Title
Direct recognition of misfolded proteins signal cell fate decisions during endoplasmic reticulum stress

Author
Lam, Mable

Publication Date
2019

Peer reviewed|Thesis/dissertation

Direct recognition of misfolded proteins signal cell fate decisions during endoplasmic reticulum stress

by
Mable Lam

DISSERTATION
Submitted in partial satisfaction of the requirements for degree of
DOCTOR OF PHILOSOPHY

in

Biochemistry and Molecular Biology

in the

GRADUATE DIVISION
of the
UNIVERSITY OF CALIFORNIA, SAN FRANCISCO

Approved:

DocuSigned by:
Peter Walter
9C44B4D1D50740D...

Peter Walter
Chair

DocuSigned by:
Avi Ashkenazi
DocuSigned by:
Shaeri Mukherjee
7AA908684B40471...

Avi Ashkenazi

Shaeri Mukherjee

Committee Members

I dedicate this dissertation with love and gratitude to my parents,

Michael Lam Dao and Van Tuyet Duong Lam.

Acknowledgements

I am forever grateful to my parents for demonstrating that tenacity and work ethic can repeatedly turn misfortune into opportunity. After one failed attempt to emigrate from Vietnam, they finally arrived in the US as refugees in their late twenties. They somehow managed to start and run three restaurants, working seven days a week from 9 am – 11 pm to finance a home and my future. They are the main reason I was able to graduate from college and pursue a Ph.D., and to this day, they still fully support my intellectual, yet financially impractical, ambitions.

I thank Peter Walter, who has taught me how to think boldly but act cautiously. He nudged me toward visionary scientific ideas and but gave me the freedom to determine if they would come to fruition. His guidance helped me focus and believe in early results in the peptide binding of my receptor of interest, even when others were skeptical of its cellular relevance. I also thank Avi Ashkenazi at Genentech Inc., who is essentially my co-advisor and encouraged an interdisciplinary approach to examine the interaction in cells. Together, we were able to piece together the location and role of this novel receptor function in the cell. I was very happy that Shaeri Mukherjee agreed to join my thesis committee later in my graduate career. Her enthusiasm for science is infectious and rejuvenated me after every thesis committee meeting.

Executing these ideas would not have been possible without past alumni of the Walter lab, who are fantastic scientific role models: Ciara Gallagher, Gulsun Elif Karagoz, and Brooke Gardner. I am always striving to think as rigorously about science as these ladies do.

I wouldn't have had the motivation to finish the Ph.D. without the support and friendships of my labmates and classmates. I am super lucky that Kelly Crotty and Sandra Torres joined the Walter lab with me. Kelly Crotty always rallied our class to hang out, and Sandra Torres brought

the gossip, sass, and level-headedness to brighten my mood. I will also remember the monthly breakfasts with Sandra and Justin Mclaurin, who always brought a different perspective to the table. I also want to thank Han and Aylin for the picnics and mimosas. Han is always generous with her time, food, and empathy. I admire Aylin greatly for her strength and unwavering kindness.

I also knew that I could always count on Fran, Marivic, Christine, and Silke to come to the rescue even with my last minute requests.

I'd like to thank all the friends who visited me during my time at UCSF: Dalee for her crazy red-eye flights and spontaneous Night Market trips, Mindy for surprising me on my birthday(!), Wing and Heydi for staying friends with me for more than a decade now, and Eunice and Diana, who came all the way to California and planned an amazing Memorial day getaway in the mountains. I'd also like to thank Alan, who has spent the most time with me in SF. I am grateful that he shares my sense of humor through the traumas of the Ph.D. experience.

I am also grateful that I met Jeremy Chang at the gym, who inspired me to seek out Olympic weightlifting. I am glad our friendship has really deepened over the past couple of years.

Lastly, my decision to go all the way to an Olympic weightlifting gym in South San Francisco has greatly changed my life, because there I met Joyson Jacob. I hope to spend a lifetime with Joyson. He has dealt with my sweat, grime, and tears in the last three years (minus one day!), and constantly reminds me of my capabilities. He is both compassionate and tough, providing much needed balance in my life. I am grateful that he wants me to come with me on my next scientific adventure.

Direct recognition of misfolded proteins signal cell fate decisions during endoplasmic reticulum stress

Mable Lam

Abstract

Disruption of protein folding homeostasis in the endoplasmic reticulum activates a signaling pathway termed the unfolded protein response, or UPR, which can mediate cell recovery or apoptosis. Understanding how the decision to live or die is made by the UPR is integral to affecting the outcome of ER stress-related pathologies. In cases of unwanted cell proliferation, inhibiting the cytoprotective branches of the UPR has shown promise in controlling cell populations. However, for cases of unwanted cell death, developing strategies to inhibit pro-apoptotic signaling of the UPR requires a deep, mechanistic understanding of the molecular events that commit the cell to an untimely fate. Chapter 1 gives an overview of both cytoprotective signaling and pro-apoptotic mechanisms of the UPR that pinpoint Death Receptor 5 (DR5) as a key driver of cell death. Chapter 2 provides published experimental evidence that reaffirms the role of DR5 in ER stress-induced apoptosis. Chapter 3 describes the experiments that demonstrate that apoptosis is driven by the direct interaction between DR5 and the source of ER stress, which is misfolded protein. In this way, DR5 assumes a terminal quality control pathway to detect unresolved protein folding stress along the secretory pathway and commit apoptosis to mitigate the consequences of secreting or displaying dysfunctional proteins.

Table of Contents

List of Figures

List of Tables

Chapter 1

Introduction: How the Unfolded Protein Response mediates cell recovery or cell death during endoplasmic reticulum stress

Introduction

A third of the mammalian proteome consists of transmembrane or secretory proteins, which begin their folding in the endoplasmic reticulum (ER). ER-resident chaperones and folding enzymes coordinate removal of the signal peptide, addition of proper glycan groups, and formation of disulfide bonds for nascent proteins to adopt their functional 3D structure. However, when physiological and pathological stresses induce an increase in secreted or transmembrane proteins, cells need accordingly to adjust the folding capacity of the ER. An accumulation of unfolded or misfolded proteins in the ER, termed ER stress, activates the Unfolded Protein Response (UPR). UPR signaling initially orchestrates a cytoprotective response through the transcriptional upregulation of ER-resident chaperones and components of the ER-associated degradation machinery (Travers *et al.*, 2000), as well as the downregulation of new protein synthesis to reduce input into the ER (Harding *et al.*, 2000; Hollien *et al.*, 2009). Upon sustained ER stress, UPR signaling leads to a pro-apoptotic program (Tabas and Ron, 2011), causing unwanted cell death associated with pathological conditions. How UPR signaling switches from a cytoprotective program to a pro-apoptotic pathway is of great interest for potential therapies in protein-folding disease states.

Cytoprotective signaling by the UPR

The UPR consists of three branches: IRE1 (inositol requiring enzyme 1), PERK (protein kinase RNA-like ER kinase), and ATF6 (activating transcription factor 6), which are ER-resident transmembrane proteins with domains in the ER lumen that monitor conditions in the ER and domains in the cytosol that transduce intracellular signals in response to those conditions.

IRE1

IRE1 is the most conserved branch of the UPR, being present even in yeast. Mammalian IRE1 exists in two isoforms: IRE1α, which is ubiquitously expressed, and IRE1β, which is only

expressed in gastrointestinal and respiratory tracts (Tabas and Ron, 2011). Its N-terminal ER-lumenal domain is followed by a single-pass transmembrane domain that links to its C-terminal cytosolic kinase and endoribonuclease (RNase) domains. Upon ER stress, activated IRE1 cleaves a subset of ER-localized mRNA's (Hollien *et al.*, 2009), leading to their degradation to reduce the incoming load into the ER. Degradation of one mRNA in particular, encoding for a mediator of apoptosis called death receptor 5 (DR5), delays the onset of apoptosis (Lu *et al.*, 2014). One major exception to IRE1-mediated degradation of mRNA is the processing of *Xbp1* (X-box binding protein 1) mRNA (Calfon *et al.*, 2002)(Kanda *et al.*, 2016). Site-specific cleavage of *Xbp1* mRNA by IRE1 releases an intronic element and subsequently allows cytoplasmic splicing of the transcript to encode for the XBP1s transcription factor. XBP1s is a potent transcription factor that upregulates several ER-resident chaperones, co-chaperones, protein disulfide isomerases, and other protein folding factors (Lee, Iwakoshi and Glimcher, 2003). Understanding the mechanisms that govern the *Xbp1*-targeted cleavage versus the promiscuous RNase activity of IRE1 continues to be an ongoing area of research.

One crucial prerequisite to activating IRE1 is the oligomerization of its kinase-RNase domains, which drives autophosphorylation of the kinase domains and positions the RNase domain to recognize RNA substrates. Both yeast and mammalian IRE1 form stress-dependent higher-order oligomers, as evident by cluster formation during live cell imaging of GFP-tagged IRE1 (Kimata *et al.*, 2007a; Aragón *et al.*, 2009; Li *et al.*, 2010a). Recombinant, purified kinase-RNase domains of IRE1 (IRE1KR) from yeast crystallized as filamentous oligomers and exhibited highly cooperative RNase activity in solution (Korennykh *et al.*, 2009), while human IRE1KR crystallized as a dimer and harbors RNase activity as a dimer (Ali *et al.*, 2011). Corresponding oligomeric states have also been observed for the N-terminal lumenal domain of IRE1 (IRE1LD), where the crystal structure of yeast IRE1LD appeared as a helical oligomer (Credle *et al.*, 2005a) and the crystal structure of human IRE1LD showed a dimer (Zhou *et al.*, 2006). Importantly, oligomerization of IRELD upon protein misfolding in the ER (as opposed to

lipid saturation) links stress in the ER to the activity of IRE1KR and is the primary driver of IRE1 clustering and activity in cells, as shown by mutations to IRE1LD that disrupt foci formation and inhibit *Xbp1* splicing (van Anken *et al.*, 2014; Karagöz *et al.*, 2017). How IRE1LD oligomerization occurs during stress will be discussed below.

PERK

PERK is also a type I transmembrane protein with a lumenal domain and cytosolic kinase domain. Upon ER stress, PERK undergoes homo-oligomerization and *trans*-autophosphorylation, in turn phosphorylating the eukaryotic initiation factor eIF2α, leading to a general inhibition of translation that reduces the load of nascent polypeptides into the ER (Harding, Zhang and Ron, 1999). Phosphorylated eIF2α also relieves the translational repression for a select subset of mRNAs with open reading frames in their 5'-untranslated regions, including the transcript encoding ATF4 (activating-transcription factor 4) (Vattem and Wek, 2004). ATF4 upregulates CHOP (C/EBP-homologous protein), which interacts with transcription factors to co-regulate the transcription or suppression of genes for adaptation to ER stress (Ron and Walter, 2007). One notable target co-regulated by ATF4 and CHOP is GADD34 (growth arrest and DNA damage-inducible protein-34), which is a regulatory subunit of the PP1C phosphatase complex that reverses phosphorylation of eIF2α and restores general translation upon resolution of stress (Ma and Hendershot, 2003). However, sustained PERK signaling leads toward pro-apoptotic responses, including the deactivation of IRE1 and upregulation of pro-apoptotic regulators, which will be discussed below.

ATF6

ATF6 is a type II transmembrane protein with its N-terminal basic leucine zipper motif in the cytosol and its C-terminal half in the ER lumen. Upon ER stress, ATF6 is trafficked via

COPII-coated vesicles from the ER to the Golgi, where site 1 and site 2 proteases cleave apart the lumenal domain and transmembrane region of ATF6 to release a soluble transcription factor to be translocated into the nucleus (Haze *et al.*, 1999). Nuclear ATF6 binds to the ER stress response element (ERSE) to upregulate many ER-adaptive genes, including the ER-resident chaperone BiP. Unlike IRE1 and PERK, how the oligomeric state of ATF6 regulates its activation is less clear. Recent evidence has shown that oligomeric species of ATF6 are inactive and retained in the ER (Gallagher and Walter, 2016), implicating monomeric ATF6 to be the traffic-competent species during ER stress (Sato *et al.*, 2011).

ER stress sensing by IRE1 and PERK

The lumenal domains of yeast and mammalian IRE1 and PERK share a conserved stress sensing mechanism because a) domain swapping experiments have shown that the domains are functionally interchangeable (Bertolotti *et al.*, 2000; Liu, Schröder and Kaufman, 2000) and b) the domains share secondary structure homology (Gardner *et al.*, 2013). An initial model for ER stress sensing by these lumenal domains originated through the observation of stress-dependent BiP dissociation from pulldowns of IRE1 and PERK (Bertolotti *et al.*, 2000; Okamura *et al.*, 2000). In the absence of stress, BiP binds to a juxtamembrane region of IRE1 and PERK lumenal domains, preventing the proteins from self-associating. Upon the induction of stress, BiP dissociates and allows IRE1 and PERK to homo-oligomerize. Testing the sufficiency of this BiP-dependent model, members of the Kohno lab identified yeast IRE1 mutations that disrupted BiP association but showed that this mutant IRE1 was not constitutively active, as this model would predict (Kimata *et al.*, 2007b; Oikawa, Kimata and Kohno, 2007).

Mechanistic insight into the missing activation signal came from examining the architecture of the lumenal domain structures, which, in their dimeric form, harbor a groove-like region reminiscent to the peptide binding domains of the major histocompatibility complex (Gardner *et al.*, 2013). This common structural feature of the lumenal domains suggested that

binding of unstructured polypeptide chains, exposed by a misfolded or unfolded protein during ER stress, could stabilize the dimer and seed oligomerization of IRE1 and PERK. In support of this model, mutations to the groove region of yeast and mammalian IRE1LD abrogate *Xbp1* splicing in response to stress (Credle *et al.*, 2005b; Li *et al.*, 2010b). Recombinant, purified yeast and human IRE1LD's have been shown to bind to peptides (Gardner and Walter, 2011; Karagöz *et al.*, 2017), and recombinant PERKLD has been shown to inhibit aggregation of proteins in refolding assays (Wang, Li and Sha, 2016). Although crosslinking-mass spectrometry techniques have mapped bound peptide to the groove that bridges dimeric human IRE1LD (Karagöz *et al.*, 2017), a recent crystal structure of PERKLD showed peptide bound at a different interface of the LD oligomer (Wang *et al.*, 2018). Whether these different binding sites for polypeptide domains occur concurrently or are specific to either IRE1 or PERK remains to be determined.

Pro-apoptotic signaling by the UPR

Although initial ER stress triggers cytoprotective adaptation, unresolved ER stress induces cell death as a programmed response rather than a secondary consequence that impinges on other stress pathways. Studies in isolated cell culture showed that treatment with tunicamycin (an inhibitor of N-linked glycosylation that induces ER stress) resulted in cell cycle arrest, DNA fragmentation, and decreased viability, establishing that ER stress was sufficient to stimulate a cell death response consistent with the hallmarks of apoptosis (Larsson, Carlberg and Zetterberg, 1993; Pérez-Sala and Mollinedo, 1995). Moreover, increasing the protein folding capacity in the ER, through exogenous expression of BiP, reduced the extent of apoptosis upon tunicamycin treatment, indicating a direct link between ER protein folding stress and the induction of cell death (Morris *et al.*, 1997).

To identify components of UPR signaling responsible for cell death, Zinszner *et al*. in the laboratory of David Ron probed the role of the highly upregulated transcription factor CHOP

during ER stress through Tm treatment of mouse embryonic fibroblasts (MEFs) isolated from *chop-/-* mice and observed reduced TUNEL staining—a marker of apoptosis—compared to wild-type (Zinszner *et al.*, 1998). Protection against ER stress also applied at the tissue level, as histological slices of the *chop-/-* mouse kidneys injected with Tm, showed decreased TUNEL staining. Furthermore, treatment with genotoxic stressors (DNA-damaging agents) did not confer resistance to cell death in the *chop-/-* animals, indicating that the role of CHOP in programmed cell death was specific to ER stress. This pivotal finding has motivated other groups to examine the role of CHOP in disease models, where ER stress and UPR signaling has been speculated to play a role in augmenting disease progression. Three examples are discussed below.

The role of CHOP in Charcot Marie Tooth 1B (CMT1B) neuropathy

Charcot Marie Tooth neuropathy results in slow, progressive degeneration of peripheral nerves leading to muscle weakness and atrophy in the limbs (Juneja *et al.*, 2019). The CMT1 subgroup is characterized by abnormalities in myelinating Schwann cells caused by duplications, mutations, or deletions of myelin-related genes. In particular, CMT1B is characterized by dominant negative point mutations in myelin protein zero (MPZ), a transmembrane protein at the surface of Schwann cells that mediates myelin compaction (Wrabetz *et al.*, 2006). A specific mutant of MPZ carrying the deletion of S63 (S63del) has been shown to cause pathology through maladaptive UPR signaling (Pennuto *et al.*, 2008). Sciatic nerves harvested from mouse models harboring a mutation equivalent to human MPZ S63del exhibited upregulation of UPR target transcripts BiP and CHOP as well as ER retention of MPZ S63del. These nerves exhibited greater amounts of TUNEL-staining, a marker of apoptosis, by post-natal day 180 compared to nerves with WT MPZ. Importantly, deletion of CHOP and PERK rescued the demyelinating effect caused by the MPZ S63del mutation (Pennuto *et al.*, 2008; Sidoli *et al.*, 2016), indicating that pro-apoptotic UPR signaling was a direct cause for the

neuropathy. However, although deletion of CHOP reduced Schwann cell death, a recent study showed that induced expression of CHOP in myelinating cells of mouse models did not lead to cell death or any discernable phenotype throughout development and into adulthood (Southwood *et al.*, 2016), indicating that upregulation of CHOP-driven factors is necessary but not sufficient to drive cell death.

The role of CHOP in RHO-associated retinitis pigmentosa

As a member of the G-protein-coupled receptor family, rhodopsin consists of a multipass transmembrane protein rod opsin (RHO) and a chromophore (11-*cis*-retinal) (Mendes *et al.*, 2005). Retinitis pigmentosa is a group of diseases caused by the death of rod photoreceptor cells that lead to cone degeneration and is associated with various point mutations RHO. One particular class of mutations results in misfolding and intracellular retention of RHO. Retinas from transgenic rat models expressing RHO P23H exhibited 2-3 fold increase in BiP mRNA expression and 4-6 fold increase in CHOP mRNA expression during development, indicating activation of the UPR (Lin *et al.*, 2007). To test the role of CHOP in the pathology of mutant RHO, transgenic mice carrying the human P23H mutation were crossed with a CHOP knockout background. Deletion of CHOP conferred mild protection at early developmental stages (P60) against rod cell degeneration but still lead to eventual rod cell death at later time points, indicating that pro-apoptotic UPR signaling may be an early driver of rod cell death but secondary mechanisms of cell death also play a significant role once the UPR is bypassed (Chiang *et al.*, 2016).

The role of CHOP in INS-induced Type 2 diabetes

Type 2 diabetes occurs upon pancreatic beta cell dysfunction, which can be caused by a progressive and persistent demand for insulin secretion to compensate for acquired insulin resistance. In a mouse model that mimics conditions of hyperglycemia and reduced beta cell

number, termed the Akita mouse, the insulin 2 gene harbors a C96Y mutation that abrogates proper disulfide bond formation within the insulin chain and induces a transcriptional increase in both BiP and CHOP mRNA. Knocking out CHOP in the heterozygous *Ins2*$^{WT/C96Y}$ delayed the reduction of beta cell mass, while homozygous *Ins2*$^{C96Y/C96Y}$ mutants were perinatally lethal with or without CHOP (Oyadomari *et al.*, 2002).

Although the genetic deletion of CHOP has consistently provided an ameliorative effect on cell death-induced pathologies, expression of CHOP itself does not directly promote cell death (McCullough *et al.*, 2001; Han *et al.*, 2013), prompting more detailed studies on the timing of the UPR signaling and molecular events downstream or in parallel that feed into the programmed cell death machinery.

Mechanisms linking UPR signaling to the programmed cell death machinery

After the initial recovery phase of the UPR, differential deactivation of the three branches during sustained ER stress largely determines the cell fate decision toward recovery or apoptosis. Attenuation of IRE1 and ATF6 signaling occurs while PERK activity persists, a pattern that consistently precedes apoptosis (Lin *et al.*, 2009; Lu *et al.*, 2014; Chang *et al.*, 2018). Apoptosis during ER stress requires Bak/Bax-mediated permeabilization of the mitochondrial outer membrane to release cytochrome C and form the apoptosome-caspase 9 complex, since double deletion of Bak and Bax confers resistance to ER stress-induced cell death (Wei *et al.*, 2001). While this pivotal finding identified the mitochondrial (or intrinsic) pathway to apoptosis as the central downstream cell death machinery, several upstream mechanisms linking unresolved ER stress to activation of Bak/Bax have been proposed.

Disputed pro-apoptotic mechanisms for IRE1

One proposed mechanism for cell death involves the recruitment of TRAF2 to the cytosolic domain of IRE1 to initiate JNK signaling. This model was initially supported by

evidence that JNK activation during ER stress required IRE1, as genetic ablation of IRE1 lead to attenuated JNK signaling; and that IRE1 and TRAF2, a scaffolding protein and E3 ubiquitin ligase in the JNK signaling pathway, form a complex in cells (Urano *et al.*, 2000). However, JNK signaling has since been shown to mediate both apoptosis and cell proliferation, and to date, no manipulation of the IRE1-TRAF2 interaction has been performed to interrogate the role of JNK signaling on apoptosis (Hetz and Papa, 2018). Furthermore, how TRAF2 recruitment to IRE1 occurs remains disconnected from stress conditions inside the lumen of the ER.

Another study found that caspase 2 activation, reported to be upstream of the mitochondrial apoptotic pathway, required the kinase-RNase activity of IRE1 (Upton *et al.*, 2012). The authors found increased levels of microRNAs that suppressed the translation of *Casp2* mRNA in an *Ire1*α*-/-* background, suggesting that IRE1 downregulated the levels of these microRNAs to derepress translation of caspase 2. However, this model would require sustained IRE1 activity to activate apoptosis, which is contrary to the observed timing of UPR signaling. Moreover, subsequent studies on ER stress using cells from *casp2-/-* mice do not report a role of caspase 2 in mediating ER stress induced apoptosis (Sandow *et al.*, 2014), indicating that activation of caspase 2 is not a primary driver of apoptosis.

Pro-apoptotic signaling by CHOP

CHOP has been reported to upregulate pro-apoptotic BH3-only proteins, such as Bim and PUMA, as well as pro-apoptotic receptors, such as Death Receptor 5 (DR5) (Yamaguchi and Wang, 2004; Puthalakath *et al.*, 2007; Cunha *et al.*, 2012). Anti-apoptotic Bcl2 proteins antagonize the pro-apoptotic activity of BH3-only proteins. Since overexpression of anti-apoptotic Bcl2 reduced apoptosis during ER stress, BH3-only proteins became likely mediators of cell death. PUMA expression has been found to have a pro-apoptotic role during ER stress primarily in neurons (Reimertz *et al.*, 2003). Upregulation of Bim was previously identified as the key switch to apoptosis in multiple cell types, since Puthalakath *et al*. observed increased levels

of Bim mRNA, but not Bid or PUMA, with treatment of ER stress inducers (Puthalakath *et al.*, 2007). Consistent with a role for Bim in apoptosis, cells ablated for Bim showed a reduction in cell death during ER stress. However, later studies showed that Bim was instead a secondary response to induce apoptosis. Puthalakath himself showed that Bim is dispensable for ER stress-induced apoptosis (Glab *et al.*, 2017), which conflicts with his original conclusion (Puthalakath *et al.*, 2007).

From re-examining the protein levels of these BH3-only proteins upon late time points of Tg treatment, truncated Bid appeared concurrently with cleavage of PARP and before an increase in Bim levels (Lu *et al.*, 2014). The production of truncated Bid by caspase 8 processing of full-length Bid did not require transcriptional upregulation of Bid. Moreover, acute depletion of caspase 8 by siRNA prevented Bid cleavage and conferred resistance to apoptosis upon ER stress, demonstrating that caspase 8 activation preceded downstream mitochondrial apoptotic events. Caspase 8 is activated by death receptors that mediate the extrinsic apoptotic pathway, and only one of these receptors, DR5, was found to be transcriptionally upregulated at later time points of ER stress. Knockdown of DR5, likewise, blocked caspase 8 activation and conferred resistance to apoptosis with Tg treatment, positioning it upstream of caspase 8 as a primary step toward activation of apoptosis during ER stress. The activation of DR5 in response to ER stress was found to be intracellular and independent of the ligand that typically activates this receptor*, i.e.,* Apo2L/TRAIL (Lu *et al.*, 2014). This highlights an important mechanistic question: how does DR5 become activated in response to the accumulation of misfolded protein in the ER lumen?

Since then, other independent studies have reported the requirement for specific death receptors in activation of ER stress-induced apoptosis. CRISPR-Cas9-mediated genetic ablation of either DR5 or DR4 in HeLa cells reduced apoptosis during glucose deprivation (Iurlaro *et al.*, 2017). TALEN-induced knockouts of either DR5 or DR4 in multiple cell lines, including HCT116, MDA-MB-231, and SW40, inhibited apoptosis during ER stress, implicating a

role for DR4 as well (Dufour *et al.*, 2017). Controversially, one group reported the generation of CRISPR-Cas9 HCT116 clones ablated in DR5 and caspase 8 that remained susceptible to ER stress-induced apoptosis (Glab *et al.*, 2017). We have characterized these specific clonal cell lines in our hands and found that, on the contrary, the caspase 8 knockout exhibited robust resistance to Tg treatment while the DR5 knockout exhibited reduced resistance (Lam *et al.*, 2018). This study has been reprinted in Chapter 2 of this dissertation.

Pro-apoptotic signaling of death receptors

Death receptors mediate the extrinsic apoptotic pathway, where these receptors reside at the cell surface and recognize external death-inducing ligands as an "instruction" to trigger death of the receiving cell (Ashkenazi and Dixit, 1998). In the physiological setting, this pathway functions in the immune system to eliminate cells expressing death receptors that readily undergo cell death upon binding a death ligand, such as stimulated lymphocytes that remain after an immune response. In the clinical setting, this pathway presented an attractive therapeutic avenue for cancers because certain death ligands, *i.e.*, Apo2L/TRAIL, induced the death of tumor cells but not healthy cells (Ashkenazi, 2015). Based on similar sequence and structural homology, death receptors belong to the tumor necrosis factor (TNF) receptor family and have 2-4 cysteine-rich domains in the extracellular matrix followed by a single-pass transmembrane domain that connects to an intracellular 80-amino acid long sequence known as the death domain (Tartaglia *et al.*, 1993). These receptors cluster upon binding to their cognate TNF superfamily ligand, a homotrimeric cytokine presented as a type II transmembrane protein on another cell or proteolytically shed into the extracellular space. Clustering of the cytosolic death domains forms a platform for assembly and activation of the intracellular cell death-triggering enzymatic machinery.

Well-characterized death receptors include Fas (also known as CD95 or Apo1), DR4 (TRAIL-R1), DR5 (TRAIL-R2), and TNFR1 (p55), and less understood receptors include DR3

and the neuron-expressed receptors, DR6 and p75NTR (Ashkenazi and Dixit, 1998). For Fas, DR4, and DR5, death ligand-induced receptor clustering recruits the cytosolic adaptor Fas-associated death domain protein (FADD) and pro-caspase 8 (A M Chinnaiyan *et al.*, 1995; Bodmer *et al.*, 2000; Kischkel *et al.*, 2000; Sprick *et al.*, 2000), assembling a platform at the membrane, termed the death inducing signaling complex (DISC) (Kischkel *et al.*, 1995). In Type I extrinsic apoptosis, DISC assembly mediates robust cleavage of the initiator caspase 8 that is sufficient to directly activate the downstream executioner caspase 3 and bypass experimental inhibition of the mitochondrial apoptotic pathway (Scaffidi *et al.*, 1998). By contrast, the type II pathway requires that activated caspase 8 cleave Bid to produce truncated Bid, an antagonist of anti-apoptotic Bcl2, to activate mitochondrial intrinsic apoptotic signaling (Li *et al.*, 1998). Caspase 8-mediated apoptosis during ER stress occurs through the type II extrinsic pathway, as evident by the requirement for Bax/Bak-mediated mitochondrial outer membrane permeabilization (Lu *et al.*, 2014). TNFR1 signaling, on the other hand, typically exhibits limited stimulation of apoptosis and instead mediates a pro-inflammatory response. Binding of its cognate ligand TNF recruits the adaptor protein TNFR-associated death domain (TRADD) and instead assembles TRAF2 and receptor-interacting protein (RIP1) to mediate NF-κB signaling (Hsu *et al.*, 1996). In cases where NF-κB signaling is suppressed, TRADD can also engage FADD (Arul M. Chinnaiyan *et al.*, 1995), as well as Nemo (IKKγ) and RIP1 leading to caspase 8 mediated apoptosis (Biton and Ashkenazi, 2011).

Activation of death receptors

Ligand-induced oligomerization of death receptors is critical to their activation. Death receptors bind to different death ligands, where TNFR1 binds to TNFα and TNFβ, Fas binds to FasL, and DR4 and DR5 share a common ligand TRAIL (also known as Apo2L). The current mechanistic understanding of ligand-induced receptor activation originated from crystal

structures of the ectodomains (ECD) of death receptors in complex with their respective ligands (Banner *et al.*, 1993; Hymowitz *et al.*, 1999; Mongkolsapaya *et al.*, 1999). Soluble ligands of the TNF family form homotrimers with three-fold symmetry. Two subunits of the ligand trimer interact with a monomer of the death receptor ECD, forming a 3:3 conical complex that tapers towards the juxtamembrane region. In addition to TNF ligand binding, antibodies and multivalent peptides that cluster death receptors also activate their signaling in cells (Engelmann *et al.*, 1990; Chuntharapai *et al.*, 2001; Li *et al.*, 2006; Pavet *et al.*, 2010; Valldorf *et al.*, 2016). In particular for DR5, divalent linkage of a 16 amino acid-long peptide was sufficient to induce apoptosis in BJAB cells when added to the media in a DR5-depdendent manner (Pavet *et al.*, 2010). However, with no apparent contact sites between the death receptor ECD's on these crystallized complexes, it was originally thought that death receptors were monomeric when inactive and required the binding of a ligand to mediate its oligomerization.

Contrary to this model, oligomerization of the ectodomain without ligand has been reported, and oligomerization of the transmembrane-death domain region can be decoupled from the ectodomain. Pre-ligand associated oligomers of in TNFR signaling have been reported to enhance ligand-stimulated activation (Chan *et al.*, 2000; Clancy *et al.*, 2005), demonstrating that the inactive death receptor is not monomeric. More surprisingly, removing the ectodomain all together did not prevent signaling, since expression of the transmembrane-tethered death domain of TNFR1 was sufficient to induce apoptosis (Boldin *et al.*, 1995). In fact, the transmembrane region alone is sufficient to mediate oligomerization as shown by NMR structures of the a trimeric Fas transmembrane domain reconstituted in bicelles (Fu *et al.*, 2016). More recently, the transmembrane domain of DR5 has been shown to form a dimer of trimers, a conformation validated by mutations that abolished apoptotic activity in cells (Pan *et al.*, 2019). If transmembrane-death domain regions formed clusters at steady state, then there must be a mechanism to inhibit clustering in the absence of ligand.

Turning again to structure for insight, the apo-ectodomain of TNFR1 has been crystallized as a dimer held together by interactions at the N-terminal Cys-rich domain with two different conformations (Naismith *et al.*, 1995). In one conformation, the monomers run parallel to each other, positioning the juxtamembrane regions adjacently. In the anti-parallel conformation, the monomers interact in the N-terminal region but point their C-termini away from other each, imposing a 100 Å separation between the juxtamembrane regions. This structure suggested that the ectodomain could mediate an auto-inhibitory conformation in the absence of ligand to physically separate the transmembrane and death domains. Recently, an autoinhibitory state has been demonstrated for DR5 as well (Pan *et al.*, 2019). By expressing an engineered TEV-protease cleavage site in the juxtamembrane region of the DR5 ectodomain, Pan *et al.* showed that proteolytic release of the DR5 ectodomain was sufficient to trigger pro-apoptotic signaling. All together, our current understanding is that death receptors occupy an auto-inhibited state as pre-assembled dimers at steady state. The autoinhibition is released by ligand binding, which allows the transmembrane regions and death domains to cluster.

Summary

The onset of ER stress activates ATF6, IRE1, and PERK to orchestrate a cytoprotective response through the transcriptional upregulation of the ER protein folding capacity and the translational downregulation of newly synthesized protein into the ER (Fig 1). Importantly, IRE1-mediated decay of transcript encoding the pro-apoptotic receptor DR5 delays caspase activation. However, with sustained ER stress, IRE1 attenuation and CHOP upregulation allows the production of DR5 to activate caspase 8 signaling. Importantly, depletion of either caspase 8 or DR5 leads to inhibition against apoptosis during ER stress. DR5 is a death receptor member of the TNFR family involved in the extrinsic pathway for apoptosis. Given that death receptors are auto-inhibited until activated by external death ligands, how and why DR5 is activated by a

source of stress initiated within the lumen of the ER became a central question of this dissertation.

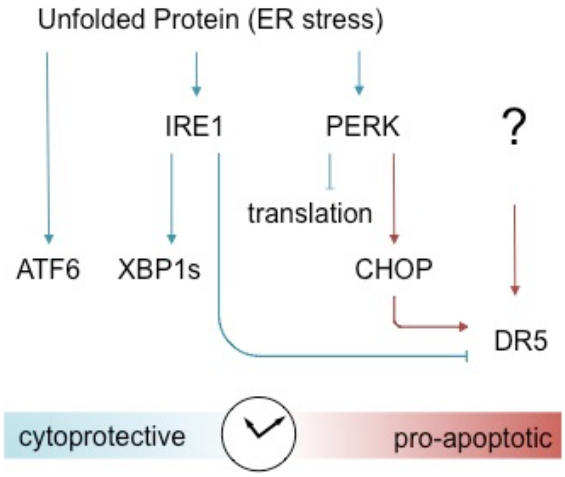

Figure 1: Cytoprotective versus pro-apoptotic signaling by the Unfolded Protein Response

References

Ali, M. M. U. *et al.* (2011) 'Structure of the Ire1 autophosphorylation complex and implications for the unfolded protein response', *EMBO Journal*, 30(5), pp. 894–905. doi: 10.1038/emboj.2011.18.

van Anken, E. *et al.* (2014) 'Specificity in endoplasmic reticulum-stress signaling in yeast entails a step-wise engagement of HAC1 mRNA to clusters of the stress sensor Ire1.', *eLife*, 3, p. e05031. doi: 10.7554/eLife.05031.

Aragón, T. *et al.* (2009) 'Messenger RNA targeting to endoplasmic reticulum stress signalling sites', *Nature*, 457(7230), pp. 736–740. doi: 10.1038/nature07641.

Ashkenazi, A. (2015) 'Targeting the extrinsic apoptotic pathway in cancer: lessons learned and future directions.', *The Journal of clinical investigation*. American Society for Clinical Investigation, 125(2), pp. 487–9. doi: 10.1172/JCI80420.

Ashkenazi, A. and Dixit, V. M. (1998) 'Death receptors: signaling and modulation.', *Science (New York, N.Y.)*. American Association for the Advancement of Science, 281(5381), pp. 1305–8. doi: 10.1126/SCIENCE.281.5381.1305.

Banner, D. W. *et al.* (1993) 'Crystal structure of the soluble human 55 kd TNF receptor-human TNFβ complex: Implications for TNF receptor activation', *Cell*, 73(3), pp. 431–445. doi: 10.1016/0092-8674(93)90132-A.

Bertolotti, A. *et al.* (2000) 'Dynamic interaction of BiP and ER stress transducers in the unfolded-protein response', *Nature Cell Biology*, 2(6), pp. 326–332. doi: 10.1038/35014014.

Biton, S. and Ashkenazi, A. (2011) 'NEMO and RIP1 Control Cell Fate in Response to Extensive DNA Damage via TNF-α Feedforward Signaling', *Cell*, 145(1), pp. 92–103. doi: 10.1016/j.cell.2011.02.023.

Bodmer, J. L. *et al.* (2000) 'TRAIL receptor-2 signals apoptosis through FADD and caspase-8', *Nature Cell Biology*, 2(4), pp. 241–243. doi: 10.1038/35008667.

Boldin, M. P. *et al.* (1995) 'Self-association of the "death domains" of the p55 tumor necrosis

factor (TNF) receptor and Fas/APO1 prompts signaling for TNF and Fas/APO1 effects', *Journal of Biological Chemistry*. American Society for Biochemistry and Molecular Biology Inc., 270(1), pp. 387–391. doi: 10.1074/jbc.270.1.387.

Calfon, M. *et al.* (2002) 'IRE1 couples endoplasmic reticulum load to secretory capacity by processing the XBP-1 mRNA', *Nature*, 415(6867), pp. 92–96. doi: 10.1038/415092a.

Chan, F. K. *et al.* (2000) 'A domain in TNF receptors that mediates ligand-independent receptor assembly and signaling.', *Science (New York, N.Y.)*, 288(5475), pp. 2351–4. Available at: http://www.ncbi.nlm.nih.gov/pubmed/10875917 (Accessed: 31 August 2018).

Chang, T.-K. *et al.* (2018) 'Coordination between Two Branches of the Unfolded Protein Response Determines Apoptotic Cell Fate', *Molecular Cell*. Cell Press, 71(4), p. 629–636.e5. doi: 10.1016/J.MOLCEL.2018.06.038.

Chiang, W.-C. *et al.* (2016) 'Ablation of Chop Transiently Enhances Photoreceptor Survival but Does Not Prevent Retinal Degeneration in Transgenic Mice Expressing Human P23H Rhodopsin', in *Advances in experimental medicine and biology*, pp. 185–191. doi: 10.1007/978-3-319-17121-0_25.

Chinnaiyan, A. M. *et al.* (1995) 'FADD, a novel death domain-containing protein, interacts with the death domain of fas and initiates apoptosis', *Cell*, 81(4), pp. 505–512. doi: 10.1016/0092-8674(95)90071-3.

Chinnaiyan, A. M. *et al.* (1995) 'FADD, a novel death domain-containing protein, interacts with the death domain of Fas and initiates apoptosis.', *Cell*, 81(4), pp. 505–12. doi: 10.1016/0092-8674(95)90071-3.

Chuntharapai, A. *et al.* (2001) 'Isotype-Dependent Inhibition of Tumor Growth In Vivo by Monoclonal Antibodies to Death Receptor 4', *The Journal of Immunology*. American Association of Immunologists, 166(8), pp. 4891–4898. doi: 10.4049/JIMMUNOL.166.8.4891.

Clancy, L. *et al.* (2005) 'Preligand assembly domain-mediated ligand-independent association

between TRAIL receptor 4 (TR4) and TR2 regulates TRAIL-induced apoptosis', *Proceedings of the National Academy of Sciences*, 102(50), pp. 18099–18104. doi: 10.1073/pnas.0507329102.

Credle, J. J. *et al.* (2005a) 'On the mechanism of sensing unfolded protein in the endoplasmic reticulum', *Proceedings of the National Academy of Sciences of the United States of America*, 102(52), pp. 18773–18784. doi: 10.1073/pnas.0509487102.

Credle, J. J. *et al.* (2005b) 'On the mechanism of sensing unfolded protein in the endoplasmic reticulum', *Proceedings of the National Academy of Sciences of the United States of America*, 102(52), pp. 18773–18784. doi: 10.1073/pnas.0509487102.

Cunha, D. A. *et al.* (2012) 'Death protein 5 and p53-upregulated modulator of apoptosis mediate the endoplasmic reticulum stress-mitochondrial dialog triggering lipotoxic rodent and human β-cell apoptosis.', *Diabetes*, 61(11), pp. 2763–75. doi: 10.2337/db12-0123.

Dufour, F. *et al.* (2017) 'TRAIL receptor gene editing unveils TRAIL-R1 as a master player of apoptosis induced by TRAIL and ER stress.', *Oncotarget*, 8(6), pp. 9974–9985. doi: 10.18632/oncotarget.14285.

Engelmann, H. *et al.* (1990) 'Antibodies to a soluble form of a tumor necrosis factor (TNF) receptor have TNF-like activity.', *The Journal of biological chemistry*, 265(24), pp. 14497–504. Available at: http://www.ncbi.nlm.nih.gov/pubmed/1696947 (Accessed: 31 August 2019).

Fu, Q. *et al.* (2016) 'Structural Basis and Functional Role of Intramembrane Trimerization of the Fas/CD95 Death Receptor.', *Molecular cell*, 61(4), pp. 602–613. doi: 10.1016/j.molcel.2016.01.009.

Gallagher, C. M. and Walter, P. (2016) 'Ceapins inhibit ATF6α signaling by selectively preventing transport of ATF6α to the Golgi apparatus during ER stress', *eLife*, 5. doi: 10.7554/eLife.11880.

Gardner, B. M. *et al.* (2013) 'Endoplasmic Reticulum Stress Sensing in the Unfolded Protein

Response', *Cold Spring Harbor Perspectives in Biology*, 5(3), pp. a013169–a013169. doi: 10.1101/cshperspect.a013169.

Gardner, B. M. and Walter, P. (2011) 'Unfolded Proteins Are Ire1-Activating Ligands That Directly Induce the Unfolded Protein Response', *Science*, 333(6051), pp. 1891–1894. doi: 10.1126/science.1209126.

Glab, J. A. *et al.* (2017) 'DR5 and caspase-8 are dispensable in ER stress-induced apoptosis', *Cell Death & Differentiation*, 24(5), pp. 944–950. doi: 10.1038/cdd.2017.53.

Han, J. *et al.* (2013) 'ER-stress-induced transcriptional regulation increases protein synthesis leading to cell death.', *Nature cell biology*, 15(5), pp. 481–90. doi: 10.1038/ncb2738.

Harding, H. P. *et al.* (2000) 'Regulated translation initiation controls stress-induced gene expression in mammalian cells.', *Molecular cell*, 6(5), pp. 1099–108. Available at: http://www.ncbi.nlm.nih.gov/pubmed/11106749 (Accessed: 27 August 2019).

Harding, H. P., Zhang, Y. and Ron, D. (1999) 'Protein translation and folding are coupled by an endoplasmic-reticulum-resident kinase', *Nature*, 397(6716), pp. 271–274. doi: 10.1038/16729.

Haze, K. *et al.* (1999) 'Mammalian Transcription Factor ATF6 Is Synthesized as a Transmembrane Protein and Activated by Proteolysis in Response to Endoplasmic Reticulum Stress', *Molecular Biology of the Cell*. Edited by P. Silver, 10(11), pp. 3787–3799. doi: 10.1091/mbc.10.11.3787.

Hetz, C. and Papa, F. R. (2018) 'The Unfolded Protein Response and Cell Fate Control', *Molecular Cell*, 69(2), pp. 169–181. doi: 10.1016/j.molcel.2017.06.017.

Hollien, J. *et al.* (2009) 'Regulated Ire1-dependent decay of messenger RNAs in mammalian cells', *The Journal of Cell Biology*, 186(3), pp. 323–331. doi: 10.1083/jcb.200903014.

Hsu, H. *et al.* (1996) 'TNF-dependent recruitment of the protein kinase RIP to the TNF receptor-1 signaling complex.', *Immunity*, 4(4), pp. 387–96. Available at: http://www.ncbi.nlm.nih.gov/pubmed/8612133 (Accessed: 31 August 2019).

Hymowitz, S. G. *et al.* (1999) ‘Triggering cell death: The crystal structure of Apo2L/TRAIL in a complex with death receptor 5’, *Molecular Cell*. Cell Press, 4(4), pp. 563–571. doi: 10.1016/S1097-2765(00)80207-5.

Iurlaro, R. *et al.* (2017) ‘Glucose Deprivation Induces ATF4-Mediated Apoptosis through TRAIL Death Receptors’, *Molecular and Cellular Biology*, 37(10). doi: 10.1128/MCB.00479-16.

Juneja, M. *et al.* (2019) ‘Challenges in modelling the Charcot-Marie-Tooth neuropathies for therapy development’, *Journal of Neurology, Neurosurgery and Psychiatry*. BMJ Publishing Group, 90(1), pp. 58–67. doi: 10.1136/jnnp-2018-318834.

Kanda, S. *et al.* (2016) ‘Autonomous translational pausing is required for XBP1u mRNA recruitment to the ER via the SRP pathway.’, *Proceedings of the National Academy of Sciences of the United States of America*, 113(40), pp. E5886–E5895. doi: 10.1073/pnas.1604435113.

Karagöz, G. E. *et al.* (2017) ‘An unfolded protein-induced conformational switch activates mammalian IRE1.’, *eLife*. eLife Sciences Publications, Ltd, 6. doi: 10.7554/eLife.30700.

Kimata, Y. *et al.* (2007a) ‘Two regulatory steps of ER-stress sensor Ire1 involving its cluster formation and interaction with unfolded proteins.’, *The Journal of cell biology*, 179(1), pp. 75–86. doi: 10.1083/jcb.200704166.

Kimata, Y. *et al.* (2007b) ‘Two regulatory steps of ER-stress sensor Ire1 involving its cluster formation and interaction with unfolded proteins.’, *The Journal of cell biology*, 179(1), pp. 75–86. doi: 10.1083/jcb.200704166.

Kischkel, F. C. *et al.* (1995) ‘Cytotoxicity-dependent APO-1 (Fas/CD95)-associated proteins form a death-inducing signaling complex (DISC) with the receptor.’, *The EMBO Journal*. Wiley, 14(22), pp. 5579–5588. doi: 10.1002/j.1460-2075.1995.tb00245.x.

Kischkel, F. C. *et al.* (2000) ‘Apo2L/TRAIL-dependent recruitment of endogenous FADD and caspase-8 to death receptors 4 and 5.’, *Immunity*, 12(6), pp. 611–20. Available at: http://www.ncbi.nlm.nih.gov/pubmed/10894161 (Accessed: 11 December 2018).

Korennykh, A. V *et al.* (2009) 'The unfolded protein response signals through high-order assembly of Ire1.', *Nature*, 457(7230), pp. 687–93. doi: 10.1038/nature07661.

Lam, M. *et al.* (2018) 'Confirming a critical role for death receptor 5 and caspase-8 in apoptosis induction by endoplasmic reticulum stress.', *Cell death and differentiation*, 25(8), pp. 1530–1531. doi: 10.1038/s41418-018-0155-y.

Larsson, O., Carlberg, M. and Zetterberg, A. (1993) 'Selective killing induced by an inhibitor of N-linked glycosylation', *Journal of Cell Science*, 106(1).

Lee, A.-H., Iwakoshi, N. N. and Glimcher, L. H. (2003) 'XBP-1 Regulates a Subset of Endoplasmic Reticulum Resident Chaperone Genes in the Unfolded Protein Response', *Molecular and Cellular Biology*, 23(21), pp. 7448–7459. doi: 10.1128/MCB.23.21.7448-7459.2003.

Li, B. *et al.* (2006) 'Activation of the Proapoptotic Death Receptor DR5 by Oligomeric Peptide and Antibody Agonists', *Journal of Molecular Biology*, 361(3), pp. 522–536. doi: 10.1016/j.jmb.2006.06.042.

Li, H. *et al.* (1998) 'Cleavage of BID by Caspase 8 Mediates the Mitochondrial Damage in the Fas Pathway of Apoptosis', *Cell*. Cell Press, 94(4), pp. 491–501. doi: 10.1016/S0092-8674(00)81590-1.

Li, H. *et al.* (2010a) 'Mammalian endoplasmic reticulum stress sensor IRE1 signals by dynamic clustering', *Proceedings of the National Academy of Sciences of the United States of America*. National Academy of Sciences, 107(37), pp. 16113–16118. doi: 10.1073/pnas.1010580107.

Li, H. *et al.* (2010b) 'Mammalian endoplasmic reticulum stress sensor IRE1 signals by dynamic clustering', *Proceedings of the National Academy of Sciences of the United States of America*. National Academy of Sciences, 107(37), pp. 16113–16118. doi: 10.1073/pnas.1010580107.

Lin, J. H. *et al.* (2007) 'IRE1 Signaling Affects Cell Fate During the Unfolded Protein Response',

Science, 318(5852), pp. 944–949. doi: 10.1126/science.1146361.

Lin, J. H. *et al.* (2009) 'Divergent Effects of PERK and IRE1 Signaling on Cell Viability', *PLoS ONE*. Edited by A. Bergmann, 4(1), p. e4170. doi: 10.1371/journal.pone.0004170.

Liu, C. Y., Schröder, M. and Kaufman, R. J. (2000) 'Ligand-independent dimerization activates the stress response kinases IRE1 and PERK in the lumen of the endoplasmic reticulum.', *The Journal of biological chemistry*, 275(32), pp. 24881–5. doi: 10.1074/jbc.M004454200.

Lu, M. *et al.* (2014) 'Opposing unfolded-protein-response signals converge on death receptor 5 to control apoptosis', *Science*, 345(6192), pp. 98–101. doi: 10.1126/science.1254312.

Ma, Y. and Hendershot, L. M. (2003) 'Delineation of a negative feedback regulatory loop that controls protein translation during endoplasmic reticulum stress', *Journal of Biological Chemistry*, 278(37), pp. 34864–34873. doi: 10.1074/jbc.M301107200.

McCullough, K. D. *et al.* (2001) 'Gadd153 sensitizes cells to endoplasmic reticulum stress by down-regulating Bcl2 and perturbing the cellular redox state.', *Molecular and cellular biology*, 21(4), pp. 1249–59. doi: 10.1128/MCB.21.4.1249-1259.2001.

Mendes, H. F. *et al.* (2005) 'Mechanisms of cell death in rhodopsin retinitis pigmentosa: Implications for therapy', *Trends in Molecular Medicine*. Elsevier Ltd, pp. 177–185. doi: 10.1016/j.molmed.2005.02.007.

Mongkolsapaya, J. *et al.* (1999) 'Structure of the TRAIL-DR5 complex reveals mechanisms conferring specificity in apoptotic initiation', *Nature Structural Biology*, 6(11), pp. 1048–1053. doi: 10.1038/14935.

Morris, J. A. *et al.* (1997) 'Immunoglobulin binding protein (BiP) function is required to protect cells from endoplasmic reticulum stress but is not required for the secretion of selective proteins.', *The Journal of biological chemistry*. American Society for Biochemistry and Molecular Biology, 272(7), pp. 4327–34. doi: 10.1074/JBC.272.7.4327.

Naismith, J. H. *et al.* (1995) 'Crystallographic evidence for dimerization of unliganded tumor

necrosis factor receptor', *Journal of Biological Chemistry*, 270(22), pp. 13303–13307. doi: 10.1074/jbc.270.22.13303.

Oikawa, D., Kimata, Y. and Kohno, K. (2007) 'Self-association and BiP dissociation are not sufficient for activation of the ER stress sensor Ire1.', *Journal of cell science*, 120(Pt 9), pp. 1681–8. doi: 10.1242/jcs.002808.

Okamura, K. *et al.* (2000) 'Dissociation of Kar2p/BiP from an ER sensory molecule, Ire1p, triggers the unfolded protein response in yeast', *Biochemical and Biophysical Research Communications*, 279(2), pp. 445–450. doi: 10.1006/bbrc.2000.3987.

Oyadomari, S. *et al.* (2002) 'Targeted disruption of the Chop gene delays endoplasmic reticulum stress–mediated diabetes', *Journal of Clinical Investigation*, 109(4), pp. 525–532. doi: 10.1172/JCI14550.

Pan, L. *et al.* (2019) 'Higher-Order Clustering of the Transmembrane Anchor of DR5 Drives Signaling', *Cell*. Elsevier, 0(0). doi: 10.1016/j.cell.2019.02.001.

Pavet, V. *et al.* (2010) 'Multivalent DR5 peptides activate the TRAIL death pathway and exert tumoricidal activity.', *Cancer research*. American Association for Cancer Research, 70(3), pp. 1101–10. doi: 10.1158/0008-5472.CAN-09-2889.

Pennuto, M. *et al.* (2008) 'Ablation of the UPR-Mediator CHOP Restores Motor Function and Reduces Demyelination in Charcot-Marie-Tooth 1B Mice', *Neuron*, 57(3), pp. 393–405. doi: 10.1016/j.neuron.2007.12.021.

Pérez-Sala, D. and Mollinedo, F. (1995) 'Inhibition of N-linked glycosylation induces early apoptosis in human promyelocytic HL-60 cells', *Journal of Cellular Physiology*, 163(3), pp. 523–531. doi: 10.1002/jcp.1041630312.

Puthalakath, H. *et al.* (2007) 'ER Stress Triggers Apoptosis by Activating BH3-Only Protein Bim', *Cell*, 129(7), pp. 1337–1349. doi: 10.1016/j.cell.2007.04.027.

Reimertz, C. *et al.* (2003) 'Gene expression during ER stress-induced apoptosis in neurons: induction of the BH3-only protein Bbc3/PUMA and activation of the mitochondrial

apoptosis pathway.', *The Journal of cell biology*, 162(4), pp. 587–97. doi: 10.1083/jcb.200305149.

Ron, D. and Walter, P. (2007) 'Signal integration in the endoplasmic reticulum unfolded protein response', *Nature Reviews Molecular Cell Biology*, pp. 519–529. doi: 10.1038/nrm2199.

Sandow, J. J. *et al.* (2014) 'ER stress does not cause upregulation and activation of caspase-2 to initiate apoptosis.', *Cell death and differentiation*, 21(3), pp. 475–80. doi: 10.1038/cdd.2013.168.

Sato, Y. *et al.* (2011) 'Luminal domain of ATF6 alone is sufficient for sensing endoplasmic reticulum stress and subsequent transport to the Golgi apparatus', *Cell Structure and Function*, 36(1), pp. 35–47. doi: 10.1247/csf.10010.

Scaffidi, C. *et al.* (1998) 'Two CD95 (APO-1/Fas) signaling pathways', *EMBO Journal*, 17(6), pp. 1675–1687. doi: 10.1093/emboj/17.6.1675.

Sidoli, M. *et al.* (2016) 'Ablation of Perk in Schwann Cells Improves Myelination in the S63del Charcot-Marie-Tooth 1B Mouse.', *The Journal of neuroscience : the official journal of the Society for Neuroscience*, 36(44), pp. 11350–11361. doi: 10.1523/JNEUROSCI.1637-16.2016.

Southwood, C. M. *et al.* (2016) 'Overexpression of CHOP in Myelinating Cells Does Not Confer a Significant Phenotype under Normal or Metabolic Stress Conditions', *The Journal of Neuroscience*, 36(25), pp. 6803–6819. doi: 10.1523/JNEUROSCI.1118-15.2016.

Sprick, M. R. *et al.* (2000) 'FADD/MORT1 and caspase-8 are recruited to TRAIL receptors 1 and 2 and are essential for apoptosis mediated by TRAIL receptor 2.', *Immunity*, 12(6), pp. 599–609. Available at: http://www.ncbi.nlm.nih.gov/pubmed/10894160 (Accessed: 11 December 2018).

Tabas, I. and Ron, D. (2011) 'Integrating the mechanisms of apoptosis induced by endoplasmic reticulum stress', *Nature Cell Biology*, 13(3), pp. 184–190. doi: 10.1038/ncb0311-184.

Tartaglia, L. A. *et al.* (1993) 'A novel domain within the 55 kd TNF receptor signals cell death.',

Cell, 74(5), pp. 845–53. doi: 10.1016/0092-8674(93)90464-2.

Travers, K. J. *et al.* (2000) 'Functional and Genomic Analyses Reveal an Essential Coordination between the Unfolded Protein Response and ER-Associated Degradation', *Cell*. Cell Press, 101(3), pp. 249–258. doi: 10.1016/S0092-8674(00)80835-1.

Upton, J.-P. *et al.* (2012) 'IRE1α cleaves select microRNAs during ER stress to derepress translation of proapoptotic Caspase-2.', *Science (New York, N.Y.)*. American Association for the Advancement of Science, 338(6108), pp. 818–22. doi: 10.1126/science.1226191.

Urano, F. *et al.* (2000) 'Coupling of stress in the ER to activation of JNK protein kinases by transmembrane protein kinase IRE1', *Science*, 287(5453), pp. 664–666. doi: 10.1126/science.287.5453.664.

Valldorf, B. *et al.* (2016) 'An Apoptosis-Inducing Peptidic Heptad That Efficiently Clusters Death Receptor 5', *Angewandte Chemie International Edition*. Wiley-Blackwell, 55(16), pp. 5085–5089. doi: 10.1002/anie.201511894.

Vattem, K. M. and Wek, R. C. (2004) 'Reinitiation involving upstream ORFs regulates ATF4 mRNA translation in mammalian cells', *Proceedings of the National Academy of Sciences of the United States of America*, 101(31), pp. 11269–11274. doi: 10.1073/pnas.0400541101.

Wang, P. *et al.* (2018) 'The luminal domain of the ER stress sensor protein PERK binds misfolded proteins and thereby triggers PERK oligomerization', *Journal of Biological Chemistry*, 293(11), pp. 4110–4121. doi: 10.1074/jbc.RA117.001294.

Wang, P., Li, J. and Sha, B. (2016) 'The ER stress sensor PERK luminal domain functions as a molecular chaperone to interact with misfolded proteins.', *Acta crystallographica. Section D, Structural biology*. International Union of Crystallography, 72(Pt 12), pp. 1290–1297. doi: 10.1107/S2059798316018064.

Wei, M. C. *et al.* (2001) 'Proapoptotic BAX and BAK: A requisite gateway to mitochondrial dysfunction and death', *Science*, 292(5517), pp. 727–730. doi:

10.1126/science.1059108.

Wrabetz, L. *et al.* (2006) 'Different intracellular pathomechanisms produce diverse Myelin Protein Zero neuropathies in transgenic mice', *Journal of Neuroscience*, 26(8), pp. 2358–2368. doi: 10.1523/JNEUROSCI.3819-05.2006.

Yamaguchi, H. and Wang, H.-G. (2004) 'CHOP is involved in endoplasmic reticulum stress-induced apoptosis by enhancing DR5 expression in human carcinoma cells.', *The Journal of biological chemistry*. American Society for Biochemistry and Molecular Biology, 279(44), pp. 45495–502. doi: 10.1074/jbc.M406933200.

Zhou, J. *et al.* (2006) 'The crystal structure of human IRE1 luminal domain reveals a conserved dimerization interface required for activation of the unfolded protein response', *Proceedings of the National Academy of Sciences of the United States of America*, 103(39), pp. 14343–14348. doi: 10.1073/pnas.0606480103.

Zinszner, H. *et al.* (1998) 'CHOP is implicated in programmed cell death in response to impaired function of the endoplasmic reticulum', *Genes & Development*, 12(7), pp. 982–995. doi: 10.1101/gad.12.7.982.

Chapter 2

Confirming a critical role for death receptor 5 and caspase-8 in apoptosis induction by endoplasmic reticulum stress.

Mable Lam, David M. Lawrence, Avi Ashkenazi, and Peter Walter

Figures from this chapter are a re-print of a correspondence that was published in *Cell Death & Differentiation* on July 10, 2018.

Abstract

Elucidating the switch between cell survival and apoptosis during ER stress remains key to understanding diseases such as protein-folding disorders and cancer (Tabas & Ron, 2011; Wang & Kaufman, 2016). Several reports demonstrate a critical role for death receptors (DRs) and caspase-8 in ER stress-induced apoptosis (Chen et al., 2016; Dufour et al., 2017; Iurlaro et al., 2017; Lu et al., 2014). However, Glab et al. recently refuted this by studying cell lines bearing CRISPR knockout (KO) of DR5 or caspase-8 (Glab et al., 2017). Glab et al. kindly provided their cells to us upon request, and we have analyzed these independently at both of our laboratories. Here we confirm, using their cell lines, that DR5 and caspase-8 have critical roles in triggering apoptosis upon ER stress.

Results

We induced ER stress with thapsigargin (Tg) and measured apoptosis activation by two orthogonal assays: Annexin V/Sytox Blue staining (Figure 2.1A-2.1D) and subG1 DNA content (Figure 2.1E). Relative to HCT116 Cas9 parental cells, DR5 KO cells showed partial attenuation, while caspase-8 KO cells exhibited nearly complete inhibition of Tg-induced apoptosis. Consistently, Tg-induced PARP cleavage (evident by the ratio of cleaved to uncleaved PARP, quantified in Figure 2.1G), caspase-3 cleavage, and caspase-3/7 enzymatic activity were diminished in DR5 KO cells and abolished in caspase-8 KO cells (Figure 2.1F-2.1H).

We also performed siRNA knockdown against DR5 in Cas9 parental cells. In keeping with published data, DR5 depletion markedly inhibited Tg-induced apoptosis, as clearly indicated by decreased Annexin V/Sytox Blue staining, PARP and caspase-3 cleavage, and caspase-3/7 activity (Figure 2.2A–2.2F). Transfection of DR5 KO cells with DR5 siRNA had no further effect on Tg-induced apoptosis, verifying an on-target impact of DR5 siRNA in the Cas9 parental cells (Figure 2.3A–2.3C). Of note, DR5 CRISPR KO suppressed apoptosis less effectively than did DR5 siRNA depletion (compare Figure 2.1 and 2.2). Furthermore, although

caspase-8 KO in Cas9 cells strongly inhibited apoptosis, caspase-8 siRNA depletion in DR5 KO cells did not (Figure 2.3D–2.3E), suggesting that the residual, DR5-independent, apoptosis in DR5 KO cells is also caspase-8-independent . A plausible explanation of these findings is that long-term DR5 ablation by CRISPR has caused the selected cell line to adapt a rewired ER stress-responsive apoptotic pathway. Caspase-8 KO cells did not display this, perhaps because this enzyme funnels multiple apoptosis drivers and is therefore more difficult to bypass. Why we find caspase-8 KO cells to be resistant whereas Glab et al. found these to be sensitive to ER stress awaits further investigation.

Inhibition of Tg-induced apoptosis was also observed upon TALEN-edited KO of DR5 and DR4 (Dufour et al., 2017). The robust apoptosis inhibition upon acute DR5 depletion and genetic caspase-8 ablation verified herein demonstrates that the DR pathway is a critical conduit for life-versus-death decisions during ER stress. This principle has now been documented for diverse ER stressors across multiple cell types (Muñoz-Pinedo & López-Rivas, 2017). In keeping with this conclusion, both our published results (Lu et al., 2014) and those of Glab *et al.* implicate the BH3-only protein Bid, whose sole proteolytic trigger is caspase-8, in ER stress-induced apoptosis.

References

Chen, P., Hu, T., Liang, Y., Li, P., Chen, X., Zhang, J., … Jia, L. (2016). Neddylation Inhibition Activates the Extrinsic Apoptosis Pathway through ATF4-CHOP-DR5 Axis in Human Esophageal Cancer Cells. *Clinical Cancer Research : An Official Journal of the American Association for Cancer Research*, *22*(16), 4145–4157. https://doi.org/10.1158/1078-0432.CCR-15-2254

Dufour, F., Rattier, T., Constantinescu, A. A., Zischler, L., Morlé, A., Ben Mabrouk, H., … Micheau, O. (2017). TRAIL receptor gene editing unveils TRAIL-R1 as a master player of apoptosis induced by TRAIL and ER stress. *Oncotarget*, *8*(6), 9974–9985. https://doi.org/10.18632/oncotarget.14285

Glab, J. A., Doerflinger, M., Nedeva, C., Jose, I., Mbogo, G. W., Paton, J. C., … Puthalakath, H. (2017). DR5 and caspase-8 are dispensable in ER stress-induced apoptosis. *Cell Death & Differentiation*, *24*(5), 944–950. https://doi.org/10.1038/cdd.2017.53

Iurlaro, R., Püschel, F., León-Annicchiarico, C. L., O'Connor, H., Martin, S. J., Palou-Gramón, D., … Muñoz-Pinedo, C. (2017). Glucose Deprivation Induces ATF4-Mediated Apoptosis through TRAIL Death Receptors. *Molecular and Cellular Biology*, *37*(10). https://doi.org/10.1128/MCB.00479-16

Lu, M., Lawrence, D. A., Marsters, S., Acosta-Alvear, D., Kimmig, P., Mendez, A. S., … Ashkenazi, A. (2014). Opposing unfolded-protein-response signals converge on death receptor 5 to control apoptosis. *Science*, *345*(6192), 98–101. https://doi.org/10.1126/science.1254312

Muñoz-Pinedo, C., & López-Rivas, A. (2017). A role for caspase-8 and TRAIL-R2/DR5 in ER-stress-induced apoptosis. *Cell Death And Differentiation*, *25*, 226. Retrieved from http://dx.doi.org/10.1038/cdd.2017.155

Tabas, I., & Ron, D. (2011). Integrating the mechanisms of apoptosis induced by endoplasmic reticulum stress. *Nature Cell Biology*, *13*(3), 184–190. https://doi.org/10.1038/ncb0311-184

Wang, M., & Kaufman, R. J. (2016). Protein misfolding in the endoplasmic reticulum as a conduit to human disease. *Nature*, *529*(7586), 326–335. https://doi.org/10.1038/nature17041

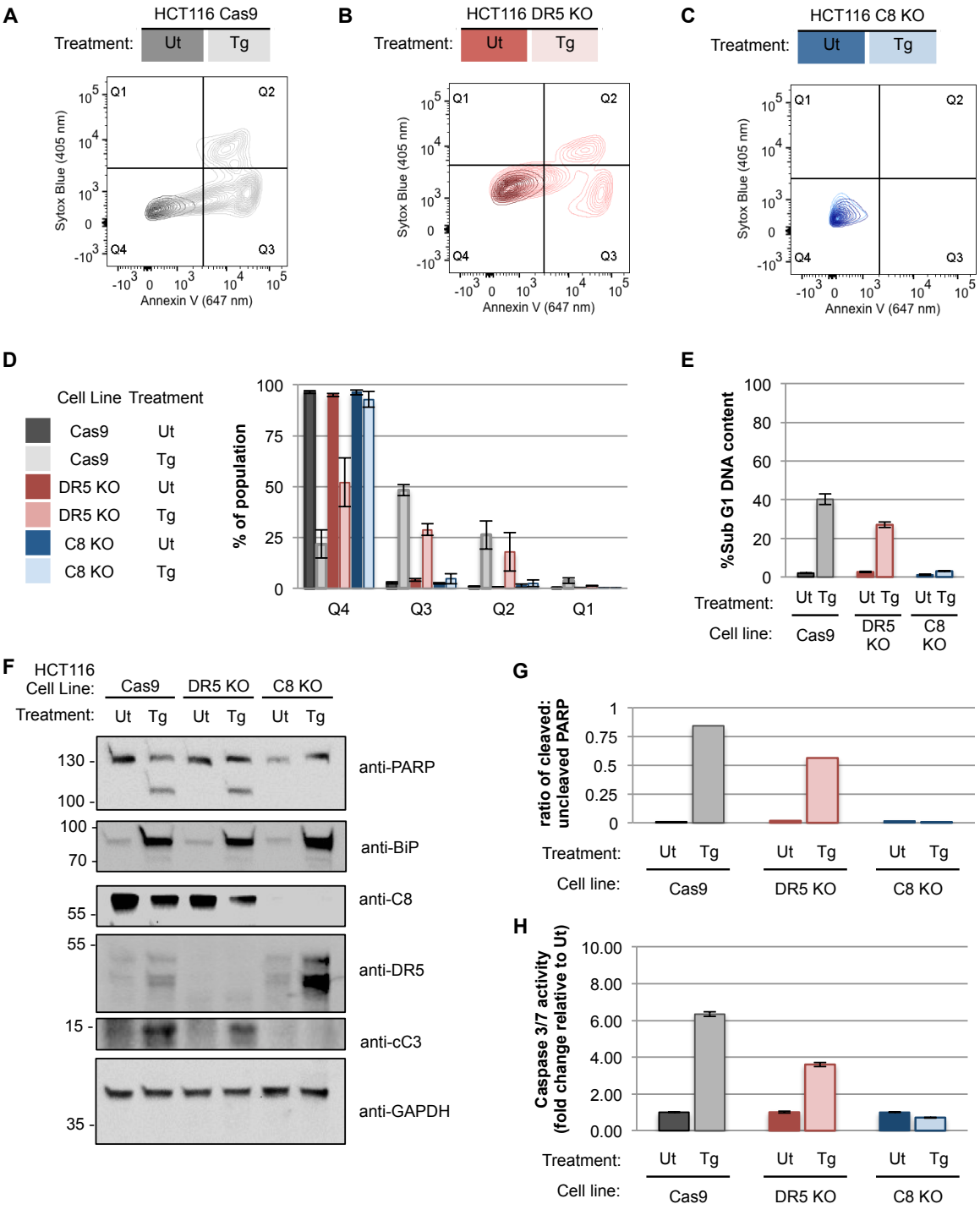
A
HCT116 Cas9
Treatment: Ut Tg
Sytox Blue (405 nm)
Annexin V (647 nm)
Q1
Q2
Q3
Q4
B
HCT116 DR5 KO
Treatment: Ut Tg
C
HCT116 C8 KO
Treatment: Ut Tg
D
Cell Line Treatment
Cas9 Ut
Cas9 Tg
DR5 KO Ut
DR5 KO Tg
C8 KO Ut
C8 KO Tg
% of population
E
%Sub G1 DNA content
Treatment: Ut Tg Ut Tg Ut Tg
Cell line: Cas9 DR5 KO C8 KO
F
HCT116
Cell Line: Cas9 DR5 KO C8 KO
Treatment: Ut Tg Ut Tg Ut Tg
anti-PARP
anti-BiP
anti-C8
anti-DR5
anti-cC3
anti-GAPDH
G
ratio of cleaved: uncleaved PARP
H
Caspase 3/7 activity (fold change relative to Ut)

Figure 2.1 Genetic ablation of DR5 partially attenuates, while disruption of caspase 8 completely blocks, Tg-induced apoptosis.

HCT116 Cas9 parental, DR5 KO cells, or caspase-8 KO cells were treated with thapsigargin (Tg, 100 nM) or vehicle alone (Ut) for 24 hours. Cells were then stained with Annexin V-AlexaFluor647 and Sytox Blue Dead Cell stain to quantify the percentage of live (Q4), early apoptotic (Q3), and late apoptotic (Q2) cells via flow cytometry for three biological replicates, each containing 10000-30000 cells (A-D). Apoptosis was also measured by analyzing subG1 DNA content via flow cytometry (E, mean -/+ standard deviation for n = 2). Lysates of DR5 KO and caspase 8 KO cells were probed for PARP cleavage and caspase 3/7 activity by Western blotting (F) and GLO assay (H, mean -/+ standard deviation for n = 3 biological replicates). The ratio of cleaved to uncleaved PARP was quantified using ImageJ to measure the intensity of the bands at 130 and 100 kDa in the anti-PARP blot (G).

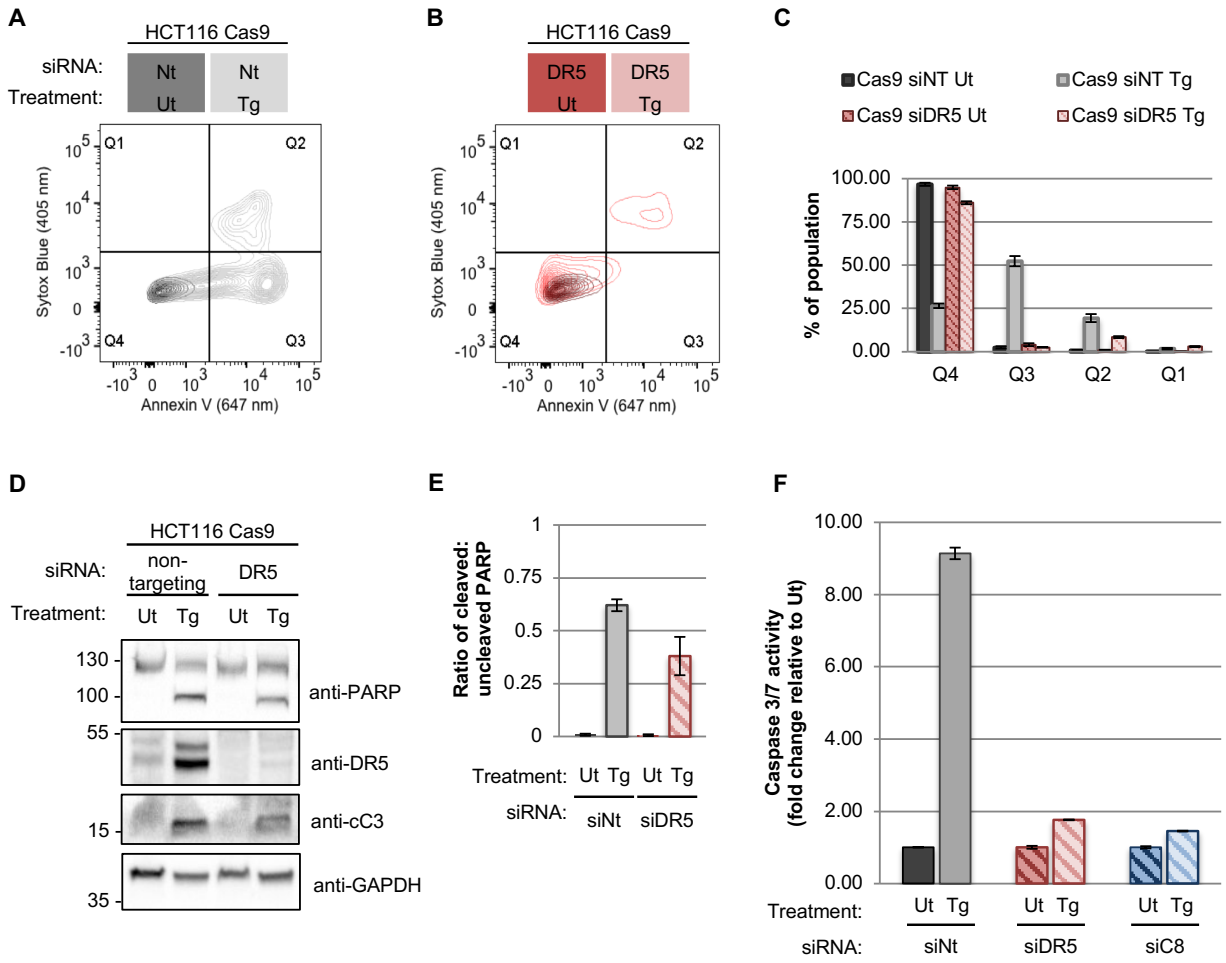

Figure 2.2 Acute depletion of DR5 via siRNA knockdown substantially inhibits ER stress-induced apoptosis.

HCT116 Cas9 parental cells were transfected with siRNA against DR5 or a non-targeting control (Nt) for 48 hours prior to treatment with 100 nM Tg for 24 hours. Cells were then stained with Annexin V-AlexaFluor647 and SytoxBlue Dead cell stain to quantify the population of live (Q4), early apoptotic (Q3), and late apoptotic (Q2) through flow cytometry (A-C). Lysates of Cas9 parental cells treated with siRNA against DR5 were analyzed for PARP cleavage via Western blotting, where one representative replicate is shown, (D) and caspase-3/7 activity through GLO assay (F, mean -/+ standard deviation for n = 3 biological replicates). The ratio of cleaved to uncleaved PARP was quantified using ImageJ to measure the intensity of the bands at 130 and 100 kDa in the anti-PARP blot (E, mean -/+ standard deviation for n = 3 biological replicates).

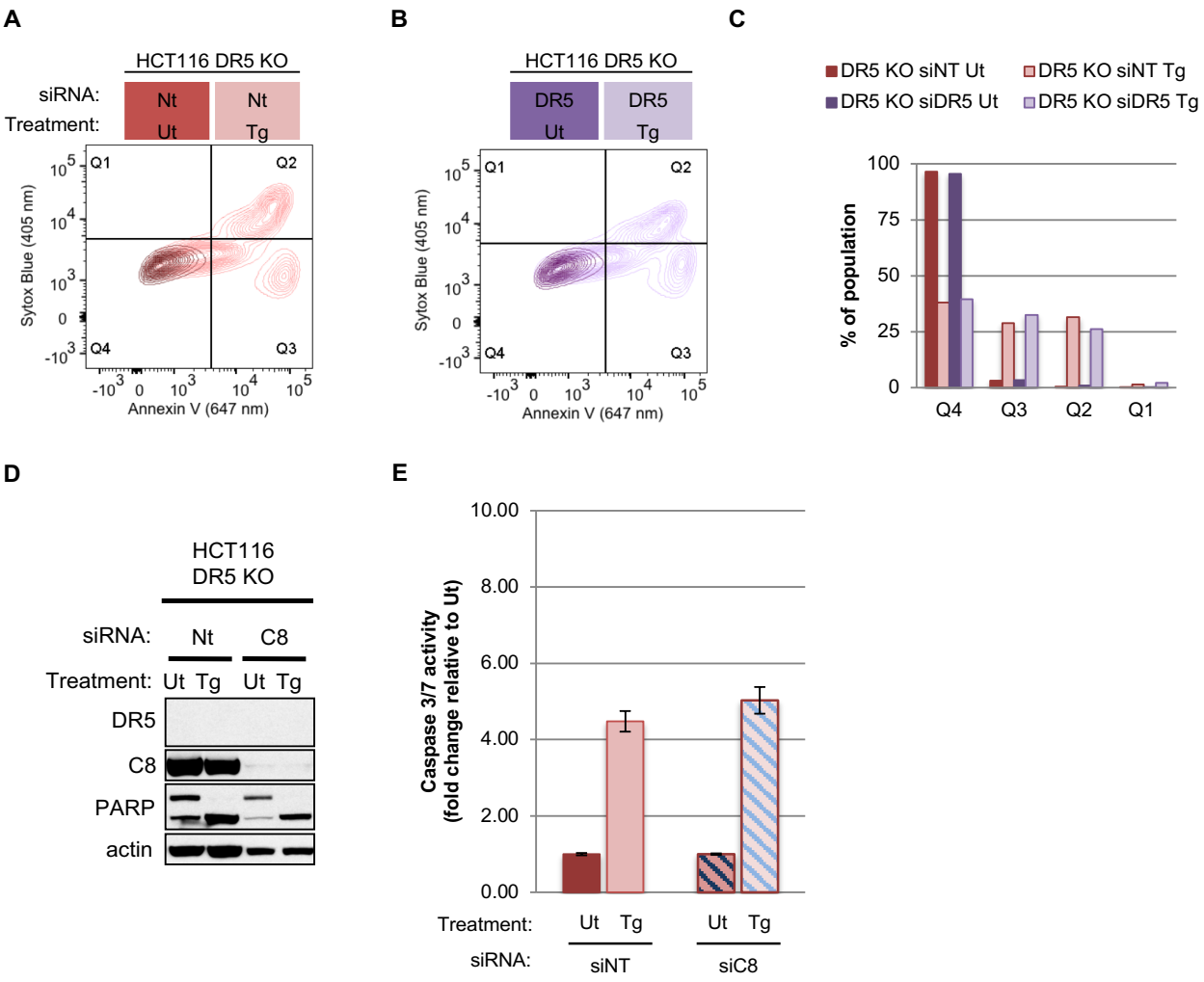

Figure 2.3 Apoptosis in DR5 KO cells occurs independently of caspase-8.

Apoptosis was measured via Annexin V-Sytox Blue staining for HCT116 DR5 KO cells transfected with siRNA against DR5 or non- targeting control (Nt) for 48 hours and treated with 100 nM Tg or vehicle alone (Ut) for 24 hours (A-C). DR5 KO cells transfected with siRNA against caspase-8 were analyzed for PARP cleavage via Western blotting (D) and for caspase-3/7 activity via GLO assay (E, mean -/+ standard deviation for n = 3 biological replicates).

Chapter 3

Misfolded proteins bind and activate death receptor 5 during unresolved endoplasmic reticulum stress

Mable Lam, Scot Marsters, Avi Ashkenazi, and Peter Walter

Abstract

Disruption of protein folding in the endoplasmic reticulum (ER) causes ER stress and activates the unfolded protein response (UPR)—a signaling network that governs cell fate. Initially, UPR signaling aims at corrective action to restore homeostasis. If this fails, the UPR drives apoptotic cell death through mechanisms that include activation of death receptor 5 (DR5). We show that misfolded protein engages DR5 intracellularly to assemble a pro-apoptotic caspase 8-activating complex at the ER-Golgi intermediate compartment. Specific peptide sequences from ER-folded proteins bind *in vitro*, through exposed hydrophobic residues, to the DR5 extracellular domain and induce its oligomerization. Disrupting DR5 recognition of unstructured polypeptides in cells inhibits apoptotic signaling. Our results suggest that DR5 directly recognizes misfolded proteins as intracellular proapoptotic ligands, thus acting as a terminal protein-folding checkpoint in the secretory pathway.

Introduction

Proper folding of transmembrane and secreted proteins is critical to cell function and intercellular communication. Quality control of protein folding begins in the endoplasmic reticulum (ER) and responds to increased protein-folding demand during physiological or pathophysiological stresses. Accumulation of unfolded or misfolded proteins in the ER, known as ER stress, activates the unfolded protein response (UPR) – a network of intracellular signaling pathways that initially mount a cytoprotective response to restore ER homeostasis, but can ultimately switch to a pro-apoptotic program under irresolvable stress (Tabas & Ron, 2011). Two key UPR sensors, IRE1 and PERK, each harboring a lumenal domain that senses ER stress through direct binding of unfolded proteins, coordinate this decision between cell survival or death through the delayed upregulation of death receptor 5 (DR5) (Karagöz et al., 2017; Lu et al., 2014; Wang, Li, Tao, & Sha, 2018). PERK-driven transcription of DR5 mRNA is initially targeted by regulated IRE1-dependent decay (RIDD), suppressing translation of nascent DR5 until PERK attenuates IRE1 activity with prolonged ER stress (Chang et al., 2018). How ER stress drives biochemical activation of DR5 downstream of its upregulation remains unclear.

DR5 is a pro-apoptotic member of the tumor necrosis factor receptor superfamily (TNFRSF) (A Ashkenazi & Dixit, 1998; Sheridan et al., 1997; Walczak et al., 1997) that forms inactive pre-ligand assembled complexes through its ectodomain (Clancy et al., 2005; Lee et al., 2005; Valley et al., 2012). In its classical activation mode, binding of the homotrimeric extracellular ligand TRAIL (also known as Apo2L) sequesters trimeric DR5 complexes on the plasma membrane into higher-order oligomeric rearrangements, in which the intracellular death domains form a scaffold that recruits the adaptor FADD and pro-caspase 8 into the death-inducing signaling complex (DISC) (Dickens et al., 2012; Jin et al., 2009; Kischkel et al., 2000; Sprick et al., 2000). In the DISC, juxtaposed pro-caspase 8 activates by auto-proteolysis. Previous studies demonstrate unexpectedly that TRAIL is dispensable for DR5 activation during ER stress (Dufour et al., 2017; Iurlaro et al., 2017; Lu et al., 2014). Indeed, upon ER stress,

most newly synthesized DR5 remains intracellular and does not reach the cell surface. Furthermore, recent studies show that the extracellular domain of DR5 is autoinhibitory, preventing receptor clustering in the absence of ligand (Pan et al., 2019). What switches DR5 from inactive pre-ligand assembled oligomers to active caspase-recruiting clusters during ER stress was unknown.

Results

To determine how ER stress triggers TRAIL-independent DR5 activation, we induced a specific protein-folding burden through ectopic expression of a GFP-tagged form of the plasma membrane-destined glycoprotein myelin protein zero (MPZ) (Fig 3.1A). Mutants of MPZ have been shown to activate the UPR and cause apoptosis in Schwann cells in a manner dependent on the UPR transcription factor CHOP (Pennuto et al., 2008). In human colon carcinoma (HCT116) cells, even expression of non-mutant MPZ induced the UPR, as indicated by a dose-dependent upregulation of CHOP, BiP, and DR5 mRNAs (Fig 3.1A, 3.2A). At low expression levels, GFP-tagged MPZ protein properly localized to the plasma membrane (Fig 3.1B); by contrast, at increased expression levels, pools of MPZ-GFP accumulated intracellularly, indicating a compromised folding state. This initiated IRE1-mediated splicing of *XBP1* mRNA after 3 hours and later attenuated *XBP1* splicing after 24 hours (Fig 3.2B). The sustained misfolding of MPZ-GFP and attenuation of IRE1 activity led to upregulation of intracellular DR5 protein, activating cleavage of caspase 8 and its downstream targets caspase 3 and PARP (Fig 3.1B, Fig 3.2C-3.2F). Moreover, cells burdened to overexpress MPZ-GFP exhibited increased Annexin V staining (Fig 3.1E), indicating engagement of the caspase-mediated apoptotic program. Acute depletion of DR5 by siRNA significantly reduced caspase activity, PARP cleavage, and Annexin V staining during overexpression of MPZ-GFP, but not cytosolic GFP (Fig 3.1C-3.1E). Sustained overexpression of two other ER-trafficked proteins, rhodopsin (RHO) and proinsulin (INS), also upregulated CHOP mRNA (Fig 3.3A) and *XBP1* mRNA splicing (Fig 3.3B), resulting in a terminal UPR that required DR5 for apoptosis induction (Fig 3.3C-3.3E). However, elevating DR5 levels in the absence of ER stress, through the ectopic expression of CHOP, was not sufficient to induce PARP cleavage or cell death to the same degree (Fig 3.4A-3.4D), indicating that activation of DR5 requires additional input signals conveyed by ER stress.

To probe the molecular components of activated DR5 assemblies, we measured the caspase 8 activity of size exclusion-fractionated cell lysates. We found increased caspase 8

activity in high molecular weight (MW) fractions of cells transfected with MPZ-GFP relative to GFP (Fig 3.1F). The fractions contained DR5 complexes and co-eluted with the leading edge of the MPZ-GFP peak (Fig 3.1F, lanes 2 and 4). Pull-down of DR5 from cell lysates enriched for FADD and MPZ-GFP (Fig 3.5A), suggesting that the co-elution of DR5 and MPZ-GFP in the high MW fractions resulted from their co-association in a physical complex.

To test if physical interaction with MPZ caused DR5 to assemble the DISC, we immunoprecipitated GFP-tagged proteins from cells transfected with vectors encoding cytosolic GFP or MPZ-GFP. DR5, FADD, and caspase 8 (both full-length p55 and its cleaved form p43) co-immunoprecipitated with MPZ-GFP but not with cytosolic GFP (Fig 3.1G, Fig 3.5B), and MPZ-GFP immunoprecipitates exhibited 2-3-fold more caspase 8 activity (Fig 3.1H, Fig 3.5C), reconstituting the DISC to a similar degree as seen after affinity purification of TRAIL-liganded DR5 (Hughes, Langlais, Cain, & MacFarlane, 2013). To determine if other ER-trafficked proteins induced caspase activity through association with DR5, we immunoprecipitated GFP-tagged proINS and RHO. RHO pull-down enriched for DR5 protein and caspase 8 activity more robustly than proINS (Fig 3.5D-3.5E), indicating that misfolded proteins differ in their propensity to engage the DR5 DISC. Thus, as shown for MPZ and rhodopsin, overexpressed ER-trafficked proteins and DR5 can interact as oligomeric complexes that induce caspase 8 activation.

Confocal imaging revealed that intracellular MPZ-GFP and DR5 co-localized in discrete puncta (3.6A), which were eliminated by DR5 siRNA knockdown (Fig 3.7A). Similarly, overexpression of RHO also resulted in intracellular puncta that overlapped with DR5 clusters (Fig 3.7B). Quantification of the mean Pearson's correlation per cell demonstrated statistically significant concurrence with DR5 signal for both MPZ-GFP and RHO-GFP (Fig 3.7C), indicating that misfolded proteins accumulate in the same compartment as DR5.

Previous findings suggested that DR5 is retained near the Golgi apparatus during ER stress (Lu et al., 2014). We observed little overlap in DR5 staining with the *cis*-Golgi marker giantin, but confirmed colocalization with the Golgi marker RCAS1 (Fig 3.8A-3.8B). Subcellular

fractionation revealed that RCAS1, DR5, MPZ, and FADD co-sedimented in segments containing ERGIC53, a marker of the ER-Golgi intermediate compartment (ERGIC), but not with those containing giantin (3.6B), thus reconciling the previously observed co-localization between DR5 and RCAS1 (Lu et al., 2014). ERGIC-associated fractions also harbored the majority of the caspase 8 activity in the cell lysate (3.6C), indicating that they contained active DR5 signaling complexes. To determine when DR5 accumulates at the ERGIC relative to misfolded proteins, we performed immunostaining of ERGIC53, which showed that intracellular puncta of MPZ appeared at 20 h — before the appearance of DR5 clusters at 24 h (Fig 3.8C). Between 20 and 24 h, the correlation of MPZ with ERGIC remained steady, whereas that of DR5 and ERGIC increased (Fig 3.8D-3.8E), indicating that DR5 accumulated after levels of MPZ at the ERGIC had saturated. At 24 h post-transfection, when caspase activity and PARP cleavage were detected (Fig 3.2C-3.2D), overlap between puncta of MPZ and DR5 with ERGIC53 was significantly higher than with giantin (3.6D-3.6E, Fig 3.8D). These results suggest that DR5 activation occurs at the ERGIC after misfolded proteins accumulate during ER stress-compromised protein trafficking.

With evidence of a physical association between misfolded protein and active DR5 oligomers at the ERGIC, we asked how misfolded protein and DR5 interact. Considering the precedence that i) DR5 binds unstructured peptides mimicking TRAIL (Kajiwara, Saito, Ogata, & Tanihara, 2004; Pavet et al., 2010) and ii) that UPR sensors directly bind misfolded protein to sense ER stress (Gardner & Walter, 2011; Karagöz et al., 2017; Wang et al., 2018), we hypothesized that DR5 may directly recognize unstructured regions of misfolded proteins through its ectodomain (ECD), which would project into the ERGIC lumen. Probing a peptide array *in vitro* with purified recombinant Fc-tagged DR5 ECD revealed promiscuous recognition of amino acid sequences throughout the ectodomain of MPZ and within extracellular loops of RHO (Fig 3.9A, Fig 3.10A-3.10B). Quantification of the relative signal intensity revealed the amino acid composition of DR5-preferred peptides, which contained aliphatic and aromatic

residues and excluded polar and acidic residues (Fig 3.10C), reminiscent of qualities that become surface-exposed in misfolded or unfolded proteins.

To validate the specificity of DR5 interactions on the array, we performed pull-down assays on the MPZ-derived peptide exhibiting the strongest signal (spots C18-C19 in Fig 3.9A, hereon referred to as MPZ-ecto) with recombinant Fc-tagged DR5 ECD versus TNFR1 ECD as a control. The MPZ-ecto peptide bound specifically to the DR5 ECD but not the TNFR1 ECD (Fig 3.9B). Under equilibrium conditions measuring the quenching of fluorescently labeled DR5 ECD, the interaction with MPZ-ecto peptide exhibited an apparent binding affinity of $K_{1/2}$ = 109 μM with a Hill coefficient of 2.6 (Fig 3.9C, green trace, 3.11A). Adding excess unlabeled DR5 ECD restored fluorescence (Fig 3.11B), and TNFR1 ECD labeled with the same fluorescent dye was not quenched in the presence of peptide (Fig 3.9C, blue), indicating that the quenching reflected a specific and reversible interaction between the DR5 ECD and the MPZ-ecto peptide. Moreover, mutation of two aromatic residues (Tyr) to disfavored acidic residues (Glu) abrogated binding (Fig 3.9C, magenta), demonstrating that the interaction is sequence-specific.

The Hill coefficient of 2.6 suggested highly cooperative binding. Therefore, we tested if the DR5 ECD forms oligomers in the presence of peptide. In the absence of peptide, the addition of a chemical cross-linker captured dimers of FLAG-tagged DR5 ECD (Fig 3.9D, 3.11C), consistent with pre-ligand assembled dimers characteristic of members of the TNFR family (Chan et al., 2000; Clancy et al., 2005; Siegel et al., 2000) . With increasing concentration of peptide (up to 200 μM), crosslinking revealed multimers of the DR5 ECD (Fig 3.9D), indicating that the peptide acts as a ligand to template assembly of DR5 oligomers. Interestingly, excess peptide (400 μM) dissociated higher-order oligomers of DR5, suggesting a lower valency of interaction when the DR5 concentration becomes limiting. Likewise, size exclusion chromatography of DR5 ECD and 100 μM MPZ-ecto (~$K_{1/2}$) showed the elution of higher-order oligomers at 7-8 ml in addition to the elution of the apo-dimer at 14 ml (Fig 3.9E). The fluorescence scan and Coomassie blue-stained gel of the fractionated samples show the

co-migration of the fluorescein-labeled MPZ-ecto peptide and DR5 ECD in the higher molecular weight fractions (Fig 3.9F, green outline). This elution pattern was similar to that of the DR5 ECD-TRAIL complex, for which both proteins co-migrated in the high molecular weight fractions (Fig 3.11E-3.11F). However, with excess MPZ-ecto peptide at 400 μM (4-times $K_{1/2}$), the proportion of both DR5 ECD and the peptide eluting as higher-order oligomers diminished and re-distributed to later eluting fractions at 12-15 ml (Fig 3.11G-3.11H, teal outline), indicating disassembly into smaller oligomers and dimers of DR5 ECD. Taken together, these data show that the MPZ-ecto peptide — used here as a proxy for an exposed, unstructured region of misfolded MPZ — enables cooperative binding of the DR5 ECD to assemble higher-order oligomers. Above saturating concentrations, excess peptide titrates DR5 ECD away from the higher-order oligomers, dissociating the complexes into smaller oligomers and dimers. In contrast, the non-binding peptide with Tyr-to-Glu mutations did not co-migrate with or induce the oligomerization of DR5 ECD (Fig 3.9E-3.9F, magenta outline).

Since mutating the Tyr residues to Glu on the MPZ-ecto peptide proved sufficient to disrupt the DR5 ECD interaction in solution, we tested the ability of this minimal MPZ-derived sequence and its mutant to bind to and activate DR5 in cells. To this end, we generated constructs that replaced the ectodomain of MPZ with either the MPZ-ecto peptide, the peptide sequence with Tyr-to-Glu mutations, or the peptide with all its aromatic residues mutated to Glu to further deplete DR5-favored residues revealed in the peptide array (3.12A). Relative to MPZ-GFP, lower expression levels of the MPZ-ecto peptide were sufficient to induce PARP cleavage in a DR5-dependent manner (Fig 3.13A-3.13B). Expressing the MPZ-ecto peptide or its mutant variants induced XBP1 mRNA splicing and transcription of CHOP and BiP, indicating that the presence of all three peptides perturb ER protein folding homeostasis to a similar degree (3.12B, 3.13C). At comparable protein expression levels, Glu mutations to the MPZ-ecto peptide drastically diminished immunoprecipitation with DR5 in both HCT116 and HepG2 (3.12C-3.12D, 3.13D-3.13E). Cells expressing the mutant peptides, relative to the MPZ-ecto peptide or full-

length MPZ, also exhibited a reduction in PARP cleavage and cell death (3.12C, 4E, 3.13D, 3.13F), demonstrating that DR5 binding of exposed polypeptides on misfolded protein is important for activating apoptosis.

Discussion

Our data identify misfolded protein as the ER stress factor that switches upregulated DR5 from inactive pre-ligand associated dimers to active multimeric clusters to mediate DISC assembly and apoptosis activation. Through characterizing the interaction between the DR5 ECD and peptide sequences of ER-trafficked proteins, we demonstrate that DR5 promiscuously binds to exposed hydrophobic stretches of misfolded proteins at an affinity of ~100 μM in a highly cooperative manner. Furthermore, we show that disrupting this affinity between DR5 and misfolded protein in a cellular context perturbs the activation of programmed cell death. To grasp how such a high concentration of misfolded protein could occur in the ERGIC, which is composed of vesicles and tubules measuring 60-100 nm in diameter and <500 nm in length, we calculate that reaching 100 μM in a vesicle with a diameter of 100 nm remarkably would require only 32 molecules (Fan, Roth, & Zuber, 2003; Sesso, de Faria, Iwamura, & Corrêa, 1994). In fact, this low affinity is likely a necessary feature that prevents aberrant DR5 oligomerization and activation in the crowded lumenal environment of membrane-bound compartments. While IRE1 and PERK act as initial UPR sensors in the ER, DR5 acts as a late sensor of misfolded protein at the ERGIC during unmitigated ER stress, triggering apoptosis to enforce a terminal quality control checkpoint for secretory and transmembrane proteins. We postulate that other members of the TNFR family, e.g. DR4, may also act in response to intracellular stimuli.

Although extensive research has focused on the therapeutic activation of death receptors including DR5 (Avi Ashkenazi, 2015), limited strategies exist to inhibit such receptors despite their demonstrated role in apoptosis-mediated disease progression (Vunnam, Lo, Grant, Thomas, & Sachs, 2017). Namely, DR5-mediated apoptosis in hepatocytes has been linked to non-alcoholic fatty liver disease, and CHOP-dependent apoptosis in Schwann cells, wherein a role for DR5 has yet to be investigated, may contribute to diabetic peripheral neuropathies (Cazanave et al., 2011; Sato, Tatsunami, Yama, Murao, & Tampo, 2015). Our finding that the assembly and disassembly of DR5 ECD oligomers can be controlled by a peptide raises the

possibility that intracellular DR5 activation could be inhibited through small ligand-induced dissociation of DR5 clusters to prevent apoptosis and thus preserve cell viability in the face of unresolved ER stress, providing a potential strategy for the growing body of work that aims to interfere therapeutically with death receptor function.

References

Ashkenazi, A. (2015). Targeting the extrinsic apoptotic pathway in cancer: lessons learned and future directions. *The Journal of Clinical Investigation*, *125*(2), 487–489. https://doi.org/10.1172/JCI80420

Ashkenazi, A., & Dixit, V. M. (1998). Death receptors: signaling and modulation. *Science (New York, N.Y.)*, *281*(5381), 1305–1308. https://doi.org/10.1126/SCIENCE.281.5381.1305

Carpenter, A. E., Jones, T. R., Lamprecht, M. R., Clarke, C., Kang, I., Friman, O., … Sabatini, D. M. (2006). CellProfiler: image analysis software for identifying and quantifying cell phenotypes. *Genome Biology*, *7*(10), R100. https://doi.org/10.1186/gb-2006-7-10-r100

Cazanave, S. C., Mott, J. L., Bronk, S. F., Werneburg, N. W., Fingas, C. D., Meng, X. W., … Gores, G. J. (2011). Death receptor 5 signaling promotes hepatocyte lipoapoptosis. *The Journal of Biological Chemistry*, *286*(45), 39336–39348. https://doi.org/10.1074/jbc.M111.280420

Chan, F. K., Chun, H. J., Zheng, L., Siegel, R. M., Bui, K. L., & Lenardo, M. J. (2000). A domain in TNF receptors that mediates ligand-independent receptor assembly and signaling. *Science (New York, N.Y.)*, *288*(5475), 2351–2354. Retrieved from http://www.ncbi.nlm.nih.gov/pubmed/10875917

Chang, T.-K., Lawrence, D. A., Lu, M., Tan, J., Harnoss, J. M., Marsters, S. A., … Ashkenazi, A. (2018). Coordination between Two Branches of the Unfolded Protein Response Determines Apoptotic Cell Fate. *Molecular Cell*, *71*(4), 629–636.e5. https://doi.org/10.1016/J.MOLCEL.2018.06.038

Clancy, L., Mruk, K., Archer, K., Woelfel, M., Mongkolsapaya, J., Screaton, G., … Chan, F. K.-M. (2005). Preligand assembly domain-mediated ligand-independent association between TRAIL receptor 4 (TR4) and TR2 regulates TRAIL-induced apoptosis. *Proceedings of the National Academy of Sciences of the United States of America*, *102*(50), 18099–18104. https://doi.org/10.1073/pnas.0507329102

Dickens, L. S., Boyd, R. S., Jukes-Jones, R., Hughes, M. A., Robinson, G. L., Fairall, L., … MacFarlane, M. (2012). A Death Effector Domain Chain DISC Model Reveals a Crucial Role for Caspase-8 Chain Assembly in Mediating Apoptotic Cell Death. *Molecular Cell*, *47*(2), 291–305. https://doi.org/10.1016/J.MOLCEL.2012.05.004

Dufour, F., Rattier, T., Constantinescu, A. A., Zischler, L., Morlé, A., Ben Mabrouk, H., … Micheau, O. (2017). TRAIL receptor gene editing unveils TRAIL-R1 as a master player of apoptosis induced by TRAIL and ER stress. *Oncotarget*, *8*(6), 9974–9985. https://doi.org/10.18632/oncotarget.14285

Fan, J.-Y., Roth, J., & Zuber, C. (2003). Ultrastructural analysis of transitional endoplasmic reticulum and pre-Golgi intermediates: a highway for cars and trucks. *Histochemistry and Cell Biology*, *120*(6), 455–463. https://doi.org/10.1007/s00418-003-0597-1

Gardner, B. M., & Walter, P. (2011). Unfolded Proteins Are Ire1-Activating Ligands That Directly Induce the Unfolded Protein Response. *Science*, *333*(6051), 1891–1894. https://doi.org/10.1126/science.1209126

Hughes, M. A., Langlais, C., Cain, K., & MacFarlane, M. (2013). Isolation, characterisation and reconstitution of cell death signalling complexes. *Methods*, *61*(2), 98–104. https://doi.org/10.1016/J.YMETH.2013.02.006

Iurlaro, R., Püschel, F., León-Annicchiarico, C. L., O'Connor, H., Martin, S. J., Palou-Gramón, D., … Muñoz-Pinedo, C. (2017). Glucose Deprivation Induces ATF4-Mediated Apoptosis through TRAIL Death Receptors. *Molecular and Cellular Biology*, *37*(10), e00479–16. https://doi.org/10.1128/MCB.00479-16

Jin, Z., Li, Y., Pitti, R., Lawrence, D., Pham, V. C., Lill, J. R., & Ashkenazi, A. (2009). Cullin3-Based Polyubiquitination and p62-Dependent Aggregation of Caspase-8 Mediate Extrinsic Apoptosis Signaling. *Cell*, *137*(4), 721–735. https://doi.org/10.1016/J.CELL.2009.03.015

Kajiwara, K., Saito, A., Ogata, S., & Tanihara, M. (2004). Synthetic peptides corresponding to ligand-binding region of death receptors, DR5, Fas, and TNFR, specifically inhibit cell

death mediated by the death ligands, respectively. *Biochimica et Biophysica Acta (BBA) - Proteins and Proteomics*, *1699*(1-2), 131–137. https://doi.org/10.1016/j.bbapap.2004.02.016

Karagöz, G. E., Acosta-Alvear, D., Nguyen, H. T., Lee, C. P., Chu, F., & Walter, P. (2017). An unfolded protein-induced conformational switch activates mammalian IRE1. *eLife*, *6*. https://doi.org/10.7554/eLife.30700

Kischkel, F. C., Lawrence, D. A., Chuntharapai, A., Schow, P., Kim, K. J., & Ashkenazi, A. (2000). Apo2L/TRAIL-dependent recruitment of endogenous FADD and caspase-8 to death receptors 4 and 5. *Immunity*, *12*(6), 611–620. Retrieved from http://www.ncbi.nlm.nih.gov/pubmed/10894161

Lee, H.-W., Lee, S.-H., Lee, H.-W., Ryu, Y.-W., Kwon, M.-H., & Kim, Y.-S. (2005). Homomeric and heteromeric interactions of the extracellular domains of death receptors and death decoy receptors. *Biochemical and Biophysical Research Communications*, *330*(4), 1205–1212. https://doi.org/10.1016/J.BBRC.2005.03.101

Lu, M., Lawrence, D. A., Marsters, S., Acosta-Alvear, D., Kimmig, P., Mendez, A. S., … Ashkenazi, A. (2014). Opposing unfolded-protein-response signals converge on death receptor 5 to control apoptosis. *Science*, *345*(6192), 98–101. https://doi.org/10.1126/science.1254312

Pan, L., Fu, T.-M., Zhao, W., Zhao, L., Chen, W., Qiu, C., … Chou, J. J. (2019). Higher-Order Clustering of the Transmembrane Anchor of DR5 Drives Signaling. *Cell*, *176*(6), 1477–1489.e14. https://doi.org/10.1016/j.cell.2019.02.001

Pavet, V., Beyrath, J., Pardin, C., Morizot, A., Lechner, M.-C., Briand, J.-P., … Gronemeyer, H. (2010). Multivalent DR5 Peptides Activate the TRAIL Death Pathway and Exert Tumoricidal Activity. *Cancer Research*, *70*(3), 1101–1110. https://doi.org/10.1158/0008-5472.CAN-09-2889

Pennuto, M., Tinelli, E., Malaguti, M., Del Carro, U., D'Antonio, M., Ron, D., … Wrabetz, L.

(2008). Ablation of the UPR-Mediator CHOP Restores Motor Function and Reduces Demyelination in Charcot-Marie-Tooth 1B Mice. *Neuron*, *57*(3), 393–405. https://doi.org/10.1016/J.NEURON.2007.12.021

Sato, K., Tatsunami, R., Yama, K., Murao, Y., & Tampo, Y. (2015). Glycolaldehyde induces endoplasmic reticulum stress and apoptosis in Schwann cells. *Toxicology Reports*, *2*, 1454–1462. https://doi.org/10.1016/J.TOXREP.2015.10.014

Sesso, A., de Faria, F. P., Iwamura, E. S., & Corrêa, H. (1994). A three-dimensional reconstruction study of the rough ER-Golgi interface in serial thin sections of the pancreatic acinar cell of the rat. *Journal of Cell Science*, *107 (Pt 3)*, 517–528. Retrieved from http://www.ncbi.nlm.nih.gov/pubmed/8006070

Sheridan, J. P., Marsters, S. A., Pitti, R. M., Gurney, A., Skubatch, M., Baldwin, D., … Ashkenazi, A. (1997). Control of TRAIL-induced apoptosis by a family of signaling and decoy receptors. *Science (New York, N.Y.)*, *277*(5327), 818–821. Retrieved from http://www.ncbi.nlm.nih.gov/pubmed/9242611

Siegel, R. M., Frederiksen, J. K., Zacharias, D. A., Chan, F. K., Johnson, M., Lynch, D., … Lenardo, M. J. (2000). Fas preassociation required for apoptosis signaling and dominant inhibition by pathogenic mutations. *Science (New York, N.Y.)*, *288*(5475), 2354–2357. Retrieved from http://www.ncbi.nlm.nih.gov/pubmed/10875918

Sprick, M. R., Weigand, M. A., Rieser, E., Rauch, C. T., Juo, P., Blenis, J., … Walczak, H. (2000). FADD/MORT1 and caspase-8 are recruited to TRAIL receptors 1 and 2 and are essential for apoptosis mediated by TRAIL receptor 2. *Immunity*, *12*(6), 599–609. Retrieved from http://www.ncbi.nlm.nih.gov/pubmed/10894160

Tabas, I., & Ron, D. (2011). Integrating the mechanisms of apoptosis induced by endoplasmic reticulum stress. *Nature Cell Biology*, *13*(3), 184–190. https://doi.org/10.1038/ncb0311-184

Valley, C. C., Lewis, A. K., Mudaliar, D. J., Perlmutter, J. D., Braun, A. R., Karim, C. B., … Sachs, J. N. (2012). Tumor Necrosis Factor-related Apoptosis-inducing Ligand (TRAIL)

Induces Death Receptor 5 Networks That Are Highly Organized. *Journal of Biological Chemistry*, *287*(25), 21265–21278. https://doi.org/10.1074/jbc.M111.306480

Vunnam, N., Lo, C. H., Grant, B. D., Thomas, D. D., & Sachs, J. N. (2017). Soluble Extracellular Domain of Death Receptor 5 Inhibits TRAIL-Induced Apoptosis by Disrupting Receptor–Receptor Interactions. *Journal of Molecular Biology*, *429*(19), 2943–2953. https://doi.org/10.1016/J.JMB.2017.08.009

Walczak, H., Degli-Esposti, M. A., Johnson, R. S., Smolak, P. J., Waugh, J. Y., Boiani, N., … Rauch, C. T. (1997). TRAIL-R2: a novel apoptosis-mediating receptor for TRAIL. *The EMBO Journal*, *16*(17), 5386–5397. https://doi.org/10.1093/emboj/16.17.5386

Wang, P., Li, J., Tao, J., & Sha, B. (2018). The luminal domain of the ER stress sensor protein PERK binds misfolded proteins and thereby triggers PERK oligomerization. *Journal of Biological Chemistry*, *293*(11), 4110–4121. https://doi.org/10.1074/jbc.RA117.001294

Xu, D., Wang, Z., Zhang, Y., Jiang, W., Pan, Y., Song, B.-L., & Chen, Y. (2015). PAQR3 modulates cholesterol homeostasis by anchoring Scap/SREBP complex to the Golgi apparatus. *Nature Communications*, *6*(1), 8100. https://doi.org/10.1038/ncomm3.13100

Materials and Methods

Cell culture and experimental reagents

HCT116 cells (ATCC CCL-247) and HepG2 cells (ATCC CRL-10741) were cultured in DMEM with high glucose (Sigma D5796) supplemented with 10% FBS (Life technologies # 10082147), 2 mM L-glutamine (Sigma G2150), 100 U penicillin, and 100 µg/mL streptomycin (Sigma P0781). Cells were incubated at 37°C, 5% CO2 for growth and transfections. Thapsigargin was purchased from Sigma and used at 100 nM in 0.1% DMSO unless otherwise indicated.

Statistical analyses

Unpaired two-tailed t-tests for data sets were performed using GraphPad Prism 6.0, where the variance between two data sets was non-signficant, unless otherwise indicated.

Transient transfections for protein expression

For each 6-well sample seeded with 400,000 cells the evening prior to transfection, the final transfection mixture put onto the cells was composed of 2 ml OptiMEM I (Thermo Fisher Scientific #31985070), 5 µl of Lipofectamine-LTX (Life Technologies #15338100), 1000 ng of total DNA (supplemented with the empty vector in cases of variable MPZ-GFP). Plasmid preparations were preformed fresh for each transfection to maximize reproducibility. Unless otherwise noted, 1.0 µg of plasmid containing GFP-tagged ER-trafficked protein was used, while 0.25 µg of GFP supplemented with 0.75 µg of empty vector was sufficient to yield GFP protein levels in excess of ER-trafficked GFP fusions.

To prepare the transfection mixture for one well of a 6-well plate, 5 µl of Lipofectamine-LTX and 1000 ng of plasmid were each diluted separately into 200 µl of OptiMEM I and then combined and incubated at RT for 15 min, as adapted from the manufacturer's protocol. Growth media for each 6-well sample was replaced with 1.5 ml of OptiMEM I and the 400-µl transfection mixture was added dropwise to each well and incubated for 24 hours (see Cell line culture conditions).

For transfections in 15-cm dishes, the transfection mixture was scaled to the number of cells plated.

Table 3.1 Constructs used for protein expression in cells

Lab Archive	Plasmid Description	Vector	Resistance	Purpose	Construct used in Figure(s):
pPW3403	empty (no GFP)	pEGFP	KanR	empty vector	1, 3.12B, 4E, 3.3, 3.5, 3.13C, 3.13F-3.13G
pPW3404	MPZ-eGFP	pEGFP	KanR	expression of MPZ	1, 2, 4E, 3.2, 3.5A-3.5C, 3.7, 3.8, 3.13
pPW3405	cytosolic GFP	pEGFP	KanR	expression of GFP	1C-1H, 3.5
pPW3406	rhodopsin (RHO) -GFP	pRK	AmpR	expression of RHO-GFP	3.3, 3.5, 3.7B-3.7C
pPW3407	proinsulin (INS) -GFP	pRK	AmpR	expression of INS-GFP	3.3, 3.5
pPW3426	MPZ-ecto peptide-eGFP	pEGFP	KanR	expression of MPZ-ecto peptide (FTWRYQPEGGRDAISIFHY A)	4, 3.13
pPW3427	MPZ-ecto peptide Glu→Tyr-eGFP	pEGFP	KanR	expression of MPZ-ecto Glu->Tyr peptide (FTWREQPEGGRDAISIFHE A)	4, 3.13C-3.13G
pPW3428	MPZ-ecto peptide Arom→Tyr-eGFP	pEGFP	KanR	expression of MPZ-ecto Arom->Tyr peptide (ETEREQPEGGRDAISIEHE A)	4, 3.13C, 3.13G
pPW3429	DR5 long FLAG-His6x, WT with silent mutation	pRK	AmpR	expression of DR5 long isoform-FLAG, harbors silent nt mutations within signal sequence to evade siRNA (AAGACCCTTGTGCTCGTT GTC → AAaACaCTTGTGCTCGTTG TC)	3.13B

Lab Archive	Plasmid Description	Vector	Resistance	Purpose	Construct used in Figure(s):
pPW3430	CHOP (canonical isoform)	pRK	AmpR	expression of CHOP in absence of ER stress	3.4

Transfections with siRNA

For experiments shown in Fig 3.1 and Fig 3.7A, the siRNA oligonucleotides against DR5 and a non-targeting control were purchased from Dharmacon (ON-TARGETplus Human TNFRSF10B 8795 siRNA # L-004448-00-0005 and ON-TARGETplus Non-targeting siRNA #2 # D-001810-02-05). The siRNA transfection was performed as previously described in (2) using Lipofectamine RNAiMAX.

For the knockdown in Fig 3.13B, we synthesized custom siRNAs from Dharmacon siRNA (DR5siRNA-2: 5' AAG ACC CUU GUG CUC GUU GUC UU 3', Nt siRNA: 5' AAA CCU UGC CGA CGG UCU ACC UU 3'). The siRNA transfection was performed 24 hours previous to the DR5L-FLAG and MPZ ecto-peptide-GFP plasmid co-transfection for a knockdown of 48 h total.

RNA extraction and generation of cDNA

Cells were grown in 6-well plates and harvested with 0.5 ml of TRIzol reagent (Life Technologies) per manufacturer's protocol to extract RNA. For cDNA synthesis, 500 ng of total RNA was reverse transcribed with 2 µl of the SuperScript VILO master mix (Life Technologies # 11755050) in a total reaction volume of 10 µl following the manufacturer's protocol for reaction temperature and duration. The reverse transcription product was diluted to 200 µl with 10 mM Tris-HCl pH 8.2 and used at 1:100 dilution for subsequent RT-PCR reactions.

Semi-quantitative RT-PCR for *Xbp1* mRNA splicing

2 µl of cDNA was added to 0.2 µM of forward and reverse primers (Hs_XBP1_Fwd: 5' -GGAGTTAAGACAGCGCTTGG- 3'; Hs_XBP1_Rev: 5' -ACTGGGTCCAAGTTGTCCAG-3'), 0.2 mM of each dNTP, 0.5 units of Taq DNA polymerase (Thermo Scientific). The reaction was set at an annealing temperature of 60.5°C with an extension time of 30 seconds for 26 cycles. The

products were then visualized on a 3% agarose gel (comprised of a 1:1 mixture of low-melting point agarose and standard agarose) stained by 1:10000 SybrSAFE.

Quantitative PCR

PCR samples were prepared as described by manufacturer's protocols from iQ SYBR Green Supermix (BioRad #17088800).
For each experiment, qRT-PCR reactions were set up in triplicate and run using a CFX96 Real Time System (Bio-Rad). Quantitation cycles were determined with CFX Manager 3.0 software (Bio-Rad) and then normalized to GAPDH as an internal control.

Table 3.2 Primers Used for Quantitative RT-PCR

Gene	5'-forward primer-3'	5'-reverse primer-3'
MPZ	GGCCATCGTGGTTTACAC	GATGCGCTCTTTGAAGGTC
GFP	CTGACCTACGGCGTGC	CCTTGAAGAAGATGGTGCG
BiP (GRP78)	GTTCGTGGCGCCTTGTGAC	CATCTTGCCAGCCAGTTGGG
DR5 (TNFRSF10B)	TTCTGCTTGCGCTGCACCAGG	GTGCGGCACTTCCGGCACAT
CHOP (DDIT3)	AGCCAAAATCAGAGCTGGAA	TGGATCAGTCTGGAAAAGCA
GADD34	GAGGAGGCTGAAGACAGTGG	AATTGACTTCCCTGCCCTCT
GAPDH	AGCCACATCGCTCAGACAC	TGGAAGATGGTGATGGGATT

Protein analysis by Western Blot

Media and cells for each sample were collected by cell scraping into cold PBS followed by a subsequent wash with 1 ml of cold PBS. The cell pellet was then resuspended in cold lysis buffer (30 mM HEPES pH 7.2, 150 mM NaCl, 1% Triton X100, 1x Roche protease inhibitor) and lysed via needle shearing on ice. Samples were centrifuged at 1000xg for 5 min, and the supernatants were mixed with sample buffer to a final concentration of 1% SDS, 62.5 mM Tris-HCl pH 6.8, 10% glycerol, 0.1% bromophenol blue, 50 mM DTT. Samples were boiled at 95°C

and loaded on SDS-PAGE gels (GenScript). Samples were subsequently transferred onto nitrocellulose membranes, blocked with Odyssey buffer (Licor) for 1 hour at RT, and probed with primary antibodies diluted 1:1000 (unless otherwise specified) in Licor Odyssey buffer supplemented with 0.1% Tween 20% at 4°C overnight.

Table 3.3 Antibodies Used for Western Blots

Primary Antibody	Species	Catalog #
anti-DR5	rabbit	Cell Signaling Technology 8074
anti-FADD	mouse	BD Biosciences 610400
anti-GFP	mouse	Roche 11814460001
anti-PARP	rabbit	Cell Signaling Technology 9542
anti-caspase 8 5F7	mouse	MBL International M032-3
anti-caspase 3	rabbit	Cell Signaling Technology 9662
anti-GAPDH	rabbit	Abcam 9485
anti-IRE1 14C10	rabbit	Cell Signaling Technology 3294
anti-Sec31A	mouse	BD Biosciences 612350
anti-Sec23A	rabbit	Invitrogen PA5-28984
anti-RCAS1 D2B6N XP	rabbit	Cell Signaling Technology 12290
anti-Giantin	rabbit	Abcam ab24586
anti-ERGIC53	rabbit	Sigma Aldrich E1031
anti-Fc	mouse	One World Lab #603-510
anti-FLAG M2	mouse	Sigma F1804
anti-His 6x	mouse	Abcam ab15149

Bound primary antibodies were probed by HRP-conjugated secondary antibodies (Amersham, Piscataway, NJ, 1:10000) using enhanced chemiluminescence (SuperSignal; Thermo Scientific, Waltham, MA) detected by standard film or through the ChemiDoc™ XRS+ Imaging System (Bio-Rad).

Caspase activity assay

Cells harvested from a 6-well plate were resuspended in 100 µl of lysis buffer (30 mM HEPES pH 7.2, 150 mM NaCl, 1% Triton X-100) and lysed via needle shearing (25G, 10 passes) followed by a 30-min incubation on ice. Supernatant was collected after centrifuging at 1000xg for 5 min. For the caspase activity assay, 10 µl of supernatant diluted with lysis buffer (1:25,

1:50, 1:100 to stay within linear range of luminescence measurements) was incubated with 10 µl of the luminogenic caspase glo 8 substrate (Promega #PRG8200) in a 384-white walled plate (Corning 3574) for 45 min at RT before measuring luminescence on a Spectramax-M5 plate reader.

Flow cytometry staining for apoptosis analysis

Cells seeded in a 6-well plate were transfected with the specified plasmid for 24 h and harvested via trypsinization in complete media to allow a 30-minute recovery at 37°C. The samples were then centrifuged at 500xg for 5 minutes and resuspended In 150 µl of a 1:20 dilution of Annexin V-AlexaFluor 647 conjugate (Thermo Scientific #A23204). Samples were transferred to a 96-well U-bottom plate and incubated in the dark for 15 min at RT. The distribution of apoptotic cells was determined by flow cytometry on a BD LSR II.

Trypan blue staining and quantification for cell death analysis

Cells seeded in a 6-well plate were transfected with the specified plasmid for 24 h and harvested via trypsinization in complete media and ultimately resuspended in 400 µl of media to obtain a concentration of 1.0-3.0x10^6 cells/ml. The cell suspension was then mixed 1:1 with 0.4% Trypan blue (Sigma-Aldrich) and incubated at 37°C for 30 min. The percentage of cells staining positive for was then quantified using the Countess™ II FL Automated Cell Counter (ThermoFisher, catalog # AMQAF1000) default brightfield settings with disposable slides.

Size-exclusion chromatography for cell lysates

Size-exclusion fractionation of cell lysate was performed as previously described in (Lu et al., 2014) with minor modifications.

In a 15-cm dish, 4 million HCT116 cells were seeded 18 hours prior to transfection (see Transient transfections for GFP-fusion proteins). 24 hours post-transfection, cells were harvesting by collecting all media (to collect detached, dying cells) and scraping the dish in 3 ml of cold PBS. The cell suspension was centrifuged at 500xg to pellet the sample. Cells were washed with an additional 1 ml of cold PBS, pelleted, and flash frozen in liquid N_2 prior to lysis.

Cells were resuspended in 600 µl of lysis buffer (30 mM HEPES pH 7.2, 150 mM NaCl, 1%

Triton X-100) with 1x protease inhibitor (Roche) and lysed through a 25G needle with 10 passes. Lysates were clarified by centrifugation at maximum speed for 15 min at 4°C, and the supernatant (400 µl) was loaded onto a SuperDex200 10/300 GL column equilibrated with lysis buffer at a flow rate of 0.35 ml/min. Fractions were collected in 0.5 ml aliquots.

For the caspase 8 activity assay, 10 µl of each fraction was incubated with 10 µl of the caspase glo 8 substrate (Promega #PRG8200) in a 384-well white walled plate (Corning 3574) for 45 min at RT before measuring luminescence on a Spectramax-M5 plate reader.

For Western blots, every three fractions were pooled for a total of 1.5 ml and subjected to TCA precipitation to concentrate the protein content. Samples were then analyzed by SDS-PAGE and immunoblotted for GFP and DR5.

DR5 Immunoprecipitation (IP)

IP for DR5 was performed as previously described in (Lu et al., 2014), using anti-DR5 mAb 5C7-conjugated agarose beads gifted by David Lawrence of the Ashkenazi lab at Genentech Inc.

GFP Immunoprecipitation (IP)

15-cm dishes were seeded with 4 million HCT116 cells and allowed to recover for 18 hours prior to transfection. Samples were then transfected for 24 hours with the GFP-tagged ER trafficked protein, cytosolic GFP, or empty vector. To harvest apoptotic and living cells for each sample, all media and washes were collected. Cells were scraped in 2 ml of cold PBS and combined with the media and washes. Samples were centrifuged to pellet cells, washed with 1 ml cold PBS, and flash frozen in liquid N_2 prior to lysis.

The cell pellets were resuspended in 750 µl of 30 mM HEPES pH 7.2, 150 mM NaCl, 1% Triton X-100 with 1x Roche protease inhibitor cocktail (if used subsequently for caspase glo 8 assay) or with 5x Roche protease inhibitor cocktail (if used for immunoblotting). The cells were lysed by mechanical shearing through a 25G needle for 13-15 plunges followed by incubation on ice for 30 min. The lysate was centrifuged at 2000xg for 5 min to remove debris and then incubated with 30 µl of GFP-Trap magnetic agarose beads (Chromotek gtma-20) for 4 hours at 4°C. The beads were then washed with 750 µl of lysis buffer for 10 min at 4°C for three rounds.

For measuring caspase activity, a fifth of the beads was resuspended in 40 µl of 30 mM HEPES pH 7.2, 150 mM NaCl, 1% Triton X-100. 10 µl of the resuspended mixture was incubated with 10 ul of the caspase glo 8 luminogenic substrate (Promega #PRG8200) for 45 min at RT before measuring luminescence.

For Western blots, samples were eluted by adding 35 µl of non-reducing SDS gel loading buffer (50 mM Tris-HCl (pH 6.8), 2% SDS, 0.1% bromophenol blue, 10% glycerol) and incubated for 10 min at 70°C. The beads were then magnetically removed from the eluted sample before adding DTT to a final concentration of 25 mM. The entire sample was loaded onto the gel and immunoblotted for DR5, caspase 8, and GFP, in that order.

Immunofluorescence of DR5 and organelle markers in HCT116

HCT116 were seeded at 25000 cells per well in an eight-well glass-bottom µSlide (Ibidi 80827) pre-coated with Collagen IV (Sigma-Aldrich C6745, 0.03 mg/ml in PBS incubated for 30 min at RT, and then rinsed off with PBS x 3) in growth media 18 hours prior to transfection (see above for protocol). 24 hours post-transfection, the cells were fixed using 4% paraformaldehyde (PFA, Electron Microscopy Sciences) or methanol, depending on the antibody combination used for immunostaining (see table below). Samples were protected from light after fixation to preserve GFP fluorescence.

Table 3.4 Antibodies Used for Immunofluorescence

Primary Antibody	Species	Catalog #	IF Dilution	Fixation method
anti-DR5 3H3	mouse	Genentech	1:100	4% PFA/methanol
anti-cleaved caspase 8 (Asp391) (18C8)	rabbit	Cell Signaling Technology 9496	1:50	4% PFA
anti-RCAS1 D2B6N XP	rabbit	Cell Signaling Technology 12290	1:200	methanol
anti-Giantin	rabbit	Abcam ab24586	1:1000	methanol

Primary Antibody	Species	Catalog #	IF Dilution	Fixation method
anti-ERGIC53	rabbit	Sigma Aldrich E1031	1:100	methanol

For fixation with 4% PFA, 32% PFA was added directly to the well in growth media for a 1:8 dilution and incubated for 10-15 min at RT. Cells were then permeabilized with PHEM buffer (60 mM PIPES, 25 mM HEPES, 10 mM EGTA, 2 mM MgCl2-hexahydrate, pH 6.9) containing 0.1% Triton-X100 for 10 min at RT for three washes.

For fixation with methanol, media was removed and cells were washed with cold PBS. Then methanol (pre-cooled at -20°C) was added to the well and incubated at -20°C for 3-4 min. The methanol was promptly aspirated and replaced with PHEM buffer (without Triton X-100), followed by two more 10-min washes with PHEM at RT.

To block against non-specific antibody interactions, cells were rinsed in PHEM (without 0.1% Triton X-100) and then incubated with PHEM containing 2% normal goat serum (Jackson Immunoresearch Laboratories, 005-000-121) for 1 hr at RT. Primary antibodies were incubated in blocking solution overnight at 4°C at the dilution noted in the table above. Cells were then washed with PHEM buffer for 10 min at RT x 3 and incubated with secondary antibodies, anti-rmouse-AlexaFluor546 (Invitrogen A11030) and anti-rabbit-AlexaFluor633 (Invitrogen A21071), diluted 1:1000 in PHEM with 2% normal goat serum. (Secondary antibody solutions were centrifuged at 15000xg for 20 mins at 4°C to remove aggregates prior to incubating with cell samples.) After a 1-hr incubation at RT, cells were washed with PHEM buffer once, then incubated with PHEM buffer containing nuclear stain (DAPI, Molecular Probes, Eugene, OR, D-1306, 5 µg/mL), and finally rinsed with PHEM buffer twice before imaging.

Samples were imaged on a spinning disk confocal with Yokogawa CSUX A1 scan head, Andor iXon EMCCD camera, and 40x Plan Apo air Objective NA 0.95 or 100x ApoTIRF objective NA 1.49 (Nikon).

Quantification of Pearson's correlation for co-localization analyses

Images were analyzed using CellProfiler (Carpenter et al., 2006). From the 405 nm channel, cell nuclei were identified as primary objects using maximum correlation thresholding (MCT) and shape to distinguish clumped objects. Secondary objects were outlined using propagation from the nuclei (DAPI) after applying MCT from the 488 nm, 561 nm, and 633 nm channels. Tertiary objects for each cell was identified as the mask of each nucleus subtracted from the mask of its corresponding secondary object in each channel, yielding masks for intracellular GFP-tagged protein from the 488 nm channel, for intracellular DR5 from the 561 nm channel, and for the organelle marker in the 633 nm channel. For overlap between DR5 and MPZ/RHO-GFP, Pearson's correlation coefficients were calculated within the MPZ/RHO mask for each cell to filter out untransfected cells. For overlap between DR5/MPZ and organelle markers, Pearson's correlation coefficients were calculated within tertiary objects for the organelle marker in GFP+ cells. Statistical analyses for all data sets were performed using GraphPad Prism 6.0.

Subcellular fractionation

This subcellular fractionation protocol was adapted from (Xu et al., 2015).

Cells transfected with MPZ-GFP were harvested from a 15-cm dish as described in the Size Exclusion Chromatography section above. The cell pellet was resuspended in 400 µl of homogenization buffer (10 mM triethanolamine-acetic acid, pH 7.4, 0.25 M sucrose, 1 mM sodium EDTA, protease inhibitor cocktail (Roche)) and lysed via mechanical shearing through a 25-gauge needle on a 1-ml syringe with 13 passes. (Note on protease inhibitor: 4x protease inhibitor was used to lyse samples used for Western blotting to minimize degradation of proteins, while 1x protease inhibitor was used in sample lysis for caspase glo 8 assay so that excess inhibitor would not interfere with cleavage of luminescent substrate.) Homogenized sample was then centrifuged at 2000xg for 15 min at 4°C to remove unlysed cells and the nuclear fraction. 250 µl of the supernatant was loaded via capillary action onto a 9-25% iodixanol gradient in a 13x51mm polyclear centrifuge tube (Seton Scientific # 7022-29426) prepared using the BioComp Gradient Master (Model 107). The 9% and 25% layers of the gradient were made by diluting 60% iodixanol (OptiPrep^{TM} Density Medium,Sigma Aldrich # D1556) into cell suspension medium (0.85% (w/v) NaCl, 10 mM Tricine-NaOH, pH 7.4). The loaded gradients were then centrifuged in SW55Ti rotor at 44800 rpm for 2 hr at 4°C. After deceleration without braking, 300-ul fractions were collected from the top of the tube.

Fractions from samples lysed with 4x protease inhibitor were subjected to TCA precipitation to concentrate protein content for immunoblotting. Fractions from samples lysed with 1x protease inhibitor were used for the caspase glo 8 assay (10 µl of each fraction + 10 µl of the caspase glo 8 reagent (Promega #PRG8200) incubated for 45 min at RT prior to measuring luminescence).

Peptide Array Binding

Peptide arrays were purchased from the MIT Biopolymers Laboratory as described previously in (Karagöz et al., 2017) and (Gardner & Walter, 2011). The sequences of each protein were tiled from N- to C-terminus in 18-amino-acid-long peptides shifting by three amino acids from the previous spot. The arrays were incubated in methanol for 10 min, and then washed in binding buffer (50 mM HEPES pH 7.2, 250 mM NaCl, 10% glycerol) for 10 min at room temperature x 3. 500 nM of Fc-tagged DR5 extracellular domain (ECD, a kind gift from Scot Marsters) was incubated with the array in binding buffer at room temperature for 1 hr. Then, the array was washed three times for 10 minutes with binding buffer to remove unbound protein. The bound DR5 ECD was then transferred onto a nitrocellulose membrane via a semi-dry transfer apparatus (Owl HEP-1) at 80 mA for 45 min at 4°C. The membrane was then blocked with 1xPBST with 5% milk for 1 hr at room temperature and probed with 1:1000 anti-Fc (One World Lab #603-510) overnight at 4°C followed by 1:10000 anti-mouse IgG-HRP (Promega #W4021) for 1 hr at RT. The membrane was imaged using chemi-luminescence with the Bio-Rad Universal Hood II Gel Doc below saturating pixel intensities. The signal of each spot was quantified using Max Quant and normalized to the maximum intensity of all the spots on the same array.

Peptides

Peptides were ordered from GenScript at >95% purity and stored with desiccant at -20°C. Peptides were dissolved as a highly concentrated stock solution in anhydrous DMSO and diluted 1:50 in aqueous buffer to measure the stock concentration using absorbance at 280 nm. All solution mixtures containing peptide and protein had a final concentration of 0.5% DMSO.

Table 3.5 Amino Acid Sequences of MPZ-derived Peptides

peptide	peptide sequence
MPZ-ecto^{VD}	VSDDISFTWRYQPEGGRD
MPZ-ecto	FTWRYQPEGGRDAISIFHYA
MPZ-ecto$^{Tyr\rightarrow Glu}$	FTWREQPEGGRDAISIFHEA

Peptide pulldown with Fc-tagged ECD proteins

Recombinant Fc-tagged DR5 and TNFR1 ECD proteins were generated and purified at Genentech Inc by S. Marsters.

Fc-tagged proteins were incubated with Dynabeads Protein G (20 µg per 12.5 µl of beads for each sample) in 1xPBS for 1.5 hours at RT. Beads were then washed with 1xPBS via magnetic pulldown, followed by two 10-min washes with 20 mM HEPES pH 7.2, 100 mM KOAc, 0.2% Tween-20 at RT to remove unbound Fc-tagged protein. Protein bound-beads were incubated with 50 µl of 100 µM peptide in 20 mM HEPES pH 7.2, 100 mM KOAc, 0.2% Tween-20 for 1 hour at RT. Beads were then washed with 50 µl of buffer three times, and samples were eluted with 25 µl of non-reducing sample buffer (62.5 mM Tris-HCl pH 6.8, 2.5% SDS, 10% glycerol) by incubating at 65°C for 15 min to elute the complex.

Purification of recombinant of DR5 and TNFR1 ECD

Human DR5 ECD (long isoform, residues 72-213: KRSSPSEGLCPPGHHISEDGRDCISCKYGQDYSTHWNDLLFCLRCTRCDSGEVELSPCTTTRN TVCQCEEGTFREEDSPEMCRKCRTGCPRGMVKVGDCTPWSDIECVHKESGTKHSGEVPAVE ETVTSSPGTPASPCSLSG) and TNFR1 ECD (residues 22-211: IYPSGVIGLVPHLGDREKRDSVCPQGKYIHPQNNSICCTKCHKGTYLYNDCPGPGQDTDCREC ESGSFTASENHLRHCLSCSKCRKEMGQVEISSCTVDRDTVCGCRKNQYRHYWSENLFQCFN CSLCLNGTVHLSCQEKQNTVCTCHAGFFLRENECVSCSNCKKSLECTKLCLPQIENVKGTEDS GTT) were cloned into a pFastBac HTB vector containing a Gp67 (glycoprotein) signal peptide and 6xHis tag to force secretion of the expressed protein. The pFastBac HTB constructs were recombined into bacmid DNA using the Bac-to-Bac baculovirus expression system according to manufacturer's protocols (Life Technologies).

Table 3.6 Constructs used to generate bacmid for recombinant protein purification

Lab Archive	Plasmid Description	Vector	resistance	Construct used in Figure(s):
pPW3408	Gp64-His6x-DR5 long ECD-FLAG	pFastBacHT	AmpR	3.9D-3.9F, 3.11C-3.11H
pPW3410	Gp64-His6x-DR5 long ECD	pFastBacHT	AmpR	3.9C, 3.11A-3.11B
pPW3411	Gp64-His6x-TNFR1 ECD	pFastBacHT	AmpR	3.9C, 3.11A

SF21 were grown in SF-900 II media supplemented with 10% FBS at 28°C in disposable Erlenmeyer flasks rotating at 150 rpm and transfected using Cellfectin II (Thermo Fisher Scientific) according to manufacturer's protocols. The baculovirus was amplified two more times at a low M.O.I. prior to infection of SF21 with a 1:50 dilution of the virus for protein expression.

After 72-96 hr of infection, the SF21 suspension was centrifuged at 2000xg for 15 min (two rounds) to collect the media containing the secreted ECD protein. The media was then further clarified through a 0.2 um filter before loading onto a HisTrapFF column equilibrated with 25 mM imidazole pH 7.4, 150 mM NaCl (Buffer A) at a flow rate of 3.0 ml/min. The column was washed with 20 CV of Buffer A at a flow rate of 4.0 ml/min. To elute, the concentration of imidazole was increased through a linear gradient from 0-100% of Buffer B (500 mM imidazole pH 7.4, 150 mM NaCl) in 7 CV. Fractions containing the His-tagged ECD were then concentrated and further purified on a SuperDex200 10/300 GL column (GE Healthcare) equilibrated with 30 mM HEPES pH 7.2, 150 mM NaCl. For long-term storage, the protein was diluted into 30 mM HEPES pH 7.2, 150 mM NaCl, 10% glycerol and flash frozen in liquid N_2 before storing at -80°C.

Labeling of DR5 and TNFR1 ECD

Recombinant DR5 and TNFR1 ECD were labeled with AlexaFluor647 NHS Ester (Succinimidyl Ester) (Life Technologies # A37573) in a 3:1 dye:protein molar ratio in 30 mM HEPES pH 7.2, 150 mM NaCl, 1% DMF overnight at 4°C protected from light. The labeled proteins were re-loaded onto a SuperDex200 10/300 GL column to remove the excess dye, yielding labeling efficiencies of 59% and 49% for DR5 ECD and TNFR1 ECD, respectively. Labeled proteins

were diluted into buffer with 10% glycerol and flash frozen in liquid N_2 for long-term storage at -80°C.

Fluorescence quenching assay

To set up reactions, the unlabeled peptide titration (10 µl each) was made from a two-fold dilution series of the highest peptide concentration assayed. To each peptide sample, 10 µl of AlexaFluor647-labeled ECD protein was added to give a final concentration of 200 nM ECD protein in 20 mM HEPES pH 7.2, 100 mM KOAc, 0.1% Tween-20. Samples were incubated for 30 min at RT protected from light before measuring fluorescence.

Samples were then loaded by capillary action onto premium capillaries (Nanotemper Technologies, cat. #MO-K025). Fluorescence was measured on a Monolith NT.115 Instrument (NanoTemper Technologies, Germany) using the capillary scan function at 25°C.
The half-maximum binding constant ($K_{1/2}$) and Hill coefficient were determined by fitting the data points on Prism 6.0 to the model equation: $Y=B_{max}*X\text{^}h/(K_{1/2}\text{^}h + X\text{^}h)$, where Y is the % quenching, X is the concentration of peptide, B_{max} is the maximum % quenching, and h is the Hill slope.

Crosslinking for DR5 ECD and peptide

To set up the peptide titration series, two-fold dilutions were made from the highest peptide concentration used into 20 mM HEPES pH 7.2, 150 mM NaCl. An equal volume of C-terminal FLAG-tagged DR5 ECD was added to each peptide sample or buffer alone for a final concentration of 10 µM DR5 ECD. Reactions were equilibrated at RT for 30 min prior to the addition of 100 µM BS3 for 20 min at RT. Excess crosslinker was quenched by adding Tris-HCl pH 7.4 to a final concentration of 100 mM and incubated for 15 min at RT before analysis by SDS-PAGE. The resulting gel was then transferred onto a nitrocellulose membrane (120 V, 2 hours for high MW species) and blotted with anti-FLAG to visualize discrete crosslinked species.

Size exclusion of DR5 ECD and peptide complex

The specified concentration of protein and peptide were incubated overnight at 4°C. The following day, 200 ul of each sample was loaded onto a SuperDex200 10/300 GL column equilibrated with 30 mM HEPES pH 7.2, 150 mM NaCl at a flow rate of 0.5 ml/min. Fractions were collected in 1-ml aliquots.

For subsequent analysis of each fraction by SDS-PAGE, 1-ml fractions were concentrated to 50 µl using a 3kDa MW cutoff and loaded onto a gel. The fluorescein-labeled peptide was visualized using the fluorescence detection mode on a Typhoon 9400 Variable Mode Imager (GE Healthcare). Protein was visualized by staining with Coomassie.

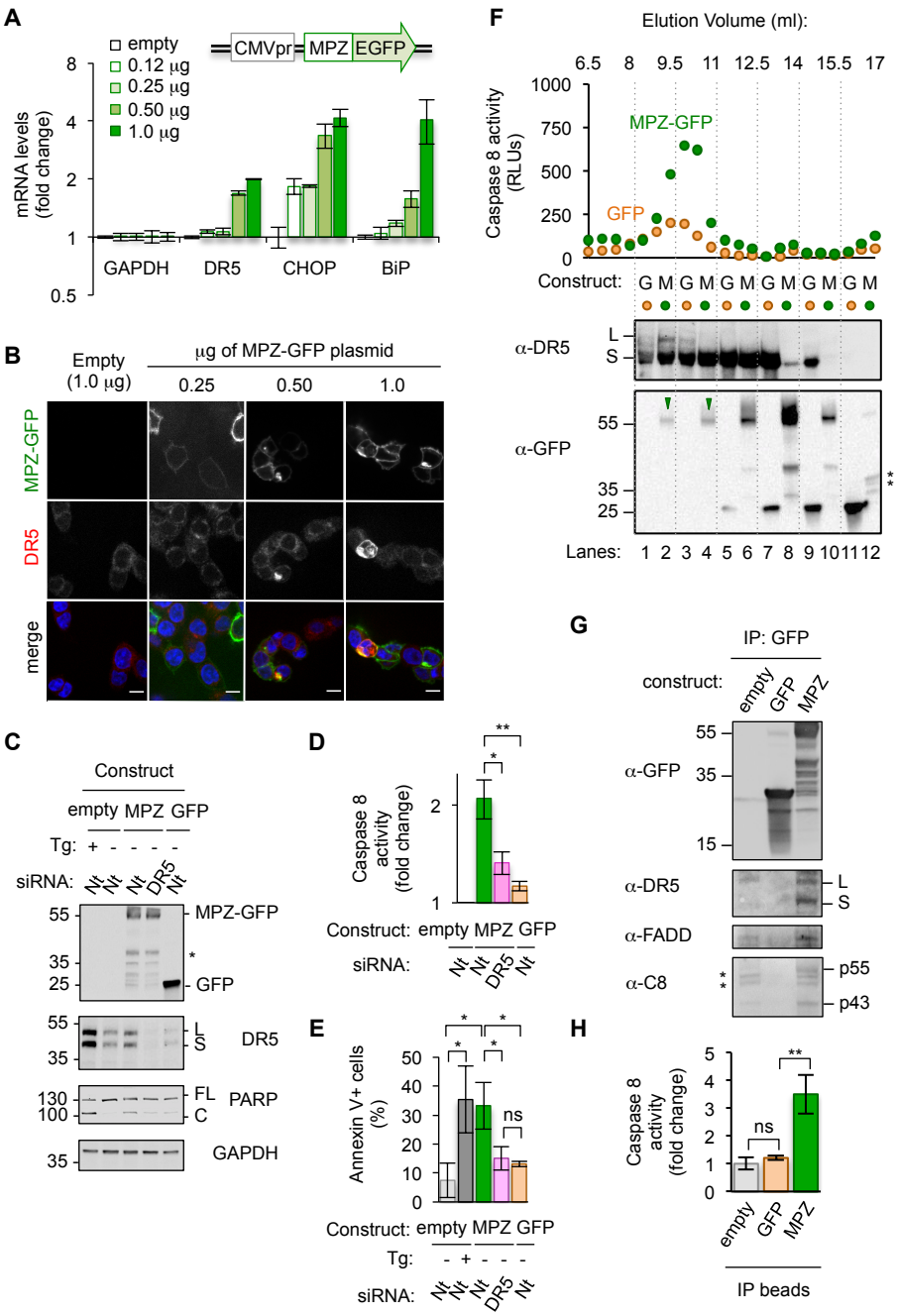

Figure 3.1 Misfolded proteins act as ligands to assemble DR5 oligomers and initiate caspase signaling during ER stress.

A) qPCR for reverse-transcribed transcripts harvested from HCT116 cells transfected with 0.12-1.0 μg of a plasmid containing myelin protein zero (MPZ) tagged with a C-terminal monomeric EGFP or 1.0 μg of the empty vector for 24 h.

B) Confocal images of HCT116 fixed 24 h post-transfection showing MPZ-GFP fluorescence (green) and immunofluorescence with an antibody against DR5 (red) (scale bar = 5 μm).
C) Western blot of HCT116 cells transfected with siRNA against a non-targeting (Nt) control or DR5 (48 h) followed by the empty vector -/+ 100 nM thapsigargin (Tg), 1.0 μg MPZ-GFP, or cytosolic GFP (24 h; * denotes degradation products; L and S denote the long and short isoforms of DR5, respectively; FL and C denote full-length and cleaved PARP, respectively).
D) Fold change in caspase 8 activity, as measured by a luminescent caspase 8 substrate, of lysates from HCT116 as transfected in C) relative to cells transfected with the empty vector control (error bars = SD for n = 3, * indicates $p < 0.05$, ** indicates $p < 0.005$).
E) Average percent of Annexin V staining for HCT116 cells transfected as described in C) from three biological replicates (error bars = SEM, * indicates $p < 0.05$, ns = non-significant). See Fig 3.2H for gating.
F) Top: Caspase 8 activity in size exclusion chromatography fractions from lysates of HCT116 cells transfected with 1.0 μg MPZ-GFP or cytosolic GFP (24 h). Bottom: Size exclusion fractions were pooled according to dotted grid lines and immunoblotted for DR5 and GFP (* denotes degradation products).
G) Immunoprecipitation of GFP-tagged proteins from lysates of HCT116 transfected as in F) with MPZ-GFP, cytosolic GFP, or the empty vector (L and S denote the long and short isoforms of DR5, respectively).
H) Fold change in caspase 8 activity relative to the empty vector control for beads with immunoprecipitated contents shown in Fig 3.1G (error bars = SD for n = 3, ** indicates $p < 0.005$, ns = non-significant).

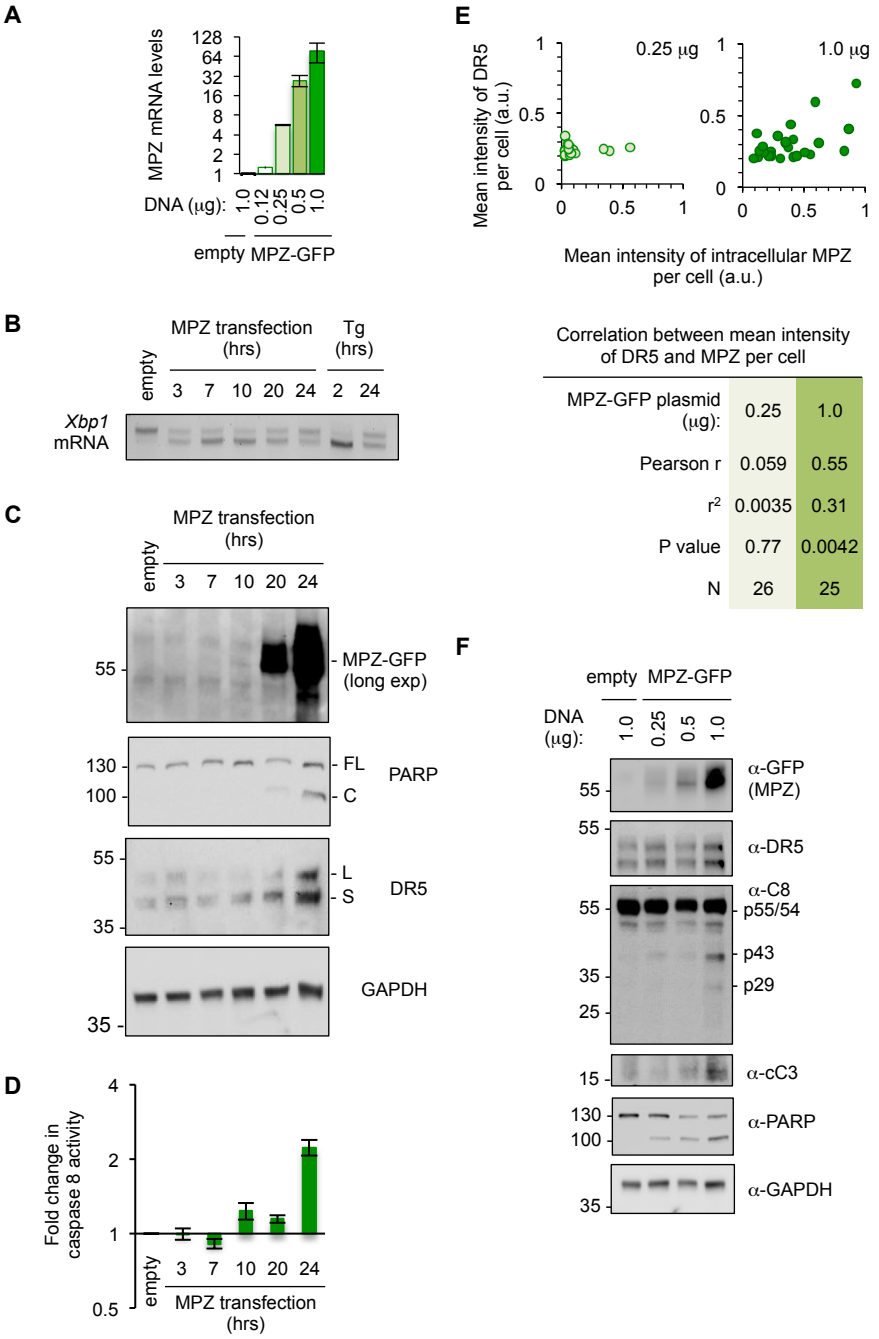

Figure 3.2 Titration and time course of GFP-tagged MPZ expression to induce pro-apoptotic UPR signaling.

A) qPCR for MPZ mRNA levels in reverse-transcribed transcripts harvested from HCT116 cells transfected with a titration of MPZ-GFP plasmid or 1.0 μg of the empty vector for 24 h.

B) RT-PCR for unspliced and spliced forms of *Xbp1* mRNA isolated from HCT116 cells transfected for 24 h with the empty vector or for various time points with 1 μg MPZ-GFP, followed by cells treated with 100 nM Tg for 2 h and 24 h.
C) Western blot of HCT116 cell lysates harvested 24 h post-transfection with the empty vector, or 3-24 h post-transfection with 1 μg MPZ-GFP.
D) Fold change in caspase 8 activity, as measured by a luminescent caspase 8 substrate, of lysates from HCT116 harvested 3-24 h post-transfection with 1 μg MPZ-GFP relative to cells transfected with the empty vector control (error bars represent SD of n = 3).
E) Quantification of the mean intensity for DR5 versus the mean intensity of intracellular MPZ-GFP per cell for HCT116 transfected with 0.25 μg (left) and 1.0 μg (right) of MPZ-GFP plasmid to show the correlation between DR5 and MPZ-GFP expression levels per cell. Intensity values given by CellProfiler algorithms were normalized to 0.02 for DR5 and 0.06 for MPZ-GFP to assign arbitrary values. P values were calculated from unpaired two-tailed t-tests.
F) Western blot of HCT116 cell lysates harvested 24 h post-transfection with a titration of MPZ-GFP plasmid or the empty vector (C8 = caspase 8, cC3 = cleaved caspase 3).

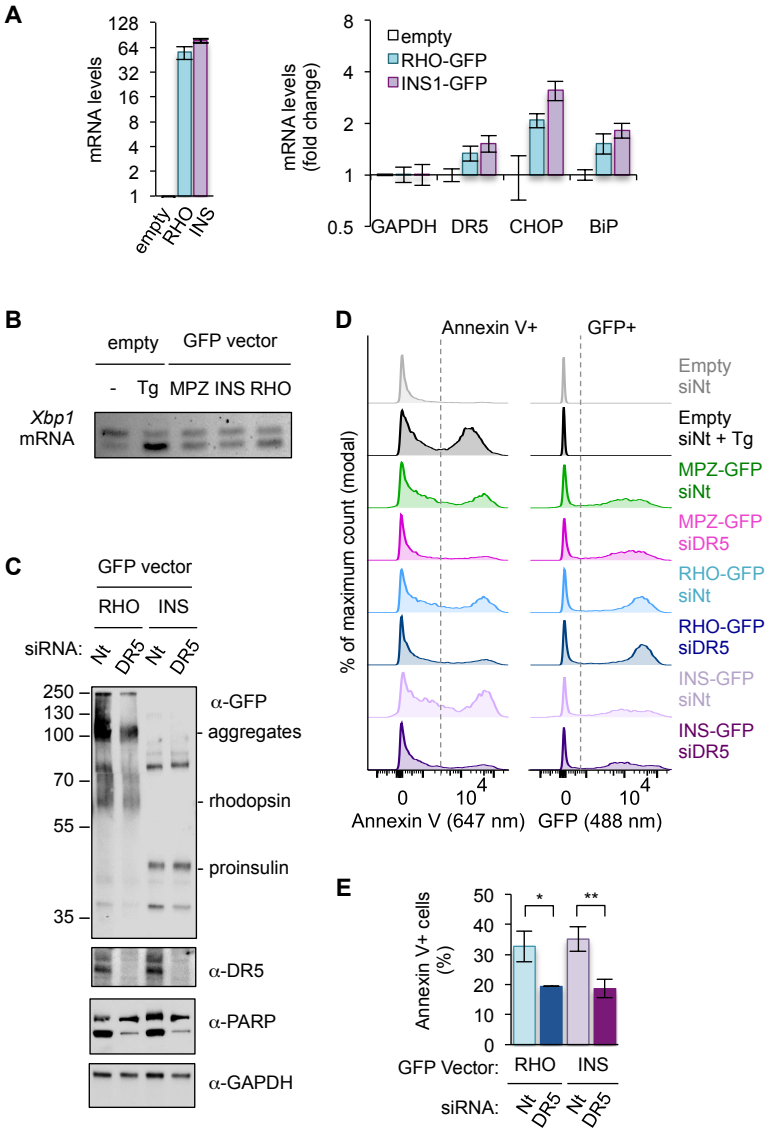

Figure 3.3 Sustained overexpression of other ER-trafficked proteins induce UPR-mediated apoptosis in a DR5-dependent manner.

A) qPCR for reverse-transcribed transcripts harvested from HCT116 cells transfected with 1.0 μg of GFP-tagged rhodopsin (RHO), proinsulin (INS), or 1.0 μg of the empty vector for 24 h.
B) RT-PCR for unspliced and spliced forms of *Xbp1* mRNA isolated from HCT116 cells transfected for 24 h with 1 μg of empty vector -/+ 100 nM Tg for 2 h, MPZ-GFP, INS-GFP, or RHO-GFP.
C) Western blot of HCT116 cells transfected with siRNA against a non-targeting (Nt) control or DR5 (48 h) followed by 1.0 μg RHO-GFP or INS-GFP (24 h).
D) Representative flow cytometry histograms of HCT116 cells transfected with the listed siRNA and vector and stained with Annexin V-AlexaFluor647. Y-axis has been scaled so that the mode = 100%. Left: Histograms of fluorescence at 647 nm to measure Annexin

V staining. Right: Histograms of fluorescence at 488 nm to compare level and distribution of GFP-tagged protein expression. To note, GFP expression profiles for the same construct are similar between different siRNA transfected samples.

E) Average percent of Annexin V-positive cells for HCT116 cells transfected with siRNA and GFP-tagged rhodopsin/proinsulin (n=3, error bars = SD, * indicates $p < 0.02$, ** indicates $p \leq 0.005$). Gating for Annexin V-positive staining is shown in S1H.

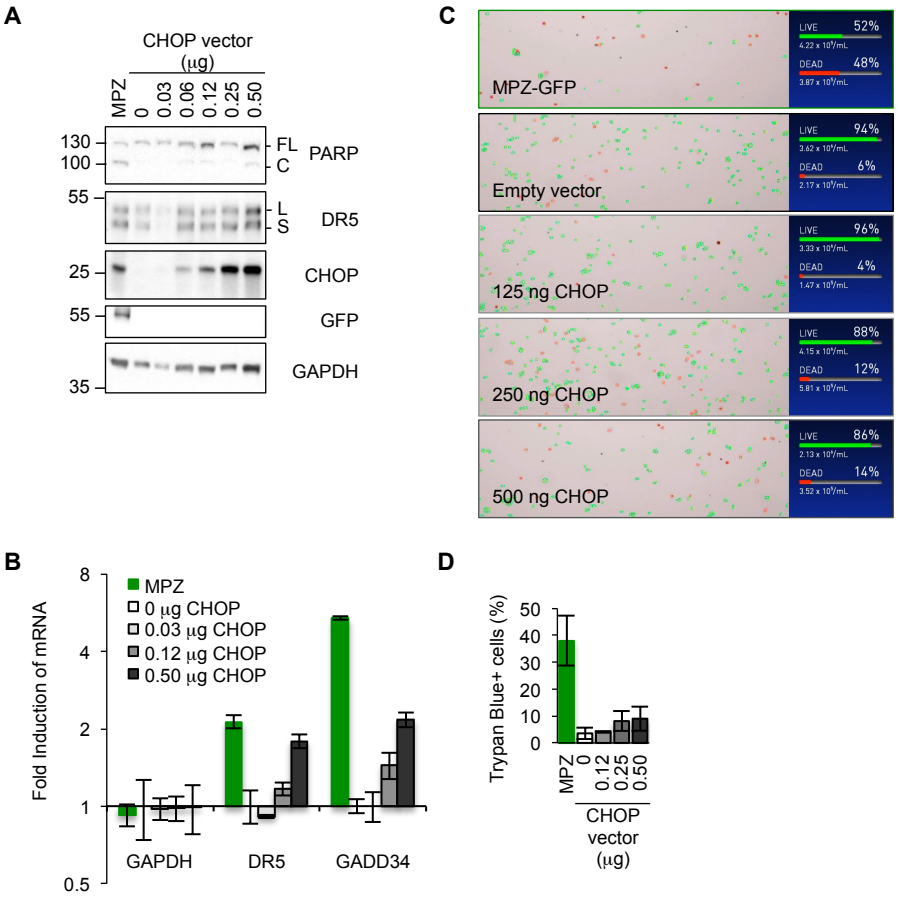

Figure 3.4 Upregulating DR5 levels in the absence of ER stress through ectopic expression of CHOP is not sufficient to induce apoptosis.

A) Western blot of HCT116 cell lysates harvested 24 h post-transfection with a titration of 0.03-0.50 μg of a CHOP expression vector, 1 μg MPZ-GFP plasmid, or the empty vector (FL = full-length, C = cleaved).
B) qPCR for reverse-transcribed transcripts harvested from HCT116 cells transfected with 0.03-0.50 μg of a CHOP expression vector, 1.0 μg of MPZ-GFP, or 1.0 μg of the empty vector for 24 h.
C) Representative images of automated counting for Trypan blue-stained cells, where green outlines denote non-stained (live) cells and red outlines denote stained cells (Trypan blue+, dead).
D) Average percentage of cells transfected as described in (3.4A) stained with Trypan blue as quantified by automated cell counting from n = 3 biological replicates (error bars = SD).

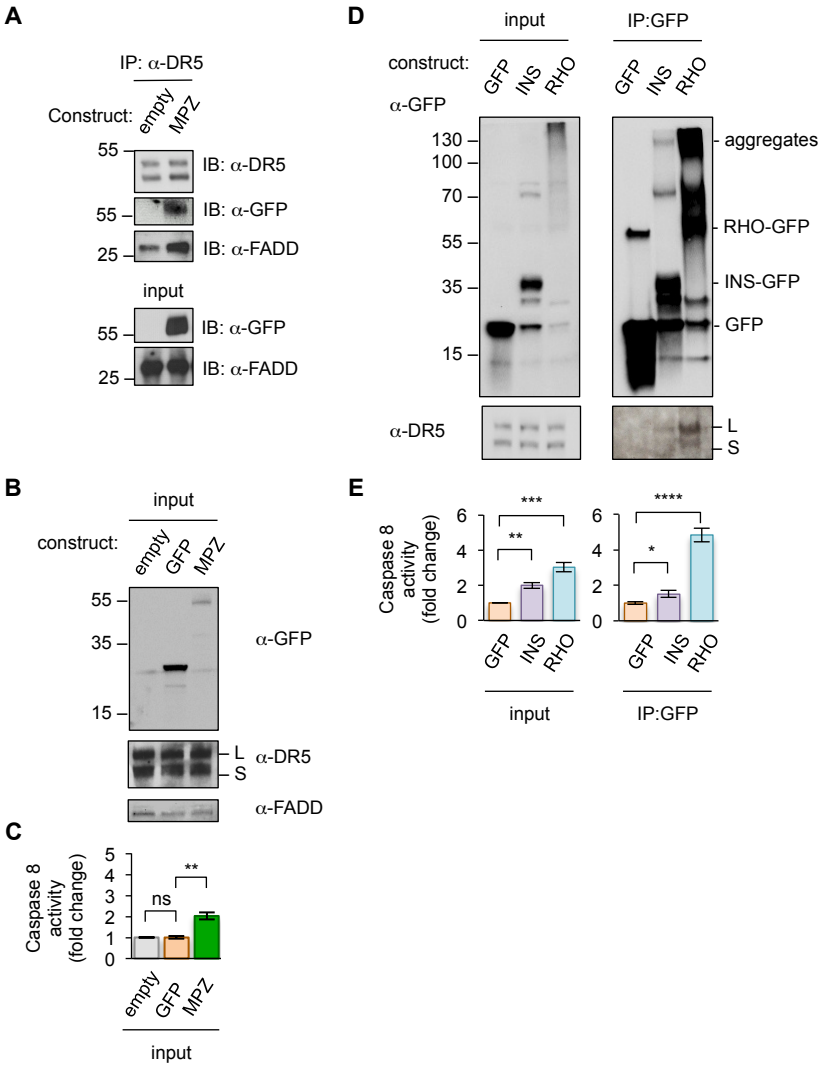

Figure 3.5 A subset of misfolded ER-trafficked protein acts as substrate for DR5 assembly and caspase activation.

A) Immunoprecipitation of DR5 from HCT116 transfected with MPZ-GFP or the empty vector and blotted for DR5, MPZ-GFP, and FADD.
B) Inputs for GFP pulldown performed in Fig. 1G.
C) Caspase 8 activity of inputs relative to the empty vector control for the GFP pulldown performed in Fig 3.1H (n = 3, error bars = SD, ** indicates $p \leq 0.005$, ns = non-significant).
D) Pulldown of GFP-tagged proteins from HCT116 transfected with INS, RHO, or cytosolic GFP. Inputs (left) and immunoprecipitated samples (right) were immunoblotted for GFP and DR5 (L and S indicate long and short isoforms, respectively).
E) Fold change in caspase 8 activity relative to cytosolic GFP for beads with immunoprecipitated contents described in Fig 3.2M as measured by caspase glo 8 luminescence (n = 3, error bars = SD, * indicates $p < 0.03$, ** indicates $p \leq 0.005$, *** indicates $p < 0.0005$, **** indicates $p < 0.0001$).

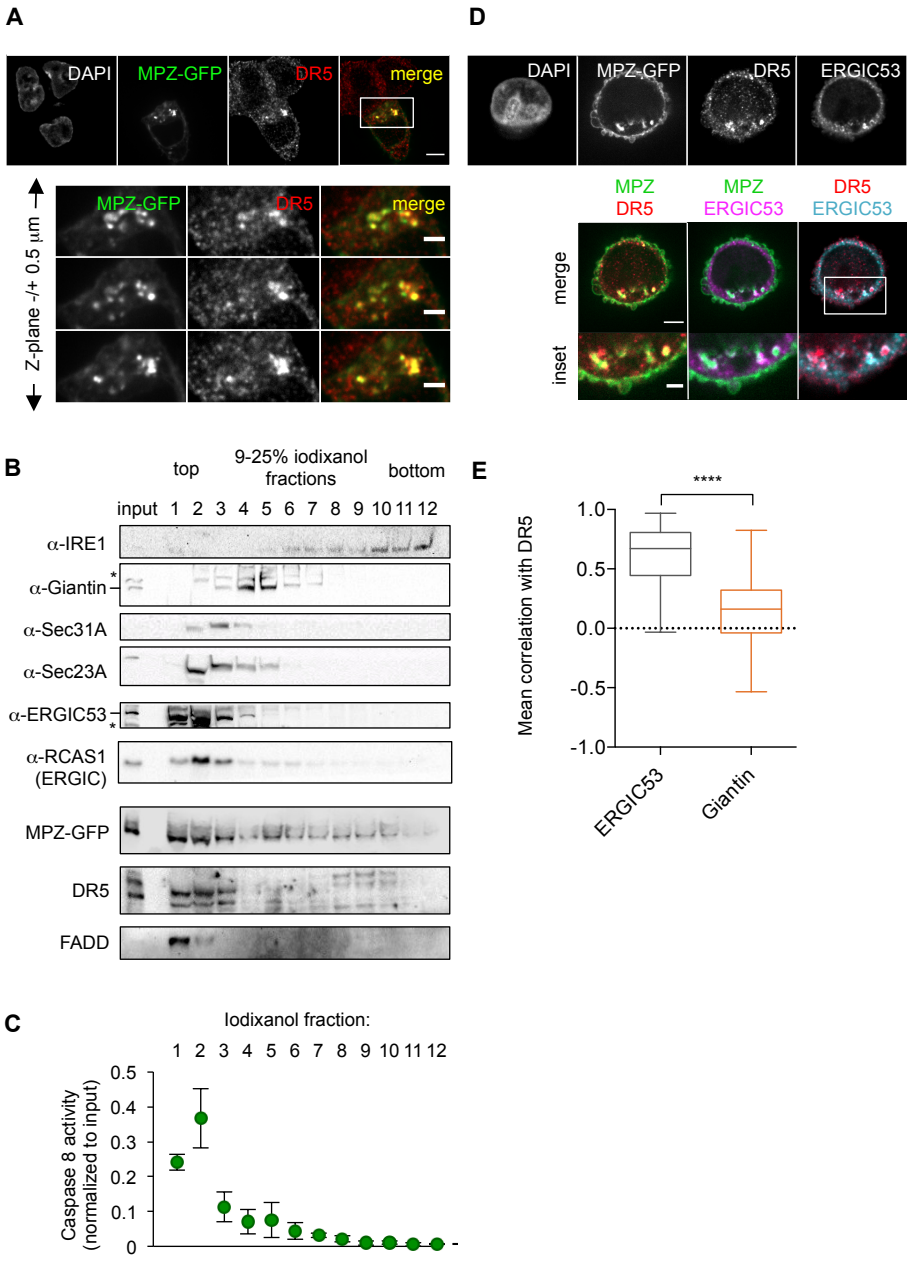

Figure 3.6 Misfolded protein engages DR5 at the ER-Golgi intermediate compartment, inducing active DR5 signaling clusters.

A) Top: Immunofluorescence of HCT116 cells transfected with MPZ-GFP (green) for 24 h and stained with anti-DR5 (red, scale bar 5 μm). Bottom: Enlargements of the inset stepping through the z-plane in 0.5 μm increments (scale bar 2 μm).
B) Subcellular fractionation of lysate expressing MPZ-GFP, where IRE1 marks the ER, Giantin marks the Golgi, Sec31A and Sec23A mark COPII vesicles, and ERGIC53 and RCAS1 correspond to ER-Golgi intermediate compartment. Bands of the expected size

are indicated by "–" and bands that may represent a modified or degraded protein are indicated by *.

C) Average caspase activity of each fraction from subcellular gradient centrifugation in (B) normalized to total lysate (input) measured by caspase 8 substrate luminescence (N = 3, error bars = SD).

D) Top: Immunostaining of DR5 and ERGIC53 in fixed HCT116 cells transfected with MPZ-GFP as in (A). Bottom: Merged images with ERGIC53 in magenta or cyan to depict overlapping signal as white (scale bar = 5 μm, insets scale bar = 2 μm).

E) Box-whisker plots quantifying the Pearson's correlation per cell between DR5 and ERGIC53 (mean = 0.61 ± 0.03) or Giantin (mean = 0.14 ± 0.02) within MPZ-positive cells (N > 55), where whiskers correspond to minimum and maximum values of the data (**** indicates $p < 0.0001$).

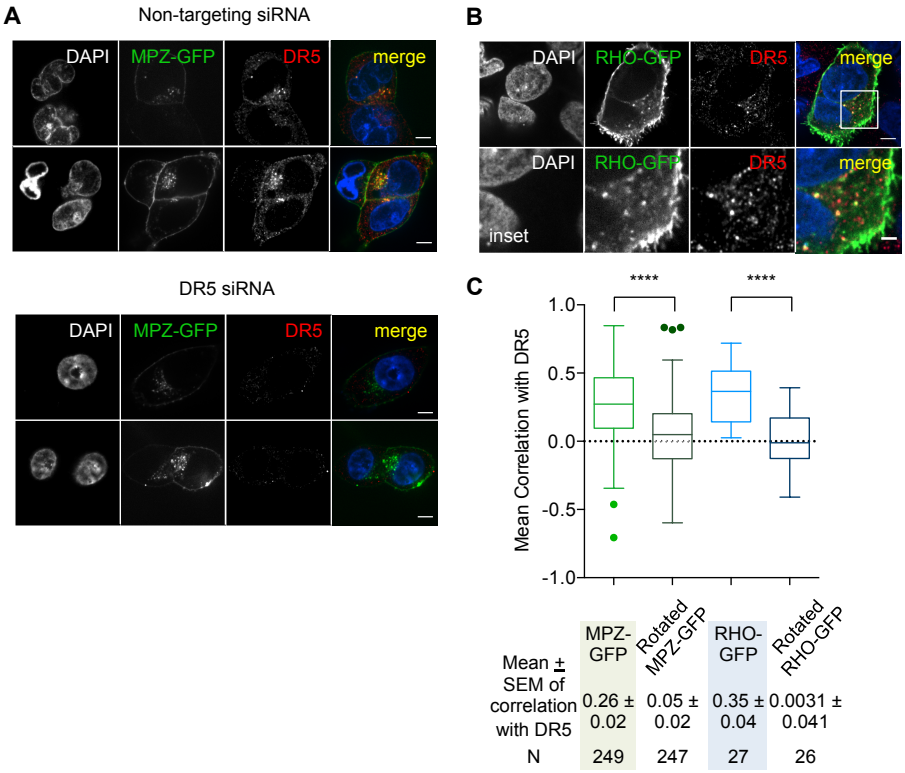

Figure 3.7 Intracellular puncta of overexpressed MPZ and rhodopsin proteins co-localize significantly with DR5 clusters.

A) Immunofluorescence of fixed HCT116 cells transfected with siRNA (top: non-targeting, bottom: siDR5) for 48 h and MPZ-GFP (green in merge) for 24 h and subsequently immunostained for anti-DR5 (red in merge). Two representative confocal images are shown for each siRNA treatment, where the scale bar corresponds to 5 μm.
B) Immunofluorescence of fixed HCT116 cells expressing RHO-GFP stained for DR5 and GFP (scale bar = 5 μm, inset scale bar = 2 μm).
C) Quantification of Pearson's correlation per cell between DR5 signal and ER-trafficked protein (MPZ and RHO) from original image files versus artificially rotated image files, for which the GFP channel was rotated 90° with respect to the other channel. Whisker-box plots depict the Tukey method. Statistics were performed through unpaired two-tailed t-tests, where **** indicates $p < 0.0001$ and the variance was non-significant.

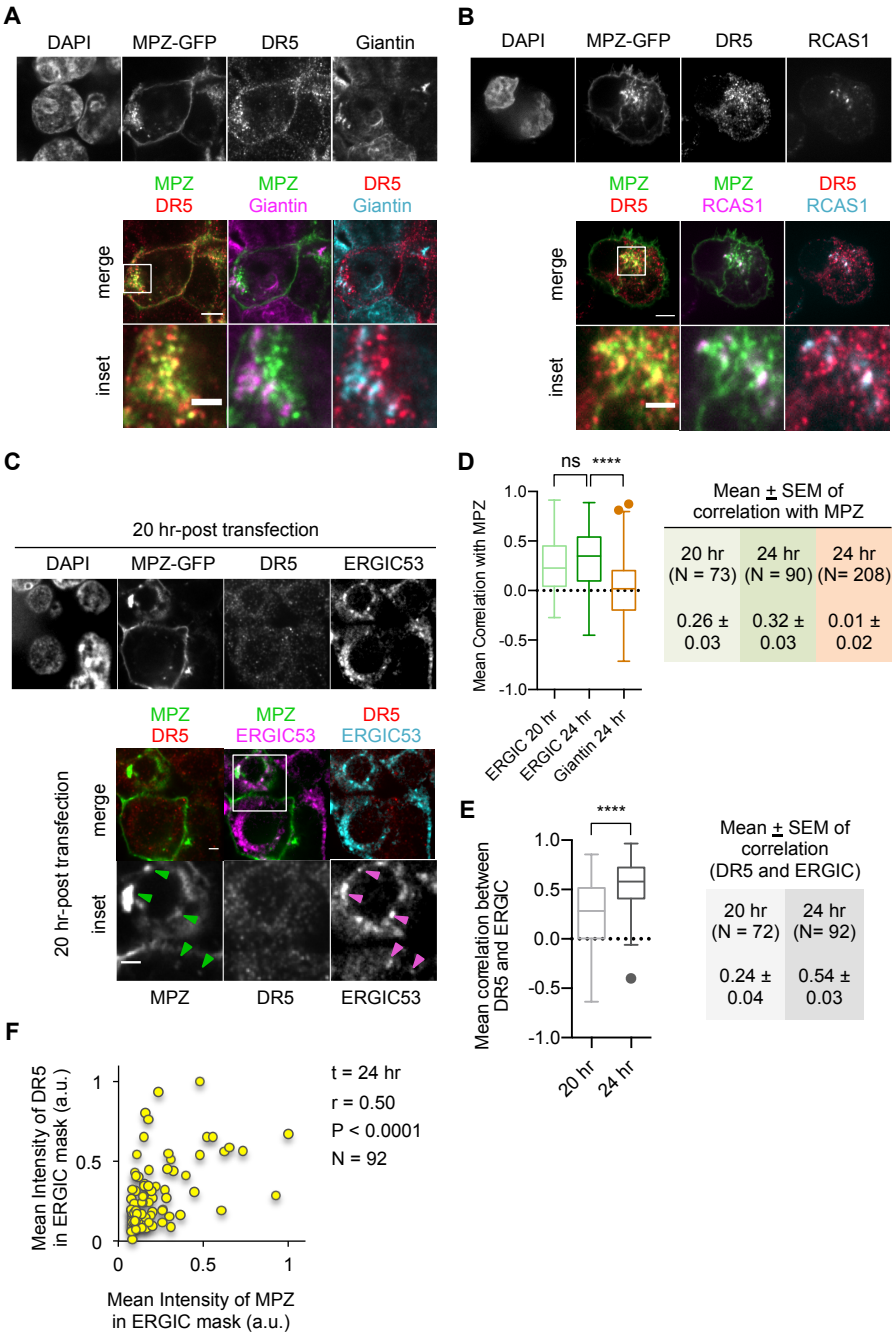

Figure 3.8 Overlapping puncta of DR5 and misfolded protein accumulate in the ERGIC, and not in the Golgi apparatus.

A) Immunostaining of DR5 and Giantin in fixed HCT116 cells expressing MPZ-GFP. Giantin is magenta in the overlay with MPZ (green) or cyan in the overlay with DR5 (red). Bottom row enlarges the inset marked in the merges images to show little overlapping signal with Giantin (scale bar = 5 μm, inset scale bar = 1 μm).

B) Immunofluorescence for DR5 and RCAS1 in fixed HCT116 cells expressing MPZ-GFP. RCAS1 is magenta in the overlay with MPZ (green) or cyan in the overlay with DR5

(red), where white puncta signify co-localized signal (scale bar = 5 μm, inset scale bar = 1 μm).

C) Immunofluorescence for DR5 and ERGIC53 in HCT116 fixed 20 hr post-transfection. ERGIC53 is magenta in the overlay with MPZ (green) or cyan in the overlay with DR5 (red) (scale bar = 5 μm). Arrows in inset images depict regions where MPZ and ERGIC53 signal overlap (scale bar = 2 μm).

D) Quantification of Pearson's correlation per cell between ERGIC and MPZ, or Giantin and MPZ of fixed HCT116 cells at the specified time after MPZ-GFP transfection. Whisker-box plots depict the Tukey method. Statistics were performed through unpaired two-tailed t-tests, where **** indicates $p < 0.0001$ and ns means not significant, and the variance was non-significant.

E) Quantification of Pearson's correlation per cell between DR5 signal and ERGIC53 of fixed HCT116 cells at 20 h and 24 h post-transfection with MPZ-GFP. Whisker-box plots depict the Tukey method. Statistics were performed through unpaired two-tailed t-tests, where **** indicates $p < 0.0001$ and the variance was non-significant.

F) Quantification of the mean intensity for DR5 within a mask of the ERGIC versus the mean intensity of MPZ-GFP within a mask of the ERGIC per cell for HCT116 transfected with 1.0 μg of MPZ-GFP for 24 h. Intensity values extracted by CellProfiler algorithms were normalized to by the maximum in each data set to assign normalized arbitrary units (a.u.). The Pearson correlation coefficient was calculated to be 0.50, and unpaired two-tailed t-tests yielded $p < 0.0001$.

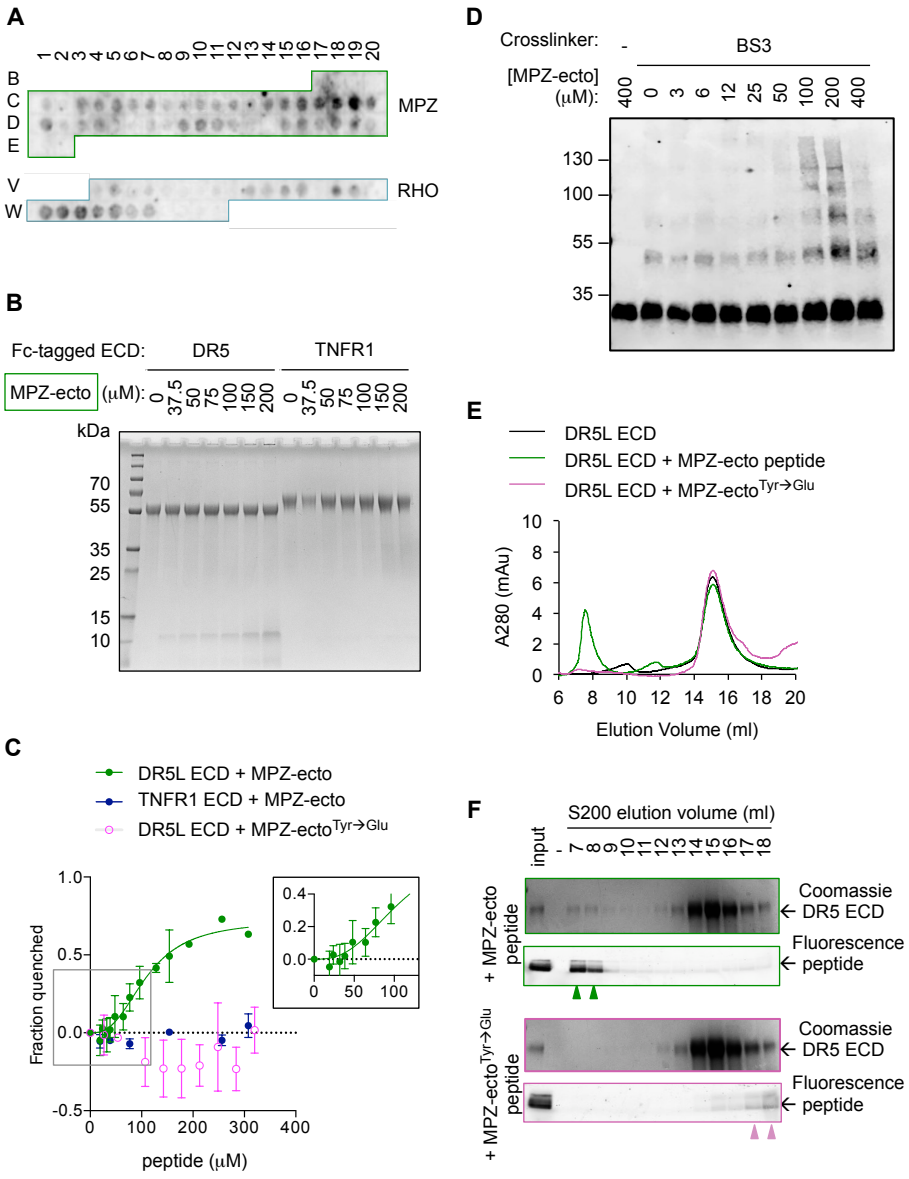

Figure 3.9 Direct binding of the DR5 ECD to exposed protein sequences of the mammalian secretome induces ECD oligomerization.

A) A peptide array tiled with sequences from the ectodomain of myelin protein zero (MPZ) and extracellular loops from rhodopsin (RHO) was incubated with Fc-tagged DR5 ectodomain domain (long isoform, 500 nM). Signal was obtained by probing with anti-Fc.

B) Coomassie stained SDS-PAGE gel of pulldown on Fc-tagged DR5L ECD (55 kDa) or TNFR1 ECD (65 kDa) incubated with increasing concentrations of the MPZ-ecto^{VD} peptide (apparent MW of 10 kDa, see Table 3.7 for sequence).

C) Fluorescence quenching of AlexaFluor647-DR5L or TNFR1 ECD was measured with increasing MPZ-ecto peptide to quantify the binding affinity, whereas quenching was not observed with the mutated MPZ-ecto$^{Tyr→Glu}$ peptide (N=3, error bars are SD). DR5L ECD binds to the MPZ ecto peptide with a $K_{1/2}$ of 109 ± 11 μM with a hill coefficient of 2.6 ± 0.5.

D) SDS-PAGE of recombinant FLAG-tagged DR5L ECD (25 kDa, 10 μM) incubated with MPZ-ecto peptide at the noted concentrations and treated with the amine crosslinker BS3 (100 μM), probed with anti-FLAG.
E) Size exclusion chromatographs of absorbance at 280 nm for 25 μM recombinant DR5L ECD alone (black), pre-incubated with 100 μM fluorescein-conjugated MPZ-ecto peptide (green) or 100 μM fluorescein-conjugated MPZ-ecto$^{Tyr \rightarrow Glu}$ peptide (magenta).
F) SDS-PAGE gels scanned for fluorescence and then stained with Coomassie for eluted size exclusion fractions in (E). Green outlines (top pair) correspond to fractions from DR5L pre-incubated with MPZ-ecto peptide, and magenta outlines (bottom pair) correspond to DR5L with MPZ-ecto$^{Tyr \rightarrow Glu}$ peptide. Lane marked by "-" denotes a blank lane between the input and 7-ml fraction to minimize spillover of signal from input sample. Arrowheads mark detectable peptide fluorescence in the indicated fractions.

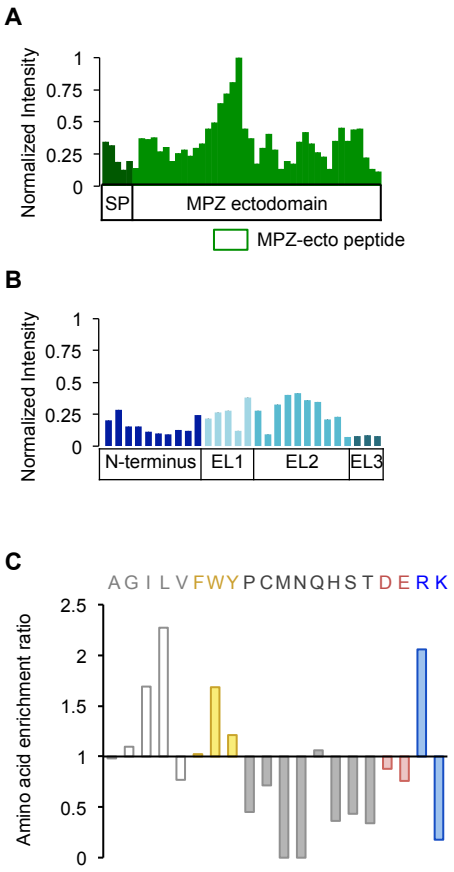

Figure 3.10 DR5 directly binds to peptide sequences of proteins in the secretory proteome.

A) Intensity values of each peptide spot in the MPZ section of the peptide array in (A) were normalized to the spot of highest intensity within MPZ. Green box below denotes the peptide chosen as a candidate binder, called MPZ-ecto, present in spots C18-C19 on the array.
B) Intensity values of the RHO peptide array section in Fig 3.9A normalized to the highest intensity from MPZ. Peptides were derived from the extracellular N-terminus tail and the extracellular loops (EL1-EL3) that connect the transmembrane domains of rhodopsin.
C) Quantification of enriched amino acids from peptides with an intensity value greater than one standard deviation above the average signal, noted as a preferred peptide, within the entire array. Enrichment ratio for each amino acid was calculated as the frequency of occurrence in preferred peptides divided by its total frequency on the array.

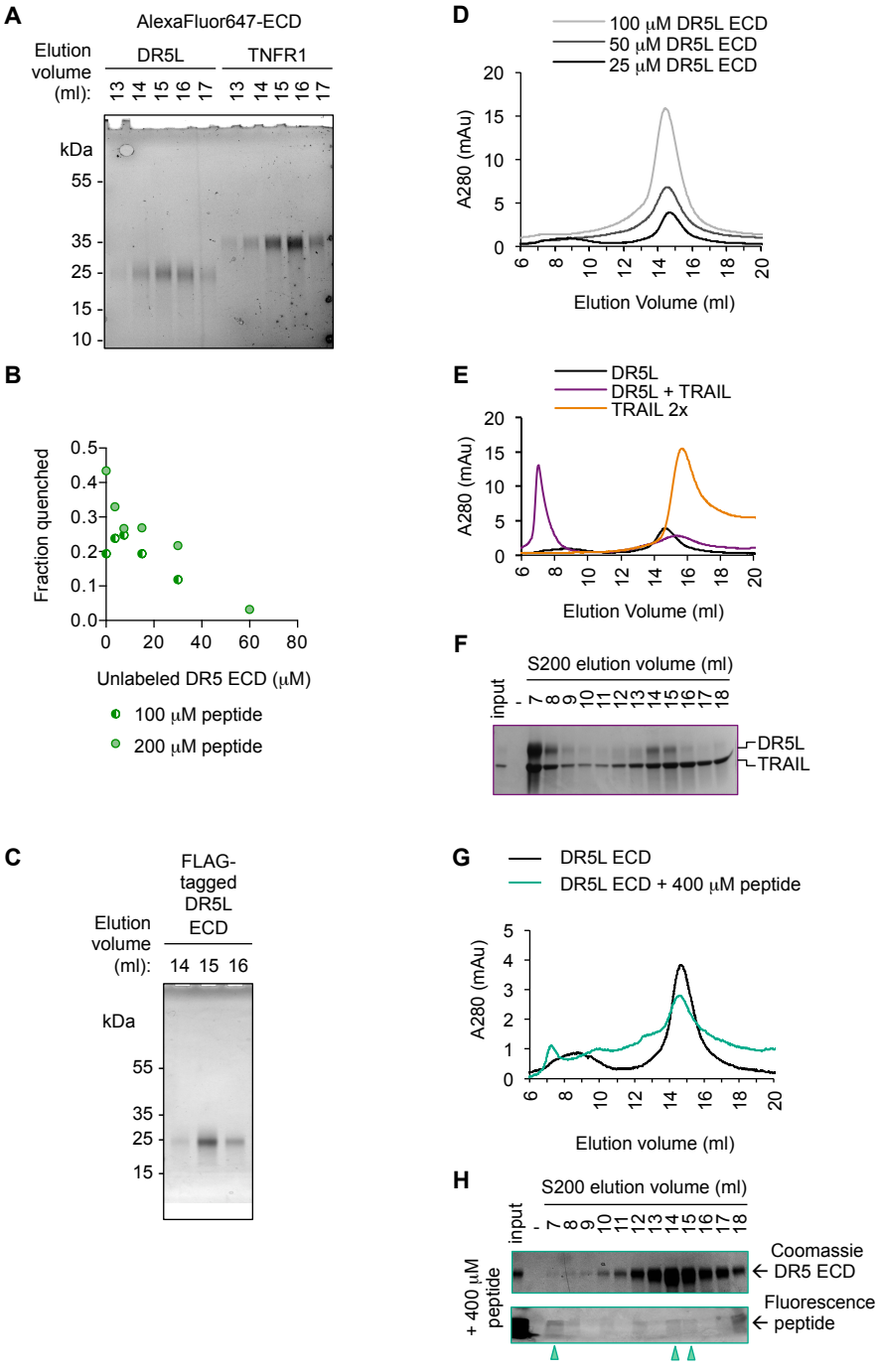

Figure 3.11 Purified recombinant DR5 ECD oligomerizes with peptide in a specific and reversible manner.

A) Fluorescence scan at 647 nm of SDS-PAGE for gel filtration-purified DR5L (25 kDa) or TNFR1 ECD (35 kDa) labeled with NHS-ester AlexaFluor647. These proteins were used in the fluorescence quenching assays shown in Fig 3.9C.

B) Fluorescence de-quenching of AlexaFluor647-DR5L ECD (200 nM) pre-incubated with 100 μM or 200 μM of MPZ-ecto peptide in the presence of increasing concentrations of unlabeled DR5L ECD.

C) Coomassie-stained SDS-PAGE of gel filtration purified FLAG-tagged DR5L ECD proteins used for the crosslinking assay in Fig 3.9D and size exclusion chromatography in Fig 3.9E.
D) Size exclusion chromatographs of absorbance at 280 nm for recombinant DR5L ECD to show that increased concentration of DR5L alone does not yield multimers.
E) Size exclusion chromatographs of absorbance at 280 nm for recombinant DR5L ECD alone (25 μM, black) or incubated with TRAIL (25 uM, purple). Trace for TRAIL alone (50 μM) is shown in light orange.
F) SDS-PAGE gels stained with Coomassie blue for eluted size exclusion fractions in Fig 3.11E depicting bands for DR5L ECD and TRAIL.
G) Size exclusion chromatographs of absorbance at 280 nm for 25 μM recombinant DR5L ECD alone (black), pre-incubated with 400 μM fluorescein-conjugated MPZ-ecto peptide (teal).
H) SDS-PAGE gels scanned for fluorescence and then stained with Coomassie for eluted size exclusion fractions in Fig 3.11G. Lane marked by "-" denotes a blank lane between the input and 7-ml fraction to minimize spillover of signal from input sample. Arrowheads mark detectable peptide fluorescence in the indicated fractions.

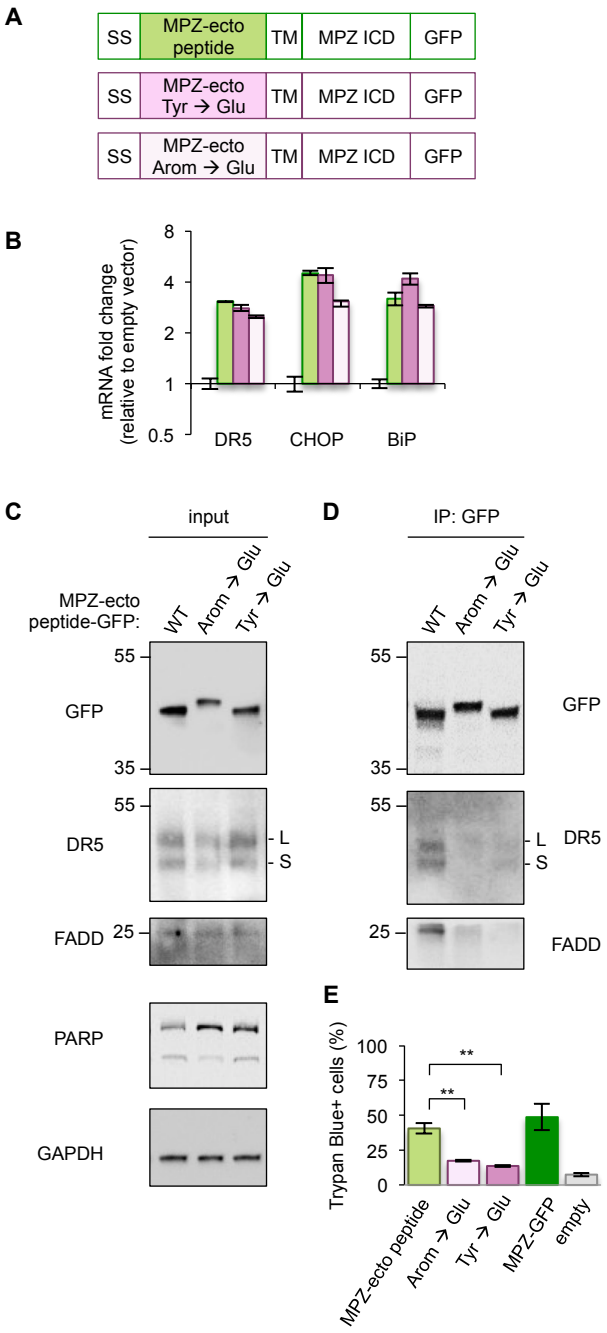

Figure 3.12 Disrupting the binding of DR5 to misfolded protein sequences attenuates ER stress-mediated apoptosis.

A) Diagram of constructs generated to replace the MPZ ectodomain with the minimal DR5-binding MPZ-ecto peptide (green), the peptide harboring Tyr → Glu mutations (magenta), or the peptide with all aromatic residues (Arom) mutated to Glu (light pink). SS = signal sequence of MPZ, TM = transmembrane domain, ICD = intracellular domain.
B) qPCR for reverse-transcribed transcripts harvested from HCT116 cells transfected with the constructs described in (A).
C) Immunoblots of HCT116 lysates expressing the constructs described in (A).

D) Immunoprecipitation of GFP-tagged proteins from the lysates shown in (C), where L and S denote the long and short isoforms of DR5, respectively.
E) Average percent of Trypan blue staining for HCT116 cells transfected with the MPZ-ecto peptide variants described in (A), full-length MPZ-GFP, or the empty vector (error bars = SEM from three biological replicates, ** indicates $p < 0.005$).

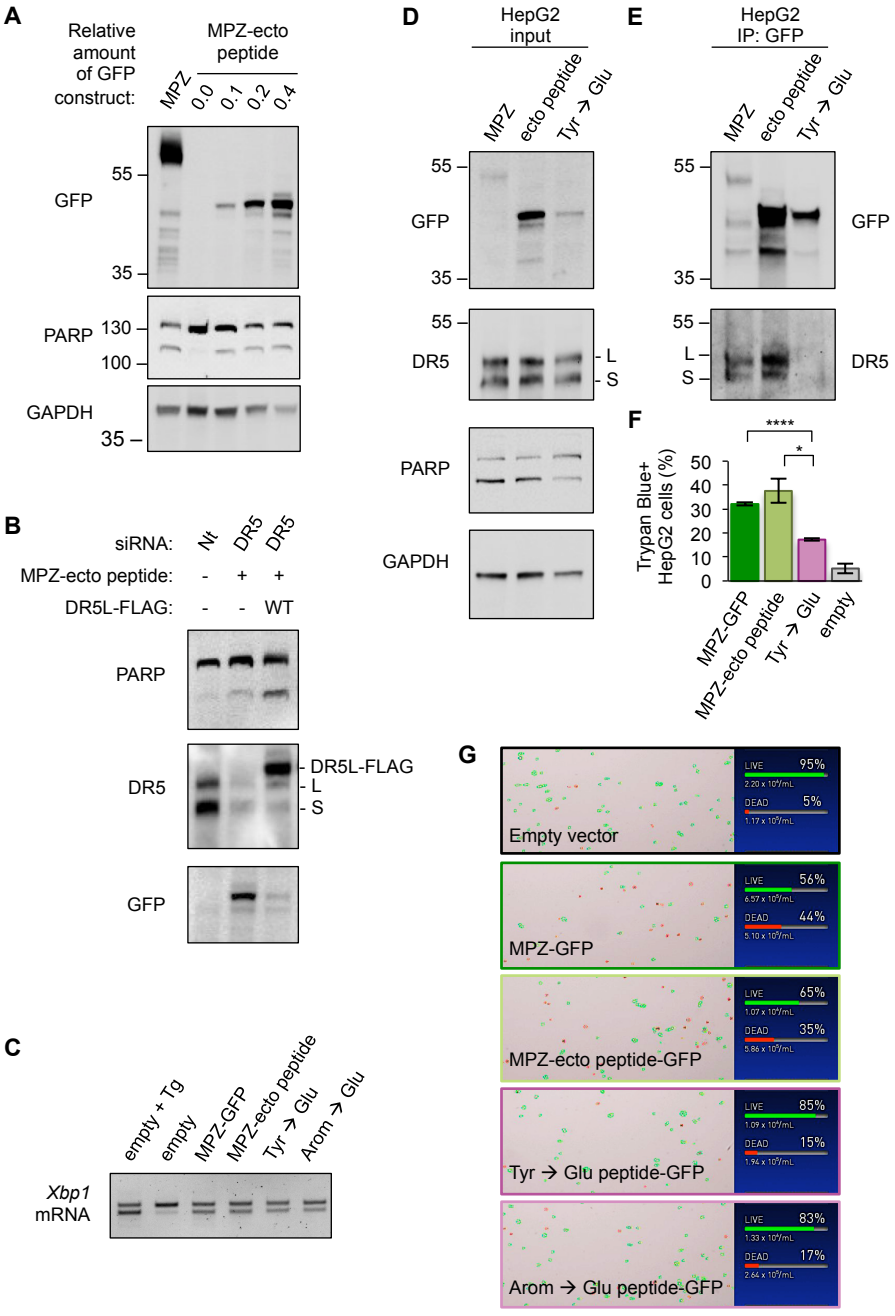

Figure 3.13 Introducing Glu mutations to the DR5-binding sequence of MPZ disrupts engagement of DR5 and apoptotic signaling.

A) Western blot of HCT116 cell lysates harvested 24 h post-transfection with 1 μg of MPZ-GFP plasmid or a titration of MPZ-ecto peptide-GFP plasmid.
B) Western blot of HCT116 cell lysates transfected with siRNA against a non-targeting (Nt) sequence or DR5 (referred to as DR5-siRNA-2 in Materials and Methods) for 48 h and co-expressing FLAG-tagged DR5 long isoform and/or MPZ-ecto peptide-GFP.

C) RT-PCR for unspliced and spliced forms of *Xbp1* mRNA isolated from HCT116 cells transfected for 24 h with the empty vector +/- 100 nM Tg, or with MPZ-GFP, or MPZ-ecto peptide GFP and its mutant variants (Tyr → Glu and Arom → Glu).
D) Immunoblots of HepG2 lysates harvested 24 h-post transfection with MPZ-GFP, MPZ-ecto peptide-GFP, or MPZ-ecto peptide-GFP with Tyr → Glu mutations.
E) Immunoprecipitation of GFP-tagged proteins from the lysates shown in (3.13D), where L and S denote the long and short isoforms of DR5, respectively.
F) Average percent of Trypan blue staining for HepG2 cells transfected with full-length MPZ-GFP, MPZ-ecto peptide and its Tyr → Glu mutant, or the empty vector (error bars = SEM from N = 3, * indicates $p < 0.05$, **** indicates $p < 0.0001$)
G) Representative images of automated counting for averages of Trypan blue-stained HCT116 cells reported in 3.12E, where green outlines denote non-stained (live) cells and red outlines denote stained cells (Trypan blue+, dead).

Appendix A

Studies toward molecular dynamics of IRE1 lumenal domain oligomerization

Introduction

Detecting and regulating the protein folding capacity of the ER lumen is critical for processing secretory and transmembrane proteins. The unfolded protein response (UPR) is activated when unfolded proteins accumulate in the ER lumen. Upon sensing the folding burden, the lumenal domain of Ire1, an ER-resident transmembrane protein, oligomerizes and activates its cytoplasmic kinase and endoribonuclease (RNase) domains. How Ire1 adjusts its activity to respond to ER stress remains unclear. Previous studies have shown that IRE1 in *S. cerevisiae* directly interacts with BiP, an ER-resident chaperone, under steady state conditions and with unfolded protein under stress, allowing IRE1 to gauge the protein folding capacity in the ER lumen (Pincus *et al.*, 2010). But how Ire1 transitions between its inactive and active state in the presence of BiP and unfolded protein is not well understood.

In both activating and deactivating UPR signaling, IRE1 oligomerization appears to be a key mechanism for communicating stress across the ER membrane. IRE1 clusters into foci under ER stress, which reversibly dissolve after resolution of stress (Li *et al.*, 2010; Pincus *et al.*, 2010). Mutations that prevent foci formation also compromise UPR activation (Kimata *et al.*, 2007; Aragón *et al.*, 2009). In addition, past studies showed that the amount of FRET between GFP and mCherry-tagged IRE1 varies with DTT concentration and that the extent of IRE1 oligomerization is tuned to the degree of stress, suggesting that ER stress adjusts UPR signaling by affecting the oligomerization status of IRE1.

Because IRE1 oligomerization is necessary for downstream signaling, modulating the oligomerization of the lumenal domain is a key regulatory step. Unfolded protein is thought to stabilize the active, oligomeric state of IRE1, since certain peptides can drive the oligomerization of purified IRE1 lumenal domain (IRE1-LD) in solution (Gardner and Walter, 2011). On the other hand, BiP, an ER-resident Hsp70 chaperone, binds to IRE1 under non-stress conditions and reversibly dissociates from Ire1 as ER stress is induced (Okamura *et al.*, 2000). Removing the BiP-binding interface on the lumenal domain of IRE1 sensitizes IRE1 to

lower ER stress levels and delays IRE1 deactivation upon resolution of stress (Kimata *et al.*, 2004; Pincus *et al.*, 2010). These results suggest BiP negatively regulates IRE1 activity through preventing oligomerization, whereas unfolded protein activates IRE1 by driving clustering. To directly probe the modulation of IRE1 oligomerization by these two factors, we reconstituted purified IRE1-LD onto supported lipid bilayers and determined how the behavior of the particles changed upon addition of unfolded protein substrate and/or BiP.

Materials and Methods

The *S. cerevisiae* IRE1-LD constructs contain the core lumenal domain (amino acids 111-461), the BiP binding domain (amino acids 462-491), and a C-terminal 10xHis tag. All Cys, except one on an unstructured loop region, have been mutated to Ser to allow for site-specific maleimide labeling with fluorescent dyes. The Cys mutations do not affect yeast growth under tunicamcyin or peptide binding by anisotropy (data not shown). These proteins were expressed from a pET16B vector in *E. coli* BL21-DE3* induced with 300 μm IPTG at OD600 ~0.7 with overnight incubation at 18^{o}C. Cells were lysed in 50 mM HEPES pH 7.2, 150 mM NaCl, 4 mM DTT, 10% glycerol through two passages on the Avestin Emulsiflex-C3 at 15,000 psi. The cell lysates were then centrifuged for 0.5 hr at 30,000xg, and the supernatant samples were loaded onto a HisTrapFF column for purification via the His tag. The 10xHis tag exhibited stronger binding the Ni-NTA beads than a standard 6xHis tag and was washed with buffer containing 20 mM imidazole pH 7.4, and eluted with a 0-100% gradient of 20 mM to 1 M imidazole over 7 CV. The proteins were further purified by size exclusion chromatography (SuperDex200 GL 10/300) and then conjugated to various fluorescent dyes via maleimide chemistry. These proteins were then re-loaded onto the SuperDex200 10/300 GL to remove unconjugated dyes. The yield of the WT IRE1-LD protein was much lower than for the interface mutant W426A.

Supported lipid bilayers (SLBs) were formed in a 96-well glass bottom microscope plate (Matriwell plates) from small unilamellar vesicles (SUVs) containing a mix of 98%

phosphatidylcholine, 1% Ni-NTA DOGS, and fluorescent dye-conjugated lipids where indicated from Avanti Lipids Inc. His-tagged proteins (100 ul of 2 nM) were incubated in wells with SLBs for 0.5 hr at RT in the dark and then washed (without drying the well) with 10x 500 μl of PBS. The nickel ion of lipid head groups on Ni-NTA DOGS chelates the 10xHis tag to tether proteins onto the lipid bilayer surface for imaging with TIRF microscopy (Fig 4.1).

For the unfolded protein substrates, Cy3-labeled C_H1 protein was a generous gift from G. Elif Karagoz (Karagöz *et al.*, 2017). For clarified lysate, 15 OD600's of *S. cerevisiae* were harvested and resuspended in 250 ul of 50 HEPES pH 7.2, 150 mM KOAc and lysed through bead beating. The lysate was then centrifuged at 20,000xg for 10 min at 4^{o}C and diluted in 1xPBS.

Preliminary Results

To limit the anticipated heterogeneity of oligomeric states for WT IRE1-LD, we initially characterized the interface mutant of IRE1-LD (W426A), for which the oligomeric state is limited to dimerization in the presence of peptide (Credle *et al.*, 2005; Gardner and Walter, 2011). Single particle tracking via TIRF microscopy with a 50 ns frame rate was used to assess the fluorescent intensity and diffusion coefficients of individual molecules. At an approximate surface density of 0.12 molecules/μm^2, the interface mutant of IRE1-LD exhibited a normal distribution of fluorescent intensities (measured at t = 0) with an average intensity value of 26.7 $\pm$ 7.1 (Fig 4.2A, 4.2D). Single particle trajectories revealed a range of diffusional behavior with traces arising from pure diffusion (Fig 4.2B) and traces corresponding to anomalous diffusion (Fig 4.2C). The average *D* of more than 400 trajectories was 0.4 $\pm$ 0.2 μm^2/s, which in agreement with the general estimate of 1 μm^2/s for lateral diffusion of membrane proteins (Yu and Groves, 2010), indicating that the supported lipid bilayers were uniform and of sufficient quality. Additionally, the average α value, which is the exponential component of mean square

displacement (MSD) over time, was 1.0 $\pm$ 0.3, indicating a linear relationship between MSD and time that is reflective of pure diffusion (Fig 4.2F).

To analyze IRE1-LD behavior at physiologically relevant concentrations, we aimed to match the surface density of IRE1-LD on SLBs to that found for IRE1 on the ER membrane. Mass spectrometry analyses of the yeast proteome estimates that an average yeast cell expresses 250 molecules of IRE1 (Ghaemmaghami *et al.*, 2003). For a yeast cell with a diameter of 5 μm, quantitative fluorescent imaging of ER membranes in yeast estimates a surface area of 100 μm^2 at steady state that expands up to 300 μm^2 under ER stress conditions (Schuck *et al.*, 2009). Therefore, the approximate surface density of IRE1 in yeast cells ranges from 1-2 molecules/μm^2. To calculate the surface density of IRE1-LD molecules on the SLBs, we held the total concentration of IRE1-LD constant and titrated the percent of labeled IRE1-LD from 1-10% (Fig 4.3A). Extrapolating to 100% labeling yielded a surface density of 1.3 molecules molecules/μm^2 when 1 nM of IRE1-LD was incubated on the SLBs (Fig 4.3B), indicating that we could recapitulate the physiological surface density of IRE1 in this *in vitro* system.

At this surface density of IRE1-LD interface mutant, we added increasing concentrations of an unfolded protein substrate C_H1 labeled with Cy3, which was purified and donated by G. Elif Karagoz. At 26 nM of C_H1 protein, no significant shifts were detected in the range of diffusion coefficients or the distribution of intensity values for the IRE1-LD interface mutant (Fig 4.4B-4.4C). At higher concentrations of C_H1 protein, we observed disruption of bilayer integrity that resulted in non-meaningful immobilization of the substrate and IRE1-LD to the surface (Fig 4.4A).

Since we were unable to detect further oligomerization of the IRE1-LD interface mutant, we investigated the WT IRE1-LD, which exhibits a higher propensity to oligomerize in solution (Gardner and Walter, 2011). As a control for membrane fluidity, we co-incubated IRE1-LD with

ubiquitin (Ub), a well-characterized monomer, labeled with a dye in a different channel. Unfortunately, the characterized peptide binder of IRE1-LD (EspP) also non-specifically disrupted lipid bilayer fluidity (data not shown). To reassess what substrates could induce measurable oligomerization of IRE1-LD, we used clarified yeast lysate. Strikingly, the addition of a 1:200 dilution of yeast lysate harvested from 15 OD600's of cells induced cluster formation of WT IRE1-LD after 300 seconds (Fig 4.5). These clusters also contained Cy5-labeled Ub and enriched for fluorescently labeled lipids (DOPE, Fig 4.6). However, the lysate did not induce clustering of the IRE1-LD interface mutant, suggesting that the effect was specific to the oligomerization propensity of WT IRE1 (Fig 4.6). Additionally, clustering of WT IRE1-LD did not occur without co-incubation with Ub-Cy5, suggesting that WT IRE1-LD clustering requires a high surface density of proteins (Fig 4.7). Lysate did not cluster Ub-Cy5 alone, and WT IRE-LD clustering was reversed by the addition of the interface mutant (Fig 4.7).

Future Directions

Further characterization of these clusters is necessary to determine if they can be categorized as phase transitions or microdomains. One goal would be to determine the minimal components to reconstitute IRE1-LD clustering and disassembly on SLBs, as a proxy for the activation and deactivation of IRE1 signaling in cells. Adding fluorescently labeled BiP to monitor its residence time with IRE1-LD with and without the clarified lysate may provide insight to the temporal dynamics of BiP dissociation from IRE1.

Furthermore, this method may be adapted to study the oligomerization dynamics of the other two branches of the mammalian UPR: PERK and ATF6. Both PERK and ATF6 have BiP binding domains, and recent published studies demonstrate that PERK also binds peptides. Studying possible differences in oligomerization dynamics between the three branches may provide a mechanistic basis for the timing of signaling responses.

References

Aragón, T. *et al.* (2009) 'Messenger RNA targeting to endoplasmic reticulum stress signalling sites', *Nature*, 457(7230), pp. 736–740. doi: 10.1038/nature07641.

Credle, J. J. *et al.* (2005) 'On the mechanism of sensing unfolded protein in the endoplasmic reticulum', *Proceedings of the National Academy of Sciences of the United States of America*, 102(52), pp. 18773–18784. doi: 10.1073/pnas.0509487102.

Gardner, B. M. and Walter, P. (2011) 'Unfolded Proteins Are Ire1-Activating Ligands That Directly Induce the Unfolded Protein Response', *Science*, 333(6051), pp. 1891–1894. doi: 10.1126/science.1209126.

Ghaemmaghami, S. *et al.* (2003) 'Global analysis of protein expression in yeast', *Nature*, 425(6959), pp. 737–741. doi: 10.1038/nature02046.

Karagöz, G. E. *et al.* (2017) 'An unfolded protein-induced conformational switch activates mammalian IRE1.', *eLife*. eLife Sciences Publications, Ltd, 6. doi: 10.7554/eLife.30700.

Kimata, Y. *et al.* (2004) 'A role for BiP as an adjustor for the endoplasmic reticulum stress-sensing protein Ire1', *The Journal of Cell Biology*, 167(3), pp. 445–456. doi: 10.1083/jcb.200405153.

Kimata, Y. *et al.* (2007) 'Two regulatory steps of ER-stress sensor Ire1 involving its cluster formation and interaction with unfolded proteins.', *The Journal of cell biology*, 179(1), pp. 75–86. doi: 10.1083/jcb.200704166.

Li, H. *et al.* (2010) 'Mammalian endoplasmic reticulum stress sensor IRE1 signals by dynamic clustering', *Proceedings of the National Academy of Sciences of the United States of America*. National Academy of Sciences, 107(37), pp. 16113–16118. doi: 10.1073/pnas.1010580107.

Okamura, K. *et al.* (2000) 'Dissociation of Kar2p/BiP from an ER sensory molecule, Ire1p, triggers the unfolded protein response in yeast', *Biochemical and Biophysical Research Communications*, 279(2), pp. 445–450. doi: 10.1006/bbrc.2000.3987.

Pincus, D. *et al.* (2010) 'BiP Binding to the ER-Stress Sensor Ire1 Tunes the Homeostatic Behavior of the Unfolded Protein Response', *PLoS Biol*, 8(7), p. e1000415. doi: 10.1371/journal.pbio.1000415.

Schuck, S. *et al.* (2009) 'Membrane expansion alleviates endoplasmic reticulum stress independently of the unfolded protein response.', *The Journal of cell biology*. The Rockefeller University Press, 187(4), pp. 525–36. doi: 10.1083/jcb.200907074.

Yu, C. and Groves, J. T. (2010) 'Engineering supported membranes for cell biology.', *Medical & biological engineering & computing*. Springer, 48(10), pp. 955–63. doi: 10.1007/s11517-010-0634-x.

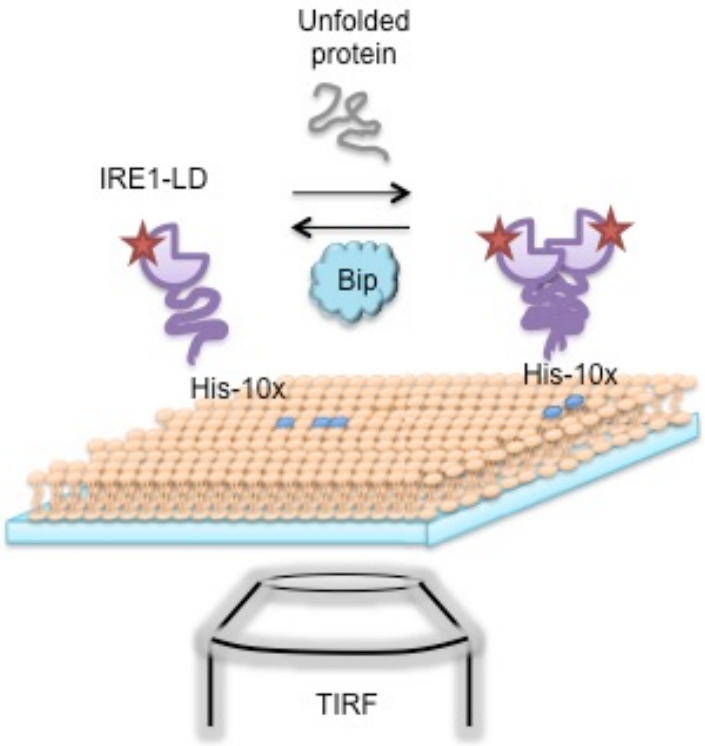

Figure 4.1 Reconstitution of IRE1 lumenal domain (IRE1-LD) onto supported lipid bilayers.

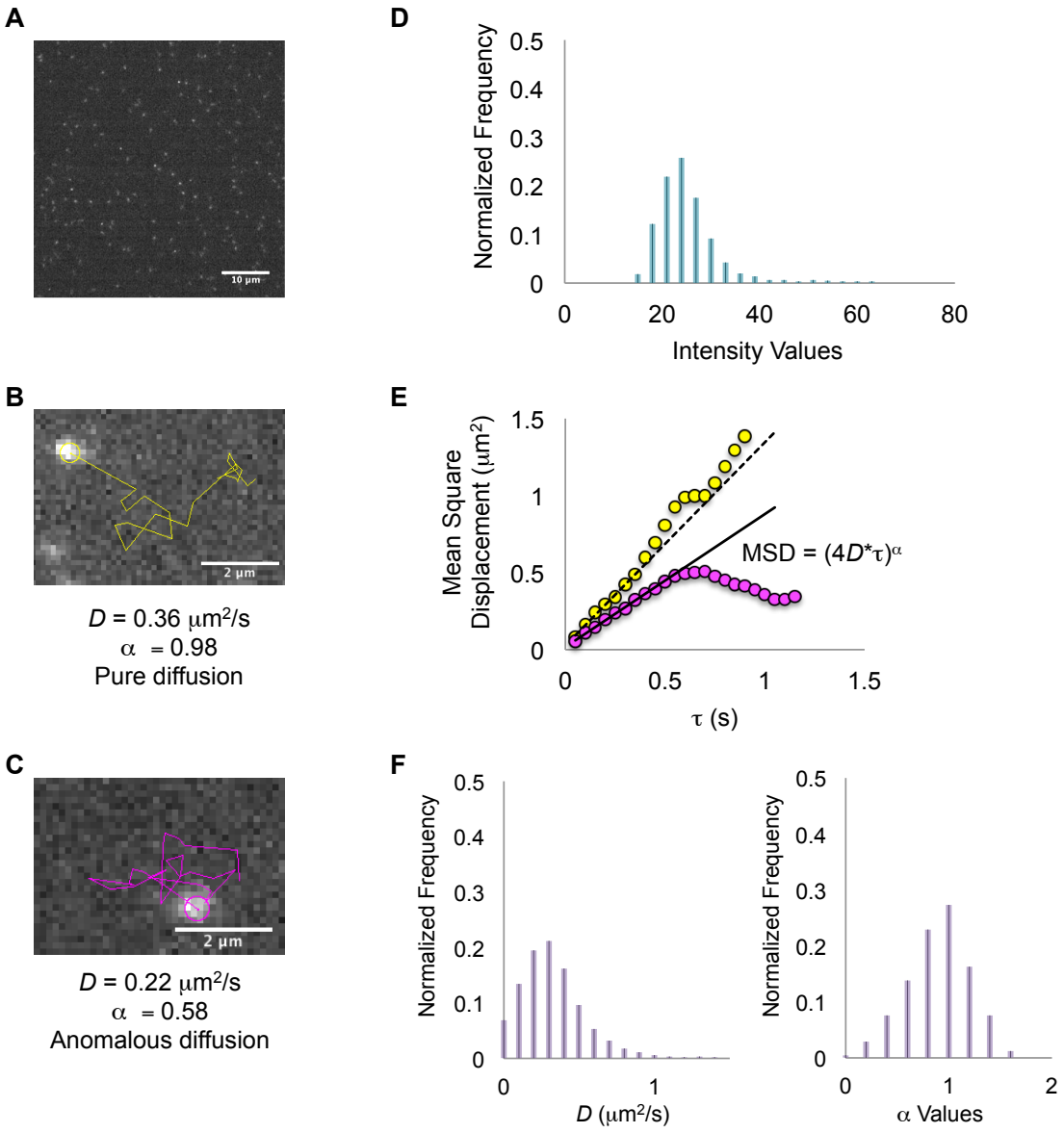

Figure 4.2 Particles of the IRE1-LD interface mutant exhibit a normal distribution of fluorescence intensities and diffusion coefficients.

A) Particles of Cy3-labeled IRE1-LD mutant are visualized by TIRF microscopy over time at a surface density of 0.12 molecules/μm^2.
B) A representative trace from single particle tracking of IRE1-LD that exhibits pure diffusion, where α (a measure of deviation from pure diffusion) is approximately 1
C) An example trace of an IRE1-LD particle that exhibits anomalous diffusion, where $\alpha < 1$
D) A histogram to show the distribution of particle intensities at t = 0 for n = 1936 particles
E) A plot of the mean square displacement (MSD) versus the time lag (t) for the trajectories shown in B) and C) to estimate the diffusion coefficient (*D*) from the slope
F) A histogram of the diffusion coefficients exhibited by 472 trajectories containing 10 frames or more. The average *D* of this sample is 0.4 $\pm$ 0.2 μm^2/s, and the average alpha value is 1.0 $\pm$ 0.3.

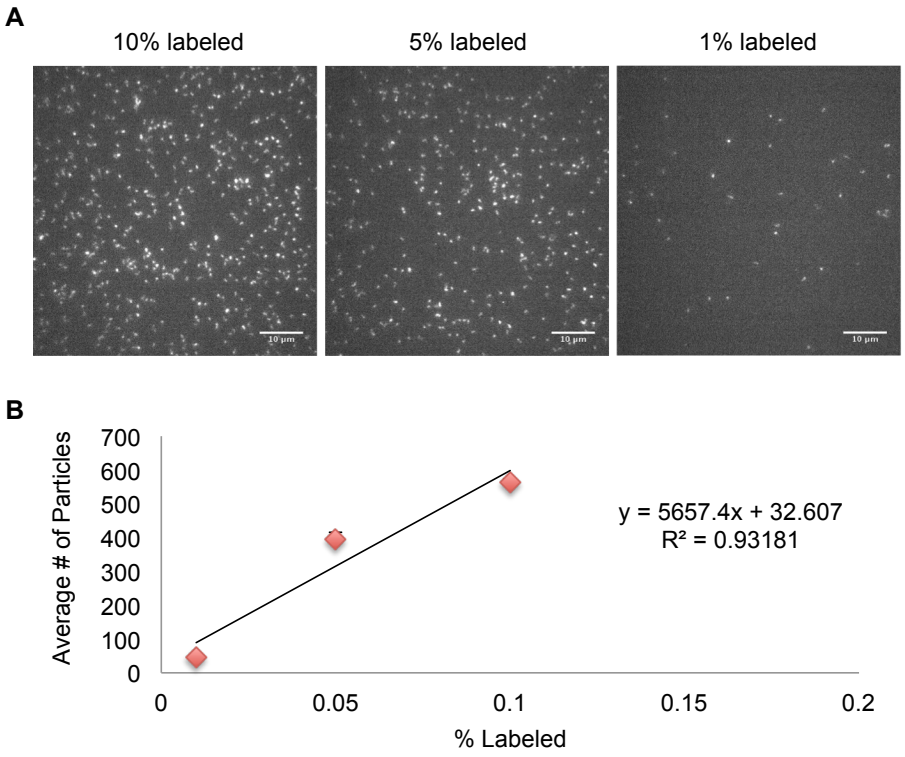

Figure 4.3 Reconstitution of the physiological surface density of IRE1 on supported lipid bilayers.

A) (left to right) The three bilayers were incubated with 1 nM of IRE1-LD consisting of 10%, 5% or 1% labeled protein, respectively (scale bar: 10 μm).
B) The average number of particles detected in the first frame of 3-4 movies was plotted against the percent of labeled protein in the sample to estimate the total number of IRE1-LD particles in each frame (63 μm x 64 μm). The estimated surface density of total IRE1-LD was 1.3 molecules/ μm^2, which is within two-fold of the *in vivo* Ire1 surface density of 2.5 molecules/ μm^2 in *S. cerevisiae* under steady state conditions.

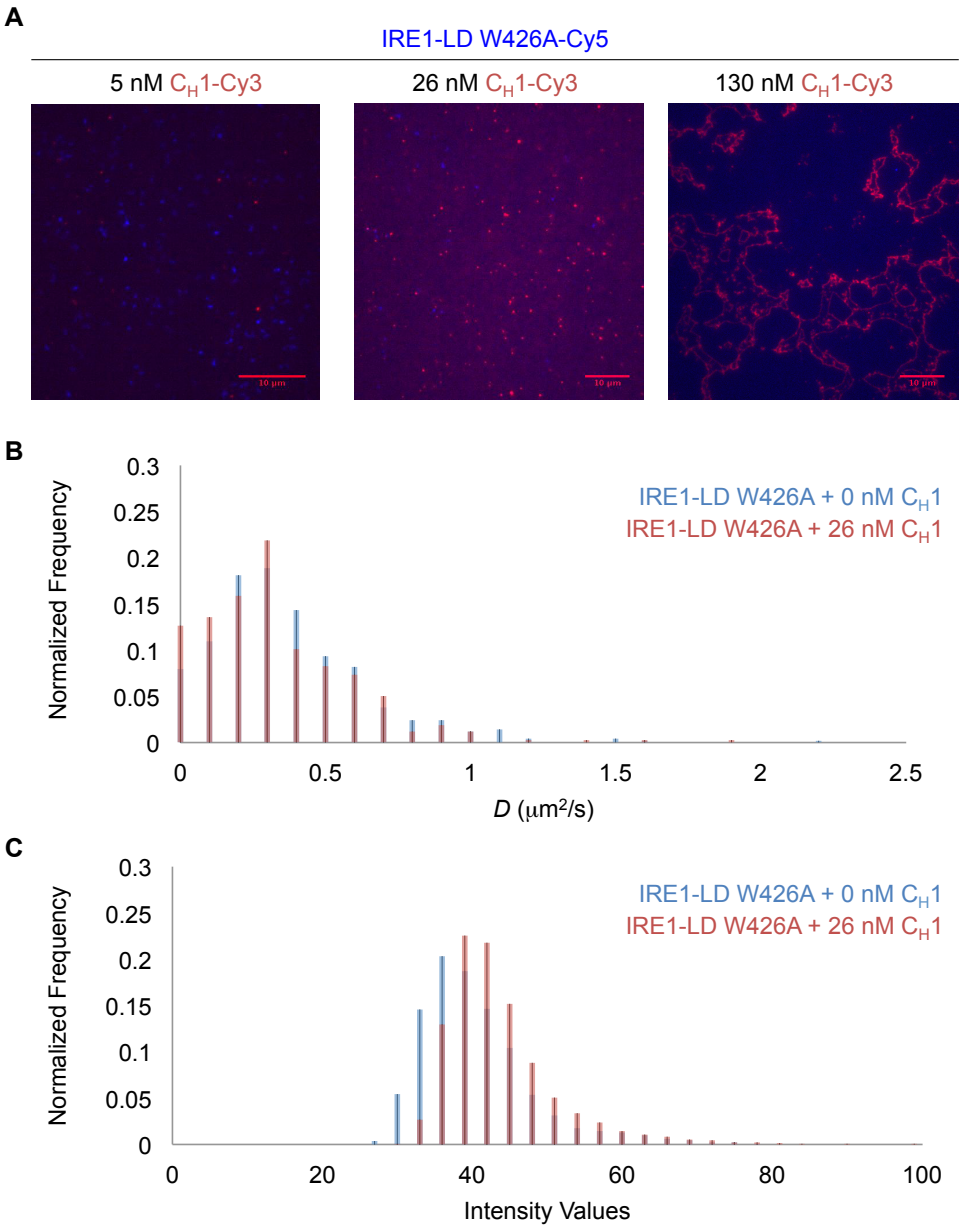

Figure 4.4 Addition of unfolded protein substrate C_H1 disrupted bilayer fluidity and caused non-specific adherence of proteins to the bilayer.

A) Wells with the interface mutant of IRE1-LD were incubated with increasing concentrations of C_H1 protein and imaged by TIRF microscopy
B) A histogram of the diffusion coefficients measured for single particle trajectories of the IRE1-LD interface mutant (n = 430-500)
C) A histrogram of particle intensity values of IRE1-LD interface mutant with and without C_H1 protein (n = 47000-50000)

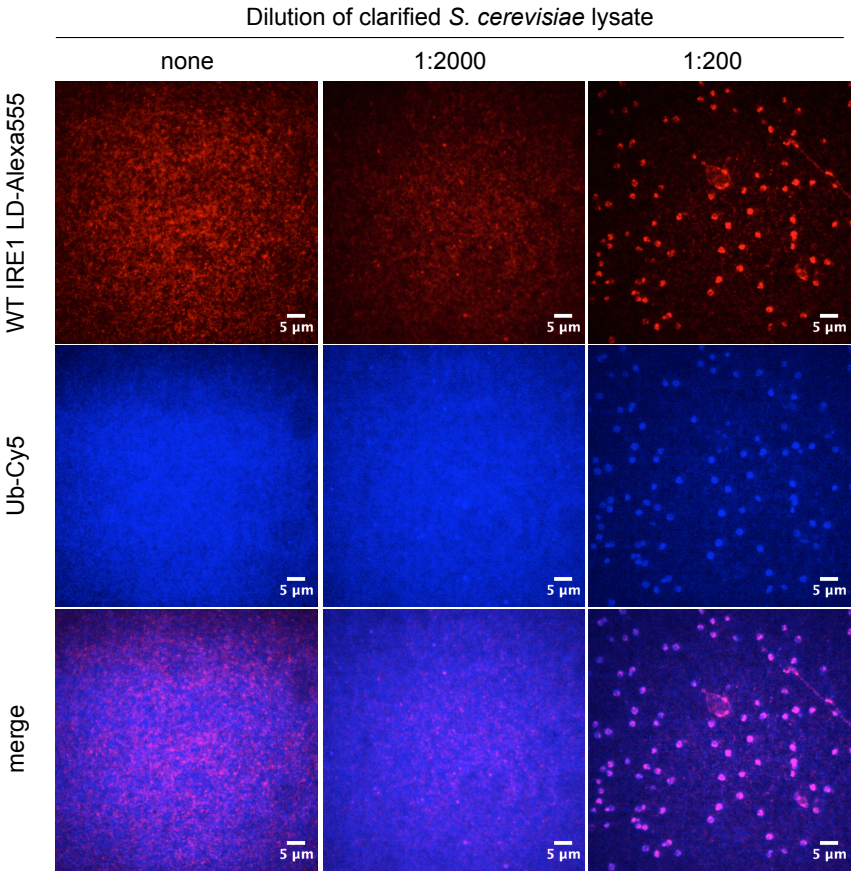

Figure 4.5 Addition of clarified yeast lysate induced clustering of WT IRE1-LD on SLBs that coalesced with Cy5-labeled ubiquitin (Ub)

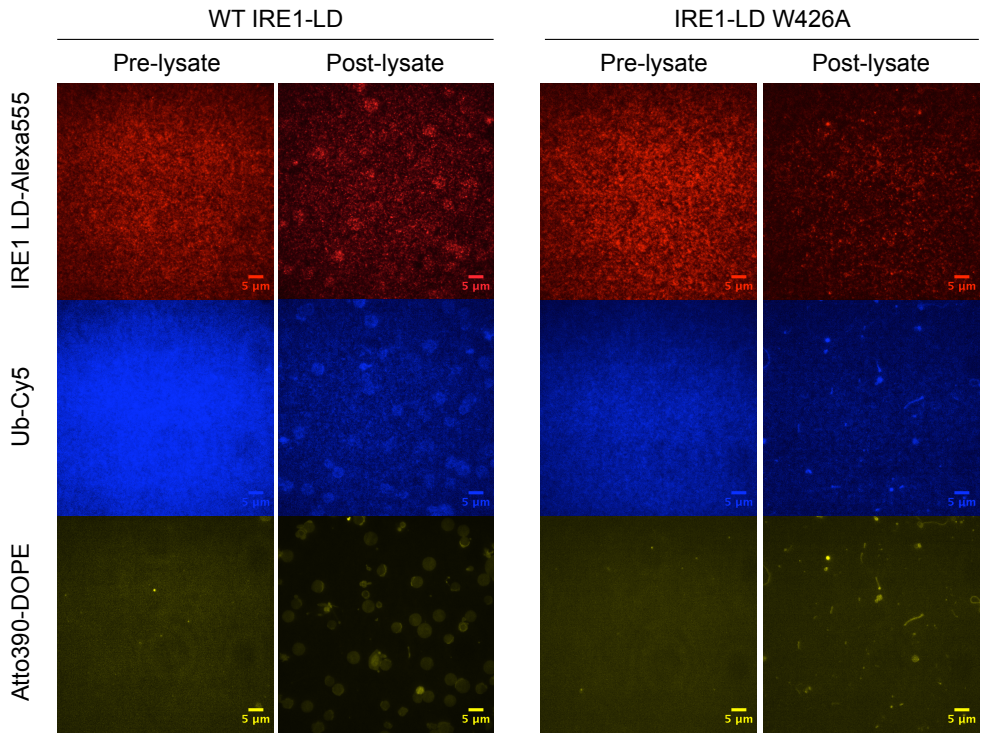

Figure 4.6 Addition of clarified yeast lysate induced clustering of WT IRE1-LD and not the interface mutant. WT IRE1-LD gathered in microdomains with clusters of Ub and fluorescently labeled lipids (Atto390-DOPE)

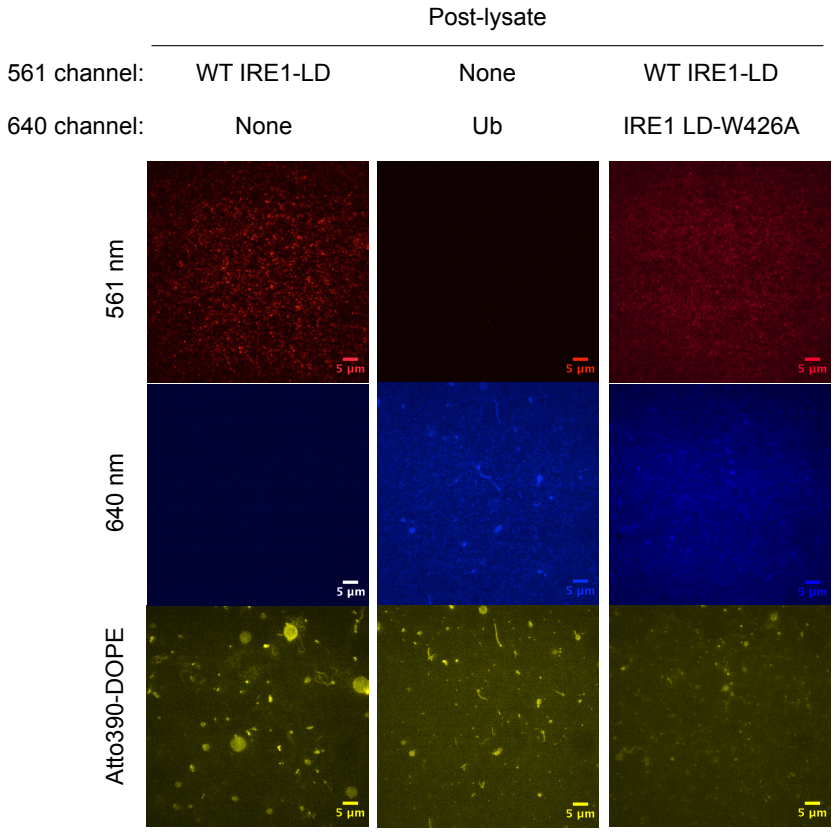

Figure 4.7 Clustering of WT IRE1-LD in the presence of clarified lysate required high protein density on the lipid bilayers but was dispersed in the presence of the interface mutant

Publishing Agreement

It is the policy of the University to encourage the distribution of all theses, dissertations, and manuscripts. Copies of all UCSF theses, dissertations, and manuscripts will be routed to the library via the Graduate Division. The library will make all theses, dissertations, and manuscripts accessible to the public and will preserve these to the best of their abilities, in perpetuity.

Please sign the following statement:

I hereby grant permission to the Graduate Division of the University of California, San Francisco to release copies of my thesis, dissertation, or manuscript to the Campus Library to provide access and preservation, in whole or in part, in perpetuity.

Author Signature

09/08/2019

Date